



Vrije
Universiteit
Brussel

Department of Chemical Engineering (VUB)
Research group Transport Modelling and Analytical Separation Science

Optimization of the separation performance by using coupled columns packed with core-shell particles operated at 1200 bar

Thesis submitted to obtain
the degree of Master of Science in Chemistry by

Jelle DE VOS

Academic year 2011 - 2012

Promotor: Prof. Dr. Sebastiaan Eeltink

Co-Promotors: Prof. Dr. ir. Gert Desmet and Prof. Dr. ir. Ken Broeckhoven

Supervisor: ir. Axel Vaast

Abstract

In this thesis the peak capacity that can be produced by operating state-of-the-art core-shell particle type ($d_p=2.6\ \mu\text{m}$) columns at its kinetic optimum at ultra-high pressures of 600 and 1200 bar is investigated. The column-length optimization, needed to arrive at this kinetic optimum was realized using column coupling. Whereas the traditional operating mode (using a single 150 mm column operated at its optimum flow rate of 0.4 mL/min) offered a peak capacity of 162 in 12 min for the separation of small molecules, a fully optimized train of 600 mm (4 x 150 mm) columns offered a peak capacity of 324 in 61 min when operated at 1200 bar. It was found that the increase in performance that can be generated when switching from a fully optimized 600 bar operation to a fully optimized 1200 bar operation these kind of separations is significant (roughly 50% reduction in analysis time for the same peak capacity or roughly 20% increase in peak capacity if compared for the same analysis time). This has been quantified in a generic way using the kinetic-plot method and is illustrated by showing the chromatograms corresponding to some of the data points of the kinetic plot curve. The effect of optimizing the performance of a separation of protein tryptic digests, by changing gradient time, has also been investigated. To work closer at the optimal flow rate for the kinetically optimized gradient separation of peptides at 1200 bar, a fully optimized train of six 150 mm core-shell columns was coupled. These chromatograms visualized the improvement in separation performance when compared with a reference system of 450 mm operated at 1200 bar. For separations of peptide mixtures containing 400-500 peptides on a fully optimized 900 mm core-shell particle column operated at 1200 bar, a peak capacity of 1360 was reported and well resolved peaks were observed.

Acknowledgements

I owe a debt of gratitude to the people who made this thesis possible. First, I would like to thank my promoter Prof. Dr. Sebastiaan Eeltink for his tireless work and sharing his extended expertise - this thesis would never have been completed without your guidance. I would also like to thank my co-promoters Prof. Dr. ir. Gert Desmet and Prof. Dr. ir. Ken Broeckhoven for their many scientific contributions and insights. ir. Axel Vaast and Dr. Catherine Stassen, for providing valuable insight and helping me to achieve my best possible work. Dr. Matthias Verstraeten and ir. Eva Tyteca for offering excellent help and assistance. I would also like to thank ir. Bert Wouters, Dr. ir. Hamed Eghbali, and Dr. ir. Anuschka Liekens for their consistent moral support. ir. Marc Sonck and ir. Bart Degreeef for helping me with mechanical problems. I would also like to thank Prof. Dr. Bart Devreese for providing the protein samples and Dr. Tivadar Farkas and Dr. Jason Anspach from Phenomenex (Torrance, CA, USA) for the kind donation of the prototype Kinetex columns. I find it appropriate to also thank all other PhD and master thesis students from the department of Chemical Engineering. I would especially like to thank my parents for offering me the opportunity and trust to study at the university, and, in addition, also all other family members and close friends who have supported me in all my endeavors. Finally, I would like to especially thank my girlfriend Calissa for cheering me up during bad times and supporting me to achieve great things – you are all my reasons.

Contents

1	INTRODUCTION	1
2	LITERATURE STUDY	3
2.1	RETENTION, SELECTIVITY, AND RESOLUTION	3
2.2	BAND-BROADENING EFFECTS IN HPLC COLUMNS	6
2.2.1	<i>Plate height and plate number</i>	6
2.2.2	<i>Random-walk theory</i>	7
2.2.3	<i>Molecular diffusion (B-term)</i>	8
2.2.4	<i>Eddy diffusion (A-term)</i>	10
2.2.5	<i>Mass-transfer effects (C-term)</i>	11
2.2.6	<i>The van Deemter curve</i>	13
2.3	PERFORMANCE LIMITS IN LIQUID CHROMATOGRAPHY	14
2.3.1	<i>Kinetic-plot method</i>	14
2.3.2	<i>Effects of ultra-high pressure</i>	18
2.3.3	<i>Fused-core particles</i>	19
3	AIM OF THE RESEARCH	21
4	EXPERIMENTAL	23
4.1	CHEMICALS AND MATERIALS	23
4.2	INSTRUMENTATION AND EXPERIMENTAL CONDITIONS	24
5	RESULTS AND DISCUSSION	27
5.1	THEORETICAL ASPECTS OF OPERATING AT THE KINETIC-PERFORMANCE LIMIT	27
5.1.1	<i>Dimensionless chromatograms</i>	27
5.1.2	<i>Efficiency analysis</i>	28
5.1.3	<i>Kinetic-plot analysis: influence of pressure on the separation performance</i>	31
5.2	KINETIC-PERFORMANCE LIMITS FOR THE SEPARATION OF SMALL MOLECULES	35
5.2.1	<i>Different regions of the kinetic-performance limit curve at 600 and 1200 bar operating pressure</i>	35
5.2.2	<i>Practical illustration of the advantage of coupled columns at 1200 bar</i>	40
5.3	KINETIC-PERFORMANCE LIMIT FOR THE SEPARATION OF PEPTIDES	43
5.3.1	<i>Peptide separations on a 450 mm core-shell column at 1200 bar</i>	43
5.3.2	<i>Quantitative assessment of peak capacity</i>	46
5.3.3	<i>Peptide separations on a 900 mm long column at 1200 bar</i>	51
6	CONCLUSION	55
	REFERENCES	57
	APPENDIX I: NEDERLANDSTALIGE SAMENVATTING	61
	APPENDIX II: LINEAR SOLVENT STRENGTH MODEL	71
	AII.1 GRADIENT RETENTION FACTOR	71
	AII.2 RETENTION FACTOR AT THE END OF THE COLUMN	73

AII.3 EXTENDING THE GENERALITY OF THE RETENTION FACTOR CALCULATIONS	73
AII.4 DETERMINATION OF RETENTION PROPERTIES OF COMPONENTS USING LSS-THEORY	74
REFERENCES	75
APPENDIX III: SIGNAL ENHANCEMENT BY TRAPPING	77
AIII.1 INTRODUCTION	77
AIII.2 EXPERIMENTAL SET-UP AND AIM	77
AIII.3 RESULTS AND DISCUSSION	79
<i>AIII.3.1 Retention characteristics of the analytical column and the trapping segment</i>	79
<i>AIII.3.2 Preconcentration experiment</i>	81

1 Introduction

The emergence of ultra-high-pressure liquid chromatography (UHPLC) instrumentation and state-of-the-art columns packed with core-shell particles have brought new opportunities for liquid chromatography method development. With these new technologies improved analytical techniques with high speed, high efficiency and high throughput can be developed. Novel chromatographic techniques are immensely important for a modern quality control laboratory in pharmaceutical, food, and agricultural industries.

Martin and Synge postulated in 1941 that the most efficient separations can be obtained using very small particles and a high pressure drop across the length of the column [1], before van Deemter introduced his equation [2] which describes the chromatographic efficiency. By using modern UHPLC instrumentation, capable of delivering system pressures of up to 1200 bar, it has become possible to perform this kind of efficient separations with columns packed with small particles. If core-shell particles instead of fully porous particles are used for packing the chromatographic column, even faster separations (smaller flow resistance) and more efficient separations (reduced mass-transfer due to thin porous layer) can be obtained. Another way for improving separation efficiency and analysis time by exploiting another advantage of UHPLC by using long columns packed with small particles, as demonstrated by Jorgenson in the late 1990s [3]. In the first part of this dissertation, the effect of using long coupled columns packed with 2.6 μm internal diameter core-shell particles operated at 1200 bar will be investigated for the gradient-elution separation of small molecules.

The high peak capacities obtained in gradient elution for small molecules by operating long columns at UHPLC conditions can be considered as an interesting starting point for the analysis of proteomic samples. Peak capacity is proportional with the square root of plate number N , and is therefore directly linked to column length and particle size. In proteomics, the efficiency of the peptide separation is important for identification of potential biomarkers. The effects of tuning column length and operating pressure to obtain more efficient separations have been shown in the first part of this master thesis. Higher throughput, a very important factor for speeding up biomarker discoveries, can be achieved by working at higher operating pressures combined with more efficient separations. In the second part of this dissertation, an investigation of peak capacities for UHPLC separations on core-shell particle columns will be performed.

2 Literature study

2.1 Retention, selectivity, and resolution

In chromatography, analyte molecules are partitioned between stationary- and mobile-phase regions inside the separation column. During separation experiments, where the mobile phase is flowing without stopping, an equilibrium state may be approached, but never reached. Because the zone center moves under equilibrium conditions [4], retention times can be expressed in equilibrium concentrations C and equilibrium partition coefficients K . The partition coefficient K describes the partitioning of the analyte molecules between the two phases. The molecules are retained proportional to their affinity for the stationary phase.

$$K = \frac{[A]_S}{[A]_M} \quad (2.1)$$

where $[A]_S$ is the concentration of the analyte in the stationary phase and $[A]_M$ the concentration in the mobile phase. Equation (2.1) can be written differently by using the number of molecules of the analyte A present in the stationary phase $n_{A,S}$ and the number of molecules of A in the mobile phase $n_{A,M}$:

$$K = \frac{n_{A,S}}{n_{A,M}} \frac{V_M}{V_S} = \frac{k}{\beta} \quad (2.2)$$

where β is the so called phase volume ratio and k the partition ratio:

$$\beta = \frac{V_S}{V_M} \quad (2.3)$$

$$k = \frac{n_S}{n_M} \quad (2.4)$$

The partition ratio k is also called the retention factor. Another way of expressing the k is based on retention times [5]:

$$k = \frac{t_R - t_0}{t_0} = \frac{t_R}{t_0} - 1 \quad (2.5)$$

where t_R is the residence time or the retention time of a certain analyte molecule and t_0 is the elution time of an unretained solute, see Figure 2.1. The retention factor is a normalized measure of solute retention that is independent of column length, radius, and flow-rate F .

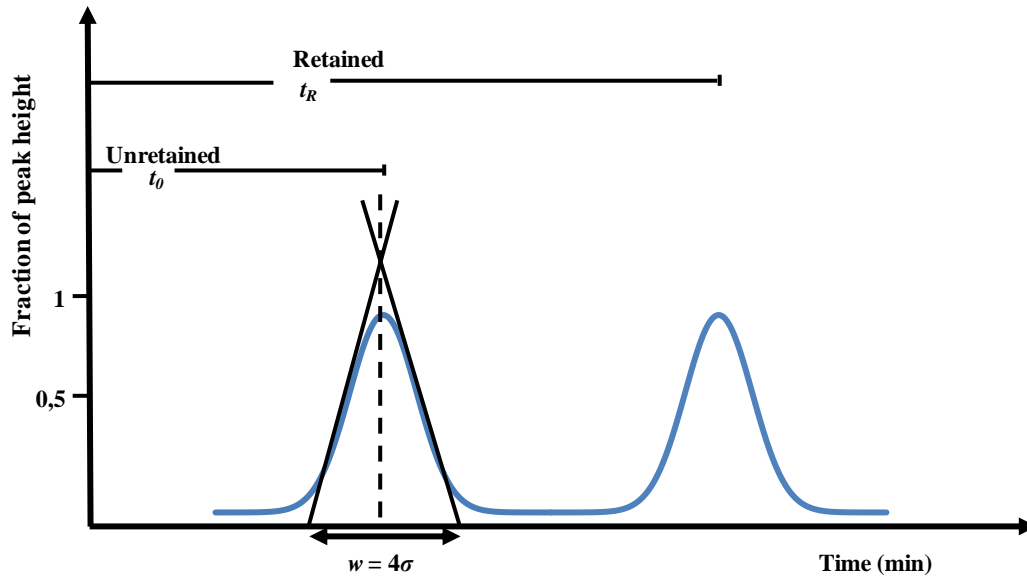


Figure 2.1: A Gaussian distribution, displaying the concentration profile of an unretained and a retained compound measured as a function of time. Also depicted are the deviation σ with its relation to peak width w and peak height.

Components within a sample can only be separated if they migrate at a different velocity through the column, *i.e.*, if they have a different retention factor. The selectivity factor α denotes the ratio of retention factors of two closely retaining components:

$$\alpha = \frac{k_2}{k_1} \quad (2.6)$$

where k_1 and k_2 are respectively the retention factors of the first and second eluting peak ($k_2 > k_1$). The selectivity factor quantifies the relative affinity of the two analyte molecules for the mobile and the stationary phase. The selectivity for a component can be optimized by selecting an appropriate stationary phase and, by altering experimental conditions (mobile-phase composition, pH and column temperature). Tuning the selectivity of analyte molecules by selecting the optimal conditions and separation column is important for optimizing the quality of the separation. A useful measure for the effectiveness of separation of two components is the resolution R_S , which is defined as the ratio of the distance between the centers of two adjacent peaks to the average width (w) of those peaks:

$$R_S = \frac{t_{R,2} - t_{R,1}}{\frac{w_1 + w_2}{2}} \quad (2.7)$$

A baseline separation is achieved when $R_S > 1,5$ and resolution increases when the peak widths are narrower, and/or the differences in retention times become larger.

When peak widths are equal for the two peaks, an alternative equation for expressing resolution can be derived [5]:

$$R_S = \left(\frac{\sqrt{N}}{4}\right) \left(\frac{\alpha-1}{\alpha}\right) \left[\frac{k}{(1+k)}\right] \quad (2.8)$$

The equation above shows that resolution can be improved by varying the plate number (N), α and k . The plate number is a measure to describe the efficiency of the separation process and is more discussed in detail in the next paragraph.

The strongest effect on resolution is acquired by improving selectivity α , as can be seen in Figure 2.2. For example, an increase in α from 1.01 to 1.02 (only 1% change) will double the resolution. When the retention factor is larger than 5 the increase in resolution is marginal and will mainly result in a slower separation. Finally, an increase in the plate number N , for example by using a longer column, will increase resolution. However, a fourfold increase in plate number (which is related to column length) is necessary to double the resolution. When the resolution of a separation is inadequate, the most effective remedy would probably be to change the chromatographic conditions, aiming at a higher relative retention. As has been emphasized above, the most profound approaches to increase α are changes in pH or in the composition of the eluent. A higher relative retention is also beneficial, as it permits the use of shorter columns.

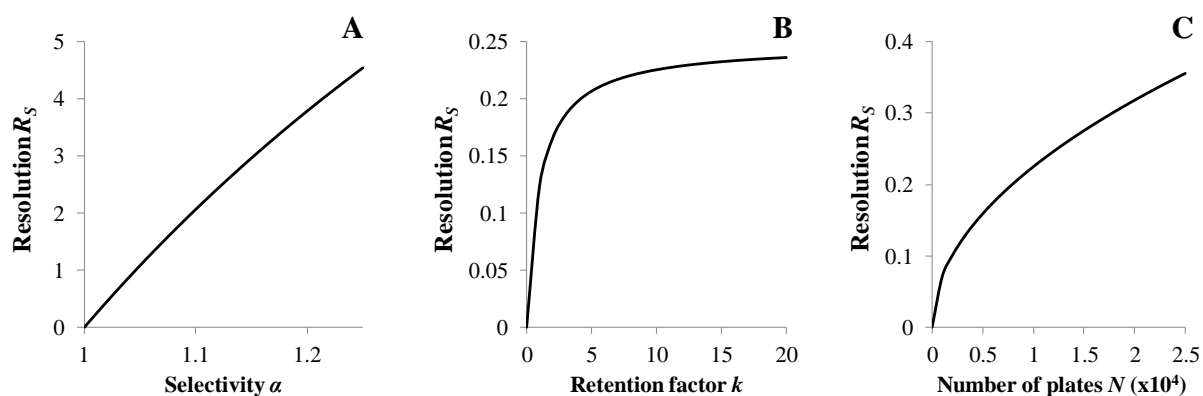


Figure 2.2: Effect of different parameters to improve resolution: (A) Selectivity α ; (B) Retention factor k ; (C) Number of plates N . To compare all parameters on a fair basis either α , k or N were varied while the other parameters were kept constant ($N= 5000$, $k=10$, $\alpha= 1.1$).

2.2 Band-broadening effects in HPLC columns

2.2.1 Plate height and plate number

At the start of a chromatographic experiment, analyte molecules are injected as one narrow concentration pulse at the column entrance. It is the intention of every chromatographer to keep the broadening of this narrow band as limited as possible. Mathematically this band is described as a δ -function. This function is zero for all independent variable values except at the origin, where it is infinite. The area under the curve is equal to one. By random diffusion or dispersion processes this initial zone is spread out and can be described by the normal or Gaussian distribution (expressed in standard deviation σ):

$$y = \frac{1}{\sqrt{2\pi}} e^{-\frac{\sigma^2}{t}} \quad (2.9)$$

A plot of this function for a retained and unretained component can be seen in Figure 2.1. σ represents the standard deviation of the concentration profile distribution, a measure of the spreading of the zone around its center as the separation process advances. Hence σ is a function of place (σ_x) and time (σ_t). Where the tangents at the inflection points intersect the baseline, it can be seen from Figure 2.1 that they cut off a distance w (with a value of 4σ) called the peak width at the base.

Since peaks are detected in function of time using a detector, the peak variance is recorded in the time domain. The transformation from a spatial concentration distribution to the time domain is done by the following relationships:

$$\sigma_x^2 = u_R^2 \sigma_t^2 \quad (2.10)$$

$$x = u_R t_R \quad (2.11)$$

where σ_t is the standard deviation around the top of the peak that elutes with retention time t_R and moves with an average zone velocity u_R . The longitudinal (or axial) coordinate inside the column is defined by x . The average zone velocity is defined by:

$$u_R = \frac{L}{t_R} \quad (2.10)$$

where L is the total column length.

In distillation procedures it was customary to describe the efficiency of the separation process by the number of plates. These plates can be thought of as discrete containers in which separations take place between two phases until equilibrium is reached. Efficiency of a separation in chromatography can be described analogous to that in a distillation process. The observed peak width is represented by a theoretical plate number N :

$$N = \left(\frac{t_R}{\sigma_t} \right)^2 \quad (2.11)$$

The number N is dimensionless and is a measure for the quality of the separation. Each container can then be given a certain length, the theoretical plate height H , in which analyte molecules spend an finite time sufficient to achieve equilibrium between the two phases. Unless columns have the same length, it is impossible to compare them based on their plate numbers. To remove this length dependence, the related parameter plate height (H) is introduced:

$$H = \frac{L}{N} \quad (2.12)$$

The column plate height can be redefined using the spatial variance σ_x (2.10) according:

$$H = L \left(\frac{\sigma_t}{t_R} \right)^2 = \frac{\sigma_x^2}{L} \quad (2.13)$$

which expresses the spreading of an analyte zone as it passes through the column.

2.2.2 Random-walk theory

In the plate theory analogy of a chromatographic process the analyte molecules are axially transported through the column during a time τ_M in the mobile phase in n steps, covering a step length of $\delta_M = L / n$. Molecules spend an infinitesimal time τ_M in the mobile phase, after which they exchange (via the process of desorption) to the stationary phase and stay there for an infinitesimal time τ_S . The number of steps n is analogous to the number of theoretical plates N , while δ_M can be seen as the height equivalent of one theoretical plate H (HETP). n and δ_M are related to the peak variance in spatial units:

$$\sigma_x^2 = n \delta_M^2 \quad (2.14)$$

Processes that obey this relationship are random-walk processes because they can be understood entirely by using statistical principles.

The rate theory presumes that there are several sources contributing independently to band broadening, and that these contributions are additive. Based on the fundamental law of additivity of variances, the total variance becomes:

$$\sigma^2 = \sum_1^i \sigma_i^2 = \sigma_1^2 + \sigma_2^2 + \sigma_3^2 + \dots + \sigma_i^2 \quad (2.15)$$

2.2.3 Molecular diffusion (B-term)

Molecules are subject to a variety of forces, such as collisional forces when contacting neighboring molecules or particles (thermal motion). Whenever a concentration gradient is present, a diffusion process tries to eliminate that gradient by a molecular transport mechanism of random movement. Diffusion of molecules in the x-direction can mathematically be described as a random-walk process, which is linked to a diffusion coefficient D_m of an analyte molecule in the mobile-phase, and the total time t required to complete the diffusion process in a number of steps:

$$\sigma_x^2 = 2 D_m t \quad (2.16)$$

When molecular diffusion occurs, the mobile phase velocity $u_m = L/t$ can be substituted in equation (2.13), linking it to the plate height:

$$H = \frac{2 D_m}{u_m} \quad (2.17)$$

Because in a chromatographic support analyte molecules have to move around particles of the packing material, an obstruction factor in the longitudinal direction $\gamma_{B,m}$ should be introduced in the diffusion equation (2.16):

$$\sigma_x^2 = 2 \gamma_{B,m} D_m t \quad (2.18)$$

This obstruction factor is generally $\gamma_B = 0.6-0.75$ for well packed columns and linked to the interstitial porosity ϵ_0 .

When molecular diffusion occurs with a mobile phase velocity u_m , it can be linked to the plate height with equation (2.13):

$$H_{B-term, longitudinal, m} = \frac{2 \gamma_{B, m} D_m}{u_m} \quad (2.19)$$

The band broadening expression in (2.19) is that for longitudinal diffusion in the mobile phase. In some cases (for example in liquid-liquid chromatography), longitudinal diffusion in the stationary phase is also important. An obstruction factor for the stationary phase $\gamma_{B, s}$ is added to the band broadening expression:

$$H_{B-term, longitudinal, s} = \frac{2 k \gamma_{B, s} D_s}{u_m} \quad (2.20)$$

where D_s is the diffusion coefficient of the analyte component in the stationary phase. The retention factor k is a consequence of the fact that the diffusion time t in equation (2.16) is now $t_s = k t_m$. The residence times of the molecule in the stationary and mobile phase are given by respectively t_s and t_m . The combined effect of longitudinal diffusion in the mobile and stationary phase is inversely proportional to the flow rate and can be given by:

$$\begin{aligned} H_{B-term, longitudinal} &= H_{B-term, longitudinal, m} + H_{B-term, longitudinal, s} \\ &= \frac{2 \gamma_{B, m} D_m}{u_m} + \frac{2 k \gamma_{B, s} D_s}{u_m} \end{aligned} \quad (2.21)$$

In Figure 2.3 the reciprocal relationship between flow rate and molecular diffusion in a chromatographic column is shown for two different flow rates.

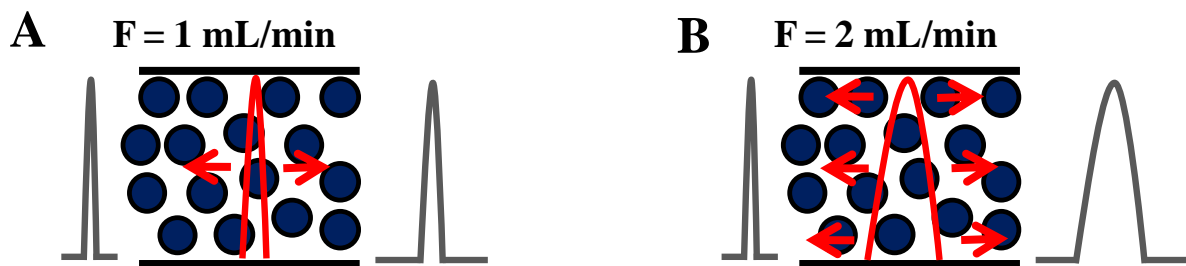


Figure 2.3: Physical visualization of longitudinal diffusion (B-term) for different flow rates: A) flow rate $F = 1$ mL/min and B) flow rate $F = 2$ mL/min.

2.2.4 Eddy diffusion (A-term)

Because of differences in particle shape, obstructions, and packing irregularities, an uneven flow distribution may be observed between nearby channels. The A-term (eddy diffusion) is a measure for the random movement of analyte molecules with overall zone velocity u_x through the chromatographic medium (see Figure 2.4).

The random-walk process is characterized by a step length δ_M related to the particle diameter d_P and $n = L / d_P$. Substituted in equation (2.14) this gives:

$$\sigma_x^2 = \left(\frac{L}{d_P}\right) d_P^2 = L d_P \quad (2.22)$$

Combined with (2.16) and knowing that $u_x = L / t$ this gives

$$D_{A-term, longitudinal} \approx \frac{d_P u_x}{2} = \lambda_{A,L} d_P u_x \quad (2.23)$$

where $\lambda_{A,L}$ is the “tortuosity” factor in the longitudinal direction (linked with the arrangement of the packing material, and typically varying between 1 and 1.5 for a well-packed bed).

When the equation for the molecular diffusion coefficient above is substituted in (2.17), the expression for the A-term contribution to band broadening in the longitudinal direction is obtained:

$$H_{A-term, longitudinal} = 2 \lambda_{A,L} \cdot d_P \quad (2.24)$$

From equation (2.24) it can be seen that the contribution to the zone broadening is independent from the zone velocity.

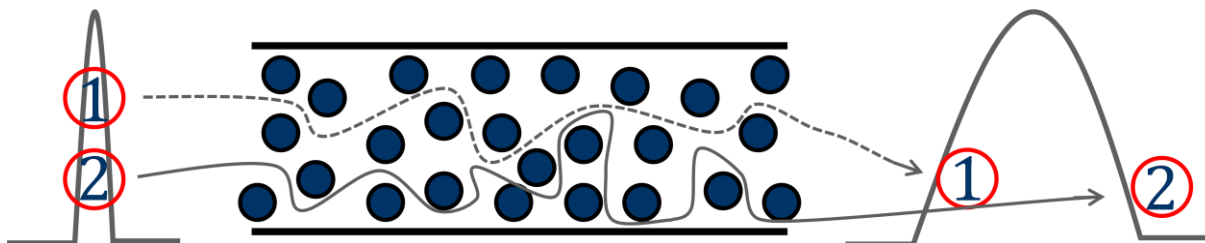


Figure 2.4: Physical visualization of eddy diffusion (A-term) on molecules 1 and 2.

2.2.5 Mass-transfer effects (C-term)

The C-term reflects the resistance to mass-transfer between the stationary and mobile phase. Molecules will diffuse from the mobile zone to the stationary zone and vice versa to maintain the equilibrium between the both zones (see Figure 2.5). Two contributions to the mass-transfer can be distinguished: resistance to mass-transfer in the mobile phase (C_m) and resistance to mass-transfer in the stationary phase (C_s). When a molecule adsorbs to the stationary phase, it will take a step back relative to the zone center, and thus moves slower relative to the zone center. Likewise, when a molecule is desorbed, it moves faster than the zone center and will elute earlier from the column. The distance travelled by the molecule in the mobile phase after this desorption process is characterized by a step length $\delta_M = (\langle u_m \rangle - u_z) \tau_M = \frac{\langle u_m \rangle \tau_m k}{1+k}$, in which u_z is the velocity of the zone center. The velocity difference between the zone center and the average of the mobile phase velocity profile $\langle u_m \rangle$ characterizes the velocity differences in the mobile phase. When a molecule adsorbs to the stationary phase, a step length $\delta_S = (0 - u_z) \tau_S = \frac{\langle u_m \rangle \tau_m k}{1+k}$ can be defined. In this definition the velocity difference between the zone center and velocity of the adsorbed molecule on the stationary phase characterizes partitioning of the molecule into the stationary phase.

The number of desorption and adsorption steps $n = 2 \cdot \left(\frac{L}{\langle u_m \rangle \tau_m} \right)$ is related to the time a molecule spends in the mobile phase τ_M . Combined with (2.14) this gives:

$$\sigma_x^2 = 2 L \langle u_m \rangle \tau_M \left[\frac{k}{(1+k)} \right]^2 \quad (2.25)$$

When (2.13) is combined with (2.25), an expression is obtained for the band broadening effect caused by the mass-transfer effects of a molecule traversing between the two phases:

$$H_{C-term} = 2 \tau_M \left[\frac{k}{(1+k)} \right]^2 \langle u_m \rangle = 2 \tau_S \left[\frac{k}{(1+k)^2} \right] \langle u_m \rangle = C \langle u_m \rangle \quad (2.26)$$

The characteristic time τ_M or τ_S are the main parameters of interest to investigate the contribution of the mobile phase and stationary phase mass-transfer effects. Giddings called this the nonequilibrium term. Velocity differences in the mobile phase throughout the entire column cross section contribute to band broadening. An equilibration time τ_M , necessary to mix the different velocity profiles in the column packing over the radial direction, can be formulated based on (2.16):

$$\tau_M \approx \frac{R_C^2}{2 D_m} \quad (2.27)$$

Where it is assumed that the band broadening occurs over a distance of the column radius R_C . When (2.26) is combined with (2.27), an expression is found for the band broadening effect caused by mass-transfer effects in the mobile phase, assuming slow diffusion in the mobile phase:

$$H_{C_M} = 2 \left(\frac{R_C^2}{2 D_m} \right) \left[\frac{k}{(1+k)} \right]^2 \langle u_m \rangle = \left(\frac{(\Omega d_p)^2}{D_m} \right) \left[\frac{k}{(1+k)} \right]^2 \langle u_m \rangle = C_M \langle u_m \rangle \quad (2.28)$$

Where $\Omega = R_C / d_p$ is the column/particle aspect ratio. In modern packed columns, an almost flat or plug-like flow profile is observed. This flat velocity profile is a consequence of splitting of the flow caused by the packing material. Because plate height decreases quadratically with particle size, it is advantageous to use smaller particle diameters (1-2 μm). A linear dependency on mobile phase velocity is observed. This is as expected: the larger the velocity, the larger the velocity differences and according band broadening.

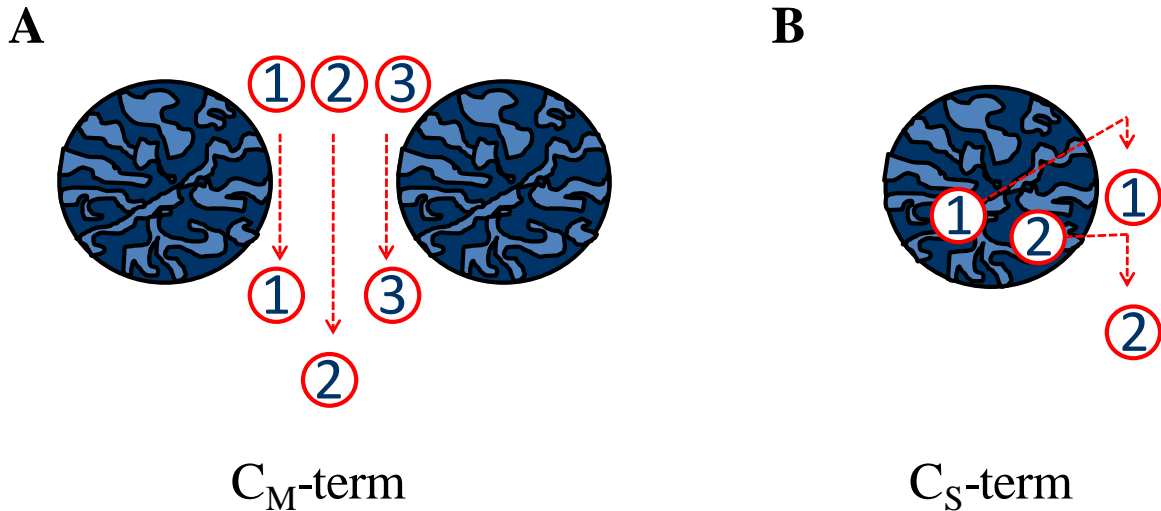


Figure 2.5: Physical visualization of mass-transfer effects in the van Deemter equation, for molecules 1, 2 and 3. (A) Resistance to mass-transfer in the mobile phase (C_M -term); where differences in velocity are depicted. (B) Resistance to mass-transfer in the stationary phase (C_S -term); where molecule 1 desorbs slower than molecule 2.

The stationary phase also contributes to band broadening in addition to the C_M term described above. When mass-transfer by diffusion is slow, $\tau_S \approx \frac{\alpha_S^2}{2 D_S}$ can be used as a characteristic time to escape from the stationary phase. In the equation above the average film thickness or depth of pores filled with liquid α_S and the related diffusion coefficient D_S is used to estimate τ_S .

The C_S term contribution to the plate height can be described by (2.26):

$$H_{C_S} = q_C \left(\frac{\alpha_S^2}{D_s} \right) \left[\frac{k}{(1+k)^2} \right] \langle u_m \rangle = C_S \langle u_m \rangle \quad (2.29)$$

The factor q_C is the so-called configuration factor, which was introduced to replace the original numerical geometrical form factor ($8/\pi^2$) introduced by van Deemter. For a spherical porous particle $q_C = 2/15$ and $\alpha_S = d_p/2$. Besides the fact that the contribution to band broadening is proportional to the flow rate (the larger the velocity, the larger the disturbance of equilibrium), equation (2.29) shows the advantage of reducing the stationary phase dimensions.

The combined equations above result in the following expression for the total C-term contribution to band broadening in packed bed columns:

$$C = C_M + C_S = f(k) \cdot \left(\frac{d_p^2}{D_m} \right) + g(k) \cdot \left(\frac{\alpha_S^2}{D_s} \right) \quad (2.30)$$

Whereas the resistance to mass-transfer in the mobile phase is dependent on the particle diameter of a stationary phase particle d_p , the stationary phase mass-transfer resistance depends on the film thickness α_S .

2.2.6 The van Deemter curve

When the plate height is plotted against the linear velocity of an unretained peak u_0 , a curved relationship called the van Deemter plot is observed (see Figure 2.6). The empirical van Deemter equation describes the relationship between plate height H and u_0 . It is composed of three independent contributions to the overall dispersion of the analyte peak and is given by:

$$H = A + \frac{B}{u_0} + C \cdot u_0 \quad (2.31)$$

At low linear velocity, the overall plate height is determined by longitudinal diffusion and at linear velocity it is determined by mass-transfer processes between the phases.

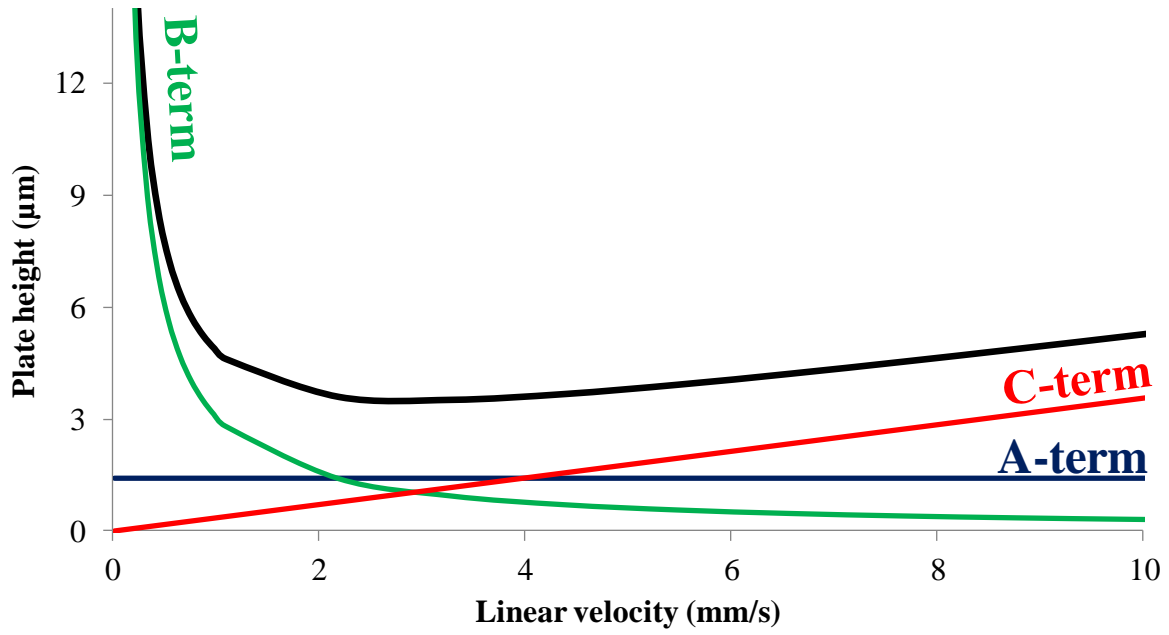


Figure 2.6: van Deemter plot for a Kinetex 2.6 μm core-shell particle column showing the relationship between column plate height H and linear velocity u_0 . The contributions to band broadening are also plotted: eddy diffusion (A-term, blue), longitudinal diffusion (B-term, green) and mass-transfer effects (C-term, red). Reproduced from [6].

In the minimum of the curve, the optimal mobile-phase velocity $u_{opt} = \sqrt{\frac{B}{C}}$ can be found where the best chromatographic separations are obtained. These separations correspond with a minimum plate height H_{min} , found by introducing u_{opt} in (2.31):

$$H_{min} = A + B \sqrt{\frac{C}{B}} + C \sqrt{\frac{B}{C}} = A + 2 \sqrt{BC} \quad (2.32)$$

2.3 Performance limits in liquid chromatography

2.3.1 Kinetic-plot method

Chromatographers desiring to decrease separation speed, for example by using UHPLC instruments capable of producing up to 1200 bar (see Paragraph 2.3.2), need to consider the minimum plate height H_{min} (or reduced equivalent $h_{min} = H_{min} / d_p$) and column permeability K_v :

$$K_v = \frac{d_p^2}{\phi} \quad (2.33)$$

Column permeability is linked with the flow resistance factor Φ . The van Deemter plot lacks permeability considerations. To assess the relative importance of both parameters, the separation impedance number E_0 is defined [7]:

$$E_0 = h^2 \Phi = \frac{H^2}{K_v} \quad (2.34)$$

Since this E_0 is defined as a dimensionless number, no information of separation speed is included in its definition. Comparison of different columns based on their E_{min} values implies B- or C-term effects that are not properly taken into account because H_{min} values are mainly influenced by A-term effects, see equation 2.32. Equation (2.34) shows that two similarly packed chromatographic columns can have a similar value for E_{min} . It is however possible that the B and/or C term region of the compared columns vary significantly.

An alternative plate height representation, the so called kinetic-plot method, visualizes the compromise between separation speed and efficiency. A kinetic plot is a tool to visualize two important chromatographic optimization problems: achieving the maximal number of plates within a given set of separation time and minimizing the separation time needed to achieve a given set of number of plates.

For isocratic separations, experimental plate height versus linear velocity data are transformed into a corresponding value of t_0 (or retention time via equation (2.5)) and N [8]:

$$N = \frac{\Delta P_{max}}{\eta} \left(\frac{K_v}{u_0 H} \right) \quad (2.35)$$

$$t_0 = \frac{\Delta P_{max}}{\eta} \left(\frac{K_v}{u_0^2} \right) \quad (2.36)$$

where ΔP_{max} is maximal allowable column or instrument pressure. These equations incorporate the flow resistance or permeability of the column, and transforms the efficiency to a pressure drop-limited plate number N . This allows to visualize the effects of increased instrument pressure on separation performance, see results and discussion paragraph 5.1.3

The knowledge of the exact retention factor experienced by the analytes when eluting from the column is difficult to determine during gradient separations. That is why the equations above are straightforward to use under isocratic conditions, but are no longer valid under gradient conditions. To measure efficiency during gradient separations, plate numbers are

seldom used. This is mainly because the migration velocity of the peak has not been constant during the recording of the chromatogram under gradient conditions. Another way to define performance of a gradient separation is by measuring experimental peak capacity $n_{p,exp}$ [9]:

$$n_{p,exp} = 1 + \sum_{i=1}^n \frac{t_{R,i+1} - t_{R,i}}{4 \cdot \sigma_{t,i+1}} \quad (2.37)$$

In this expression, the values for $\sigma_{t,i+1}$ represent the average of the peak variances measured for peak i and $i + 1$. The t_0 -marker is included as component number $i = 1$ and n denotes the last of the components. Once the gradient conditions (start and end composition of the mobile phase and the value of t_G/t_0) are determined, the performance of different column lengths should be measured over the entire range of available flow-rates or pressures. The ‘mobile phase history’ experienced by the components needs to remain the same for different column lengths and flow-rates, in order to be able to construct valid kinetic plots for gradient elution mode [10]. This condition is achieved if the gradient time (t_G) and the system dwell time (t_{dwell}) are scaled proportional to the column dead time (t_0). The system dwell time is the time needed for the mobile phase to flow from the pumping system to the point where the sample is injected (injector). This implies that the ratio of t_G/t_0 and of t_{dwell}/t_0 should remain constant when flow rates are varied and columns are coupled to maintain a longer column length. When the peak capacity is recorded for each considered flow-rate, this information can be plotted *versus* the retention time of the last peak used to calculate $n_{p,exp}$. The blue curve in Figure 2.7 denotes the fixed-length kinetic plot curve. Just like the van Deemter plot in Figure 2.6, an area where B-term effects or C-term effects influence the separation efficiency can be distinguished. Also present is the point where the minimum plate height is measured.

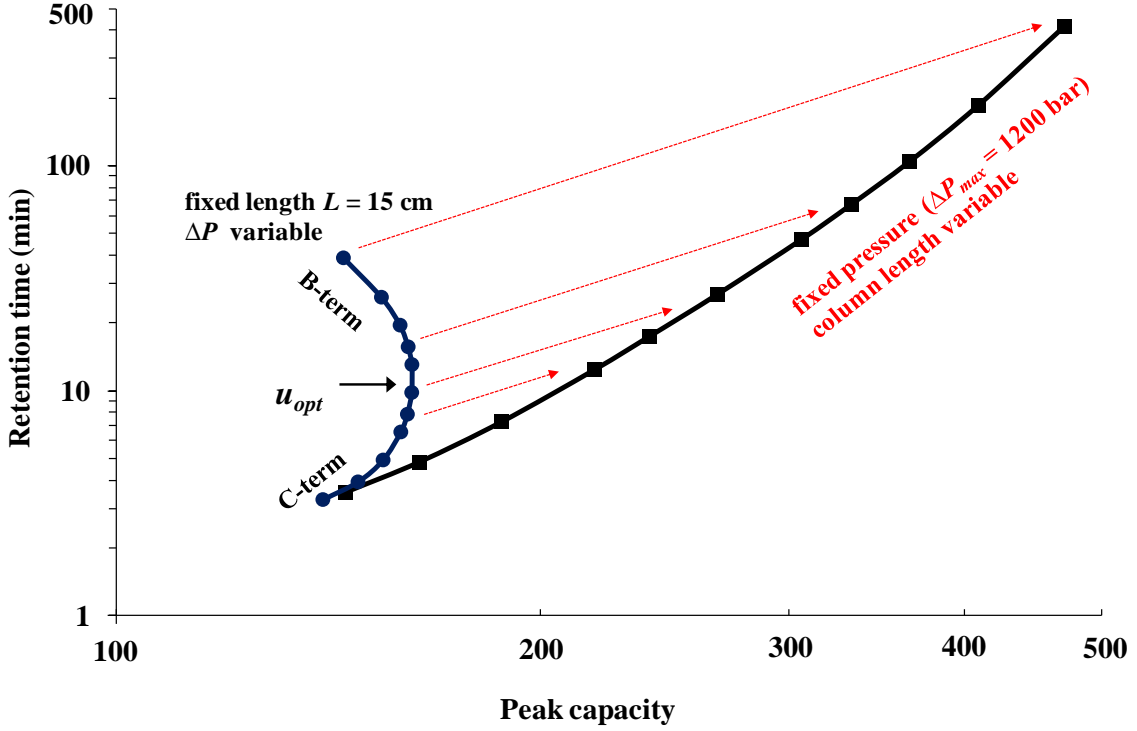


Figure 2.7: Construction of the kinetic-performance limit curve for $\Delta P_{max} = 1200$ bar in gradient elution mode (black). The blue curve depicts a fixed-length kinetic plot for a 150 mm column packed with core-shell particles. The red arrows depict how the datapoints from the fixed-length kinetic plot are extrapolated to the free-length kinetic plot according to Equations (2.38) and (2.39).

Using the kinetic-plot method for gradient elution [10], the kinetic-performance limit (KPL) of a given particle type can be directly calculated by using the experimentally determined peak capacity ($n_{p,exp}$), analysis time ($t_{R,exp}$) and pressure drop (ΔP_{exp}) measured on one specific column length. This can be done by extrapolating the abovementioned experimentally determined parameters to their corresponding value on the KPL using:

$$n_{p,KPL} = 1 + (n_{p,exp} - 1) \cdot \sqrt{\lambda} \quad (2.38)$$

$$t_{R,KPL} = \lambda \cdot t_{R,exp} \quad (2.39)$$

with a length-elongation factor λ defined as:

$$\lambda = \frac{P_{max}}{P_{exp}} \quad (2.40)$$

The free-length kinetic plot, which represents the kinetic-performance limit (KPL) is visualized by the black curve in Figure 2.7. The kinetic-performance limit of a given chromatographic support can be defined as the efficiency or peak capacity it can generate using a set of columns with widely varying length and each operated at the maximal available or allowable pressure (ΔP_{max}). The KPL of a given particle type connects the maximal

efficiency or peak capacity values that can be achieved with the particle type as a function of the allowed analysis time. It is thus impossible to find better combinations of efficiency and time than those situated on the KPL.

2.3.2 Effects of ultra-high pressure

Efforts have been made during the past 30 years to improve the separation power of standard chromatography columns, which provided 20.000 theoretical plates. One way to improve the number of theoretical plates to 100.000-300.000 is by packing the conventional 3 and 5 μm particles into long fused-silica capillary columns [11]. A drawback from this approach is that the analysis time is increased. Another way to improve separation power and achieve faster analysis times, is by decreasing the particle size to 1-2 μm . This was also deduced from equations (2.24) and (2.28), where it is shown that the A-term is dependent of the particle diameter (d_p), and the C-term is proportional to d_p^2 . The inverse proportionality between number of plates N and particle diameter d_p shows that when the particle size is decreased with a factor three from 5 μm (HPLC-scale) to 1.7 μm (UHPLC-scale), N is increased by three. The resolution increases by $\sqrt{3}=1.7$, as it is predicted by the resolution equation (2.8). Equation (2.11) shows that increased number of plates also relates to narrower peaks. This also means an increase in sensitivity because taller, narrower and better separated peaks are obtained by using smaller particles.

Unfortunately the pressure required for pumping the mobile phase through such long columns packed with small particles is higher than the 400 bar (6000 psi) pressure limit of conventional HPLC systems. This can be deduced from following equation [4]:

$$\Delta P = \frac{\Phi \eta L u_0}{d_p^2} \quad (2.41)$$

where the pressure drop ΔP , the flow resistance factor Φ and the mobile-phase viscosity η are used. New valves, pumps and columns were designed to address this problem. This technology is called ultra-high-pressure liquid chromatography (UHPLC) [3,12–14]. More than 200.000 theoretical plates in 10 min ($k \approx 1$) for a separation of small molecules with a 460 mm capillary column packed with 1 μm nonporous reversed-phase particles has operated at 2570 bar has been reported [3].

Comparing systems under fully optimized conditions, the gain in separation speed that can be obtained when switching from a 400 bar system to a 1000 bar system can be estimated to be of the order of a factor of 2 to 2.5 (significantly less if only small efficiencies, in the order of 10.000, are needed; significantly more if very large efficiencies, in the order of 50.000 to 100.000, are needed). [15]

2.3.3 Fused-core particles

Particles consisting of a solid, nonporous core surrounded by a shell of porous material were originally developed to analyze macromolecules. Pellicular (thin porous shell layer) particles with a 50 μm diameter for ion-exchange chromatography were developed by Horváth and Lipsky [16]. They argued that columns packed with such particles would provide more efficient separations because diffusion through the thin porous layer would be faster than diffusion through fully porous particles. Around the same time (late 1960s) Kirkland developed shell (thick porous shell layer) particles with a 30-40 μm diameter for improving the analysis of biomolecules [17].

Nowadays the term core-shell particles (or shell particles) is mostly used for particles which have a diameter of 2.6-2.7 μm or 1.7 μm . Their shell thickness varies from 0.5-0.23 μm . Smaller particles improve the efficiency of the separation but comes with the cost of increased back pressure, as was described in section 2.3.2. Core-shell particles have a flow resistance Φ around 550 [18,19], which is much lower compared to their fully porous counterparts (Φ around 800) [20]. The solid core in core-shell particles increases column permeability K_v , because analyte molecules only have to move through a small porous layer. This increase in permeability decreases the flow resistance, as can be deduced from Equation (2.33). The separation impedance (E_{min}) values for fully-porous and core-shell particles are reported to be respectively 2800 or higher and 1600 or less. The E_{min} -value directly determines the maximal speed with which a given particle type can produce at a given separation efficiency N or peak capacity n_p . Hence, the core-shell particle concept intrinsically allows for nearly a doubling of separation speed compared to the fully porous particle case. The former is only valid when both particle types are compared for the same pressure and on the basis of their kinetic-performance limit.

It is beneficial to use core-shell particle columns over their fully porous counterparts under UHPLC conditions when separations require high performance (low H_{min}) and high speed (u_{opt} at higher linear velocities) [21–25]. Reduction of A-term and B-term effects on efficiency are observed for core-shell particle columns. Less pronounced C-term contributions occur at higher linear velocities for this type of columns. Columns packed with core-shell particles have a reduced eddy diffusion coefficient (A-term) of up to 40% [26] compared to columns packed with fully porous particles. One explanation is that the improvement in efficiency compared to fully porous particles is obtained due to the narrow particle size distribution of core-shell particles, which may help to diminish short-range interchannel velocity biases [6]. In literature it was also suggested that the rougher external surface of the core-shell particles aid in the homogeneity of the packed bed, which decrease the long-range trans-column velocity biases. The longitudinal diffusion coefficient (B-term) was decreased with 20-30% compared with fully porous particles [27]. This diminution is due to the presence of the solid core and the more dense mesoporous network of the shell layer. The contribution of mass-transfer in the stationary phase decreases by about 50% due to the thin diffusion path length in the thin porous shell. The overall effect on the reduction of the total plate height caused by the C_S -term is however rather limited [19].

3 Aim of the research

In the first part of this study, the gradient peak-capacity limits and separation speed that can be achieved by combining both technological advancements have been investigated by assessing the gradient performance of prototype Kinetex columns packed with 2.6 μm core-shell particles, designed to withstand operating pressures up to 1200 bar. By coupling several of these columns, the total column length could be customized to operate the system at the kinetic-performance limit (KPL) of the considered particle type and size (2.6 μm). To quantify the potential advantage of elevated operating pressures, the performance limit is compared at two different operating pressures (resp. 600 and 1200 bar). The separation performance data were obtained using low molecular-weight sample mixtures, containing waste water pollutants, alkyl phenones and parabenes.

In the second part, the potential of using coupled core-shell columns at their kinetic-performance limits investigated for proteomics applications, by separating tryptic digest mixtures that differ in complexity. Therefore, three core-shell columns of 150 mm were coupled and operated at a column pressure of 1200 bar. The effect of changing the gradient time t_G , for given operating conditions, on the separation performance was studied using a tryptic digest of β -lactoglobulin, a tryptic digest of 6 proteins (bovine serum albumin, β -galactosidase, α -lactalbumin, β -lactoglobulin, lysozyme and apotransferrin) and a tryptic digest of *E. coli*.

4 Experimental

4.1 Chemicals and materials

For both studies acetonitrile (ACN, HPLC supra-gradient quality) was purchased from Biosolve B.V. (Valkenswaard, The Netherlands). Deionized HPLC-grade water ($\leq 0.055 \mu\text{S}$) was produced in-house using a Milli-Q water purification system (Millipore, Molsheim, France). For the separation of the in-house made peptide mixtures, formic acid (FA, $\geq 99\%$) was purchased from Biosolve B.V. (Valkenswaard, The Netherlands).

The following small MW sample mixtures were prepared by dissolving 100 ppm of each of the components in 50/50 (V%) ACN/H₂O and uracil (99%, HPCE) was added as the t₀-marker. All the compounds were purchased from Sigma-Aldrich (Steinheim, Germany):

1. A test mixture of 6 waste water pollutants (WWP) composed out of 2-naphtoic acid, quinoline, 2-naphtalenol, benzofuran, indene and fluorene.
2. A 19-compound mixture was made comprising the same components as 6WWP, but 9-hydroxyfluorene, 2-hydroxyquinoline, methyl 4-hydroxybenzoate, ethyl 4-hydroxybenzoate, propyl 4-hydroxybenzoate, butyl 4-hydroxybenzoate, dibenzofuran, indane, 1-indanone, acetophenone, propiophenone, butyrophenone and valerophenone were added to the mixture.
3. A complex 37-compound mixture was prepared as described for the 19-compound mixture above, with the addition of caffeine, acetanilide, phenol, trans-4-phenyl-3-buten-2-one, 3-methylacetophenone, benzene, dibenzothiophene sulfon, toluene, benzothiophene, benzophenone, xylene, naphtalene, ethylbenzene, acenaphthylene, 1,3,5-tri-isopropylbenzene, hexanophenone, mesitylene and propylbenzene.

The tryptic digest samples were prepared by dissolving the protein digest in mobile- phase A (0.05% FA in water):

1. A tryptic digest of β -Lactoglobulin (0.26 $\mu\text{g}/\mu\text{L}$).
2. A tryptic digest of six proteins (1.4 $\mu\text{g}/\mu\text{L}$): bovine serum albumin, β -galactosidase, α -lactalbumin, β -lactoglobulin, lysozyme and apotransferrin (6PMD).
3. A tryptic digest of *E. coli* (2 $\mu\text{g}/\mu\text{L}$, lyophilized) was purchased from Dionex Benelux (Amsterdam, The Netherlands).

To prepare the tryptic digest, proteins were dissolved in a solution of 1M urea in 50mM ammonium bicarbonate to concentrations of 2 nmol/ μ L and 250 pmol/ μ L for respectively the β -Lactoglobulin and 6-protein mixture. Proteins were first denatured by heating the mixture for 10 min at 60°C, subsequently 25 mM of reducing agent DTT was added to a final concentration of 2,5mM. After proper mixing, the solution was kept at 60°C for 10 min. Subsequently the proteins were alkylated by adding 75 mM IAA to a final concentration of 7,5 mM followed by 20 min incubation in the dark at room temperature. Finally trypsin was added in a 1:50 ratio (trypsin:protein) and incubated overnight at 37°C. The final concentrations of β -Lactoglobulin and 6-protein mixture were 1 nmol/ μ L and 80 pmol/ μ L.

Separations were performed on a set of prototype 2.1 internal diameter x 150 mm column length and 2.1 internal diameter x 100 mm column length Kinetex C18 columns (2.6 μ m, 100 Å), designed to withstand higher operating pressures (1200 bar). nanoVIPER 75 μ m ID x 100 mm length connections were used to couple columns.

4.2 Instrumentation and experimental conditions

The measurements were performed on an Agilent 1290 Infinity system equipped with a binary pump), an autosampler, a temperature controlled compartment set at 30°C for all experiments and a diode array detector with a Max-Light cartridge cell (10 mm path length). The instrument was operated with the Agilent Chemstation software Rev. B.04.02 (166)

The absorbance values were measured at 210 nm with a sample rate of 40 Hz (80 Hz for the peptide separations). The injected sample mixture volume was 0.5 μ L for the small molecules samples. 3.5 μ L of 6PMD and 1PD, and 5 μ L of *E. coli* digest was injected on a 450 mm column, the injection volume was scaled according to the square root of the column length for different column lengths.

Peak capacity measurements using the WWP mixture were performed on a single column (2.1 internal diameter x 150 mm column length) as well as on coupled-column systems involving 2, 3 or 4 columns. All separations were performed in gradient mode, and for the separation of small MW mixtures a linear mobile phase ramp from 15% (ϕ_0) to 72% (ϕ_f) aqueous ACN in an optimized gradient time t_G with $t_G/t_0 = 15$ (constant ratio for the different flow rates) was

used. This resulted in an elution window ranging in retention factor k between 1.8 and 12.2 for all the investigated small MW mixtures.

For the separation of the peptide mixtures a linear mobile phase ramp from 0% mobile-phase B to 50% was used. Mobile- phase A was 0.05% FA in water, mobile phase B was 0.04% FA in 80:20% (v/v) ACN:H₂O. For the experiments on the 450 mm column length reference system, gradient times t_G of 40, 80, 120 and 445 min were used for 6PMD, and for the β -Lactoglobulin digest samples the gradient time was 40 and 120 min. The *E. coli* digest chromatograms were recorded with a gradient time of 120 and 240 min on this reference system. Separations of β -Lactoglobulin digest and 6PMD were also done on a 900 mm column with a gradient time of 480 min.

5 Results and discussion

5.1 Theoretical aspects of operating at the kinetic-performance limit

5.1.1 Dimensionless chromatograms

The gradient-elution performance of different systems or operating conditions can only be compared in a fair and general way when the peak-to-peak selectivity and the width and the position of the elution window (expressed in dimensionless time units) are kept identical. This requires that the same initial gradient composition ϕ_0 and steepness factor $\beta.t_0$ are applied whenever the column length and or the flow rate are changed. The constant ϕ_0 - and $\beta.t_0$ -rule is also the requirement underlying the validity of the kinetic-plot method for gradient separations [10], which is a way to quantify the kinetic performance of a given chromatographic system that directly describes its kinetic-performance limit (KPL).

All experiments were performed at (i) the same initial mobile-phase composition ϕ_0 , (ii) the same gradient steepness ($\beta.t_0$) using the time steepness of the gradient β given by :

$$\beta = \frac{\phi_e - \phi_0}{t_G} \quad (5.1)$$

and (iii) the same ratio of t_{dwell}/t_0 in order to ensure that an identical peak-to-peak selectivity and relative elution window is obtained, regardless of the employed column length or applied flow rate (t_{dwell} is defined here as the time between the moment of injection and the time at which the gradient slope reaches the head of the column). Since the system dwell volume (112 μL) induced a t_{dwell} for the single column gradients, a constant t_{dwell}/t_0 -condition was needed when switching to the coupled column system. This was ensured by increasing the equivalent dwell time by adding an isocratic hold to the beginning of the gradient [28].

Figure 5.1 shows some examples of the chromatograms recorded at different flow rates on one single column length (150 mm), and illustrates the constant elution pattern that can be obtained when the set of rules which are described above are applied. The chromatograms on the left hand side are plotted as a function of the time, as is customarily done, whereas the chromatograms on the right hand side show the same information, although as described in [29] plotted as a function of the retention factor k (i.e. an adjusted dimensionless time) defined by Equation (1.5).

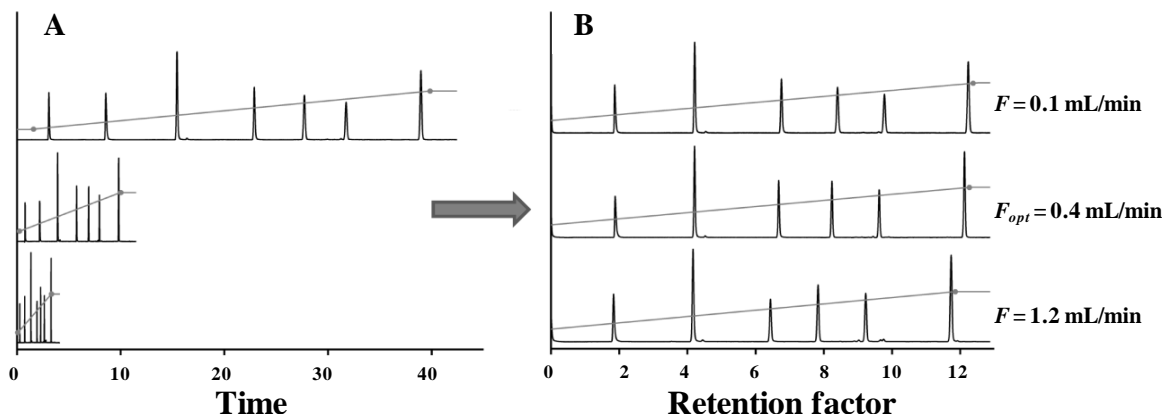


Figure 5.1: Chromatograms of the separation of 6 waste water pollutants recorded at 3 different flow rates (each one characteristic for a different region of the van Deemter curve) and plotted as a function of (A) the absolute time and (B) the retention factor k (dimensionless time $k = (t-t_0)/t_0$). The elution order of the peaks corresponds to naphtoic acid, quinoline, 2-naphtalenol, benzofuran indene, and fluorene.

The latter approach shows that the selectivity and the elution window are (nearly completely) unaffected by the flow rate when the same ϕ_0 and $\beta \cdot t_0$ -values are being used (as done in present study). The same holds for changes in length (see for example Figures 5.4-5.8 further on). Looking more in detail, the flow rate independency of the elution pattern is however not fully perfect, as the two last compounds tend to elute somewhat earlier when the flow rate increases. These deviations can be attributed to the effect of the higher degree of viscous heating [30–32] accompanying the higher flow rate. Such effects are typical for any change to a higher pressure system and cannot be captured in a simple rule such as the constant ϕ_0 - and $\beta \cdot t_0$ -rule (see also discussion of Figures 5.7 and 5.8 further on).

5.1.2 Efficiency analysis

Figure 5.2 shows the peak capacity n_p measured on one of the single columns as a function of u_0 , hence flow rate F . The resulting curve goes through a maximum (*cf.* the white diamond data point), indicating the existence of an optimal flow rate F_{opt} around = 0.4 mL/min. Since the reported peak capacity is obtained under conditions leading to a constant elution window width, the change in peak capacity observed in Figure 5.2 directly reflects the change in separation efficiency. As a consequence, the same trend can be observed as for isocratic separations, where the maximum efficiency is achieved at a given F_{opt} , and where the efficiency to the left and to the right of this optimum drops as one respectively enters the B-term and the C-term dominated region of the van Deemter curve.

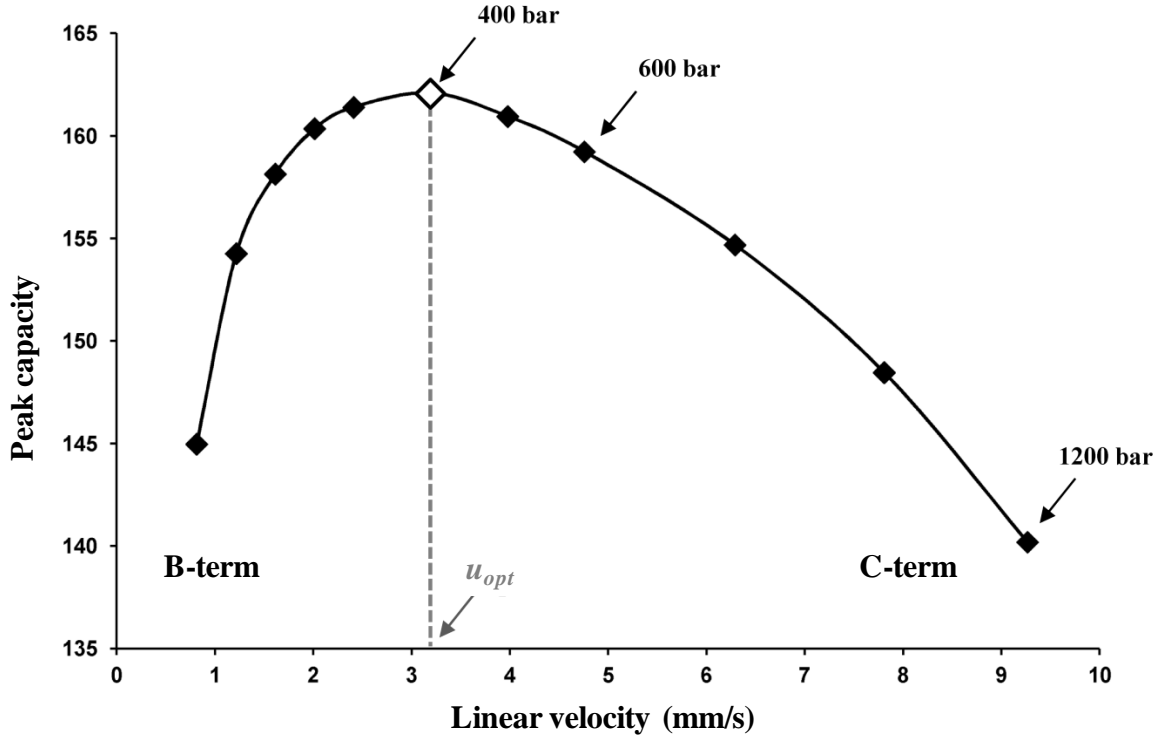


Figure 5.2: Plot of peak capacity (n_p) versus mobile phase velocity (u_0) recorded on a 150 mm long column. The white diamond denotes the optimal velocity point and the arrows denote how far one can expect to enter into the C-term region as a function of the available pump pressure. $t_C/t_0 = 15$.

Whereas the n_p -values reported in Figure 5.2 have been obtained by adding the peak capacity of the different sections of the chromatogram, using the peak width $w_p (= 4 \cdot \sigma_t)$ of the individual components to represent the peak capacity over each subsequent section, it is also possible to study the evolution of the peak widths of the individual components. From these peak widths and their corresponding σ_t -values, a representative column plate count or efficiency N can be calculated using [33]:

$$N = \frac{G^2 \cdot t_0^2}{\sigma_t^2} (1 + k_e)^2 \quad (5.2)$$

wherein the peak compression factor (G) and the retention factor at the point of elution (k_e) are given by:

$$G = \sqrt{\frac{1 + p + \frac{p^2}{3}}{(1 + p)^2}} \quad (5.3)$$

$$k_e = \frac{k_0}{b \cdot k_0 + 1} \quad (5.4)$$

with p the parameter of peak compression equation, b the general gradient slope and k_0 the retention factor at the beginning of the gradient, all given by :

$$p = \frac{k_0 \cdot b}{1 + k_0} \quad (5.5)$$

$$b = S \cdot \beta \cdot t_0 = S \cdot \frac{\phi_e - \phi_0}{t_G} \cdot t_0 \quad (5.6)$$

$$k_0 = k_w \cdot e^{-S \cdot \phi_0} \quad (5.7)$$

with S the linear solvent strength parameter, β the time steepness of the gradient, ϕ the fraction of organic modifier in the mobile-phase composition (subscript 0 for start of gradient and e for end) and k_w the extrapolated value of k for water as mobile phase. In this way, the effect of the peak compression factor and the effect of the retention factor at the moment of elution on the observed peak width are both cancelled so that the intrinsic column efficiency N is obtained. This was done for each peak in the chromatogram of the mixture containing 6 waste-water pollutants (6WWP). To determine the k_w and S -parameters of the LSS-model [9] for the components of the simplified 6WWP mixture, the retention times of the different components were recorded for five different gradient steepness values (resp. for $t_G/t_0 = 4.51, 7.90, 11.82, 16.96$ and 21.00). This resulted in the following values for naphtoic acid ($k_w = 21.43, S = 14.61$), quinoline ($k_w = 43.45, S = 9.15$), 2-naphtalenol ($k_w = 126.48, S = 8.82$), benzofuran ($k_w = 179.85, S = 8.61$), indene ($k_w = 307.07, S = 8.64$) and fluorene ($k_w = 1109.52, S = 9.30$). The details for the calculations using the LSS-model are given in Appendix I.

Calculation of the efficiency N was performed twice, once for the crude σ_t -data read out from the instrument software, and once for the case wherein the σ_t -values were corrected for the system band broadening. The extra-column contribution was found to be relatively small (improving the N -values by about 5 to 10%). For the largest retained compounds, the column produced roughly 25,000 theoretical plates around its optimal flow rate (23,000 without correction for the extra-column band broadening). Neglecting the correction for the peak compression factor by putting $G^2 = 1$ [33], these 25,000 plates turn into a value of about 33,000. Both values are situated in the area of the typical efficiencies measured under isocratic conditions on the same type of column. The column-to-column variation on these values was in the order of some 5%.

The obtained values also imply that the coupled column chromatograms typically correspond to approximately 60,000, 90,000 and 120,000 theoretical plates, for respectively two, three and four column system. The arrows added to Figure 5.2, indicate the maximal flow rate achievable in a 150 mm column using respectively 400, 600 and 1200 bar, and show that a 400 bar inlet pressure is barely enough to get to the optimal flow rate of the particles. To deeply enter the kinetically most advantageous C-term regime, higher inlet pressures, such as the currently applied 1200 bar, are needed.

5.1.3 Kinetic-plot analysis: influence of pressure on the separation performance

A kinetic plot of experimental data points (which corresponds to a plot of the KPL of a given particle type) can be established in two ways: either measuring the performance on a single column and using the kinetic-plot method to calculate the corresponding KPL-values or measuring the actual performance on different column lengths. In the present study, both approaches have been adopted as is depicted in Figure 5.3. The gray curve represents the peak capacity measured on the single column for different flow rates (see Figure 5.2) whereas the black curves have been calculated by applying equations (1.37)-(1.40) to the single column data for the case of a 600 and a 1200 bar operation. As such, the black curves represent the KPL of core-shell material under investigation.

The clear shift that can be noted between the 600 and 1200 bar KPL curves readily shows the advantage of producing 2.6 μm core-shell particles that can withstand 1200 bar instead of only 600 bar. It also visualizes the gain in performance that can be obtained when the system pressure is doubled. The increase in performance (higher peak capacity in the same time, or, the same capacity in a shorter time) that can be realized by switching to this ultra-high pressure is significant over the entire range of practically relevant analysis times.

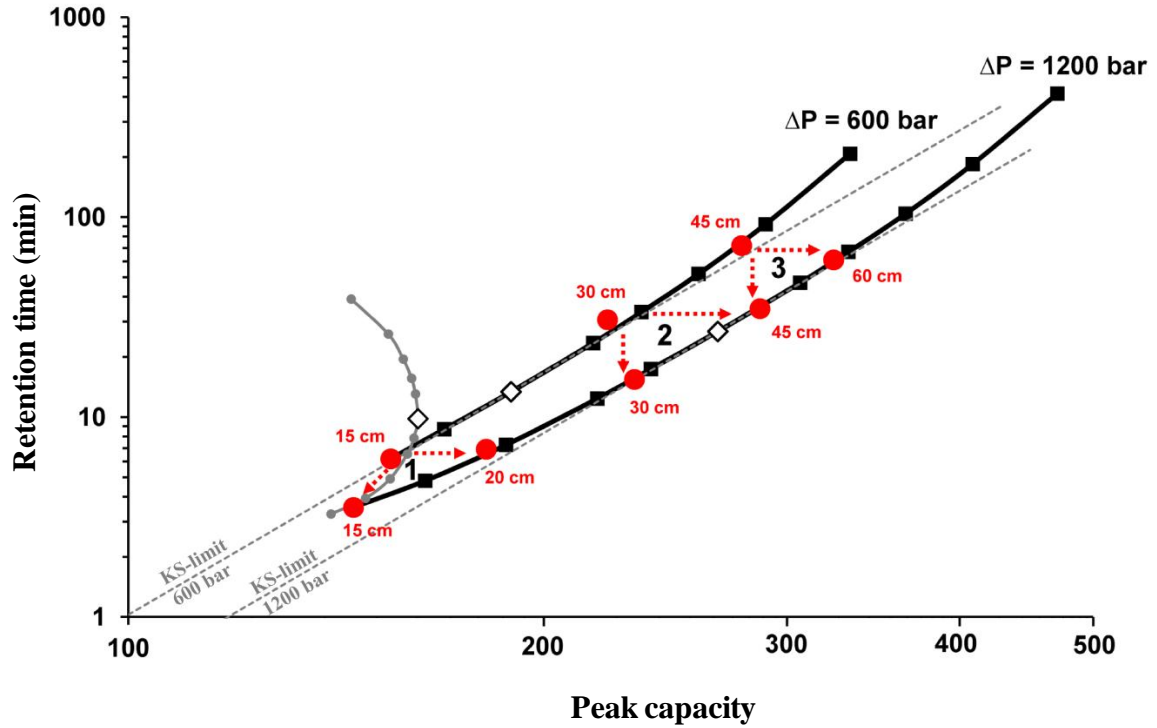


Figure 5.3: Extrapolation of the measured n_p versus t_R data measured on a single 150 mm column (grey curve, ●) to the kinetic-performance limit (KPL) curves corresponding respectively to a 600 and a 1200 bar operation (black curves). The time depicted here represents the retention time of the last eluting compound. The constructed Knox and Saleem limit lines touch the KPL-curves at the point corresponding to the optimal flow rate (white diamonds ◇). The experimental data measured on different coupled column lengths at 600 and 1200 bar are represented by the red dots (●). Three different regions (“triangles” 1,2,3) are distinguished for further discussion in Figure 5.4-5.6.

The shape of the KPL-curves in Figure 5.3 corresponds very well to the theoretical expectations, according to which the kinetic-performance limit curve (KPL-curve) should touch the Knox and Saleem limit (KS-limit) at the point corresponding to the optimal flow rate [7,34]. This can be understood as follows: adopting the LSS-theory, the relation between the peak capacity and the number of theoretical plates generated by the column can be written as [9]:

$$n_p = 1 + \frac{\sqrt{N}}{4} \cdot \frac{1}{b+1} \cdot \ln \left(\frac{b+1}{b} \cdot e^{b \cdot k_g} - \frac{1}{b} \right) \quad (5.8)$$

$$k_g = \frac{1}{b} \ln(b \cdot k_0 + 1) \quad (5.9)$$

Introducing the symbol $f(k_g)$ to group the effect of initial gradient composition and the gradient steepness, (5.8) can be written as :

$$(n_p - 1) = \frac{\sqrt{N}}{4} \cdot f(k_g) \quad (5.10)$$

Subsequently considering that the KS-limit originates from a combination of the basic kinetic plot equations [8]:

$$N = \frac{\Delta P}{\eta} \cdot \frac{K_v}{u_0 \cdot H} \quad (2.35)$$

into:

$$t_0 = \frac{\Delta P}{\eta} \cdot \frac{K_v}{u_0^2} \quad (2.36)$$

gives:

$$t_0 = \frac{H^2}{K_v} \cdot \frac{\eta}{\Delta P} \cdot N^2 = E_0 \cdot \frac{\eta}{\Delta P} \cdot N^2 \quad (5.11)$$

it can be found that, after combining (5.10) and (5.11), and by noting that, according to (1.5), $t_R = t_0 (1+k_g)$:

$$t_R = E_0 \cdot \frac{\eta}{\Delta P} \cdot \frac{256}{f(k_g)^4} \cdot (n_p - 1)^4 \cdot (1+k_g) \quad (5.12)$$

Introducing t_E as the time needed to generate a peak capacity of 2 (such that $n_p - 1 = 1$), (5.12) can also be rewritten as:

$$t_R = t_E \cdot (n_p - 1)^4 \quad (5.13)$$

In this expression, t_E is related to E_0 and thus depends on the flow rate, because E_0 varies with the square of the plate height (see equation (1.34) in paragraph 2.3.1). The definition of the Knox and Saleem limit now represents the performance of the particles for the flow rate at which t_E (or equivalently, E_0) reaches its minimum value (at which $t_E = t_{E,min}$). This value is always obtained at the optimal flow rate, *i.e.*, when $H = H_{min}$ and $F = F_{opt}$. In a plot, where typically the analysis time *versus* peak capacity is plotted, the KS-limit is hence given by:

$$t_{R, Knox \& Saleem} = t_{E,min} \cdot (n_p - 1)^4 \quad (5.14)$$

wherein $t_{E,min}$ is a constant depending on the support and packing quality ($E_{0,min}$), the employed column pressure (ΔP), the mobile phase viscosity (η), and the elution-window characteristics $f(k_g)$ and k_g :

$$t_{E,min} = \frac{256 \cdot E_0 \cdot \eta}{\Delta P} \cdot \left[\frac{b+1}{\ln\left(\frac{b+1}{b} \cdot e^{bk_g \cdot \frac{1}{b}}\right)} \right]^4 \cdot (1+k_g) \quad (5.15)$$

When $n_p \gg 1$, (5.14) represents a straight line with slope $r = 4$ in a log-log plot (as is the case for Figure 5.3). By fitting such a line until it touches the experimental KPL-curve at a single point, the position of the F_{opt} point can be retrieved and the value of $t_{E,min}$ can be determined. As can be noted, the two added KS-limit lines indeed touch the black curves close to the data point (denoted by an asterisk) corresponding to the optimal flow rate of the single column experiment. The $t_{E,min}$ -values that yield the best fit for the 600 and 1200 bar case are respectively equal to $t_{E,min} = 1.07 \cdot 10^{-8}$ and $t_{E,min} = 5.34 \cdot 10^{-9}$. Both values approximately differ by a factor of two, in agreement with the fact that the only difference between the two data sets is the different pressure value appearing in the value of $t_{E,min}$.

Another, and even more convincing argument for the fact that the KPL-curves in Figure 5.3 (obtained by using equation (1.37)-(1.40) to extrapolate the single-column data) are in line with the theoretical expectations is their good agreement with the experimental peak capacities and total analysis times measured on different coupled column length systems (red dots in Figure 5.3) for both 600 and 1200 bar. For example, the deviation in peak capacity between the experimentally measured data at 1200 bar and the KPL-extrapolation did not exceed 0.6 %, 1.3 % and 0.2% for respectively two, three and four coupled columns. The deviation in retention time was in the order of 2.3 %, 5.2 % and 0.7 % for respectively two, three and four coupled columns. This degree of agreement is in line with that observed in earlier studies [35].

5.2 Kinetic-performance limits for the separation of small molecules

5.2.1 Different regions of the kinetic-performance limit curve at 600 and 1200 bar operating pressure

As the red dots in Figure 5.3 correspond to actually measured performances, they can also be used to directly assess the gain that can be realized by increasing the system pressure from 600 bar to 1200 bar. This is illustrated in Figures 5.4-5.6, each corresponding to the three “triangles” considered in Figure 5.3. Each “triangle” represents the gain in peak capacity at constant analysis time (horizontal arrow), as well as the gain in analysis time at constant peak capacity (vertical arrow). Each triangle is also representative for a different degree of separation difficulty, with “triangle” 1 being representative for the fast separations requiring only a short analysis time ($t_R < 10$ min), “triangle” 2 representing separations of much more components, and “triangle” 3 representing more complex samples of small molecules, requiring an analysis time of over 1h. Given the different degree of difficulty, the different “triangles” have been illustrated using mixtures with a different complexity as shown in Figures 5.4-5.6. The cited peak capacity values are however always based on the same 6 reference compounds that were present in every mixture and are denoted by the asterisks.

Figure 5.4 shows the separation of the 6-compound mixture under the conditions corresponding to “triangle 1” in Figure 5.3. The reference separation (150 mm column operated at 600 bar) is represented in Figure 5.4A and generates a peak capacity of 155 in 6.5 min. To illustrate the gain in time achievable by increasing the pressure without compromising the performance (vertical arrow), the same 150 mm column as used in Figure 5.4A was operated at 1200 bar. As can be noted from Figure 5.4B, this change still allows to produce a peak capacity of 146 (i.e. only a 6% decrease), while merely 47% of the analysis time (3.5 min) is needed. To illustrate the gain in peak capacity that can be obtained in the same time-frame as that in Figure 5.4A but by increasing the pressure to 1200 bar, Figure 5.4C shows the same separation using a 200 mm coupled column system (150 mm + 50 mm). This approach generates a 17% increased peak capacity ($n_p = 181$) in about the same analysis time (6.9 min).

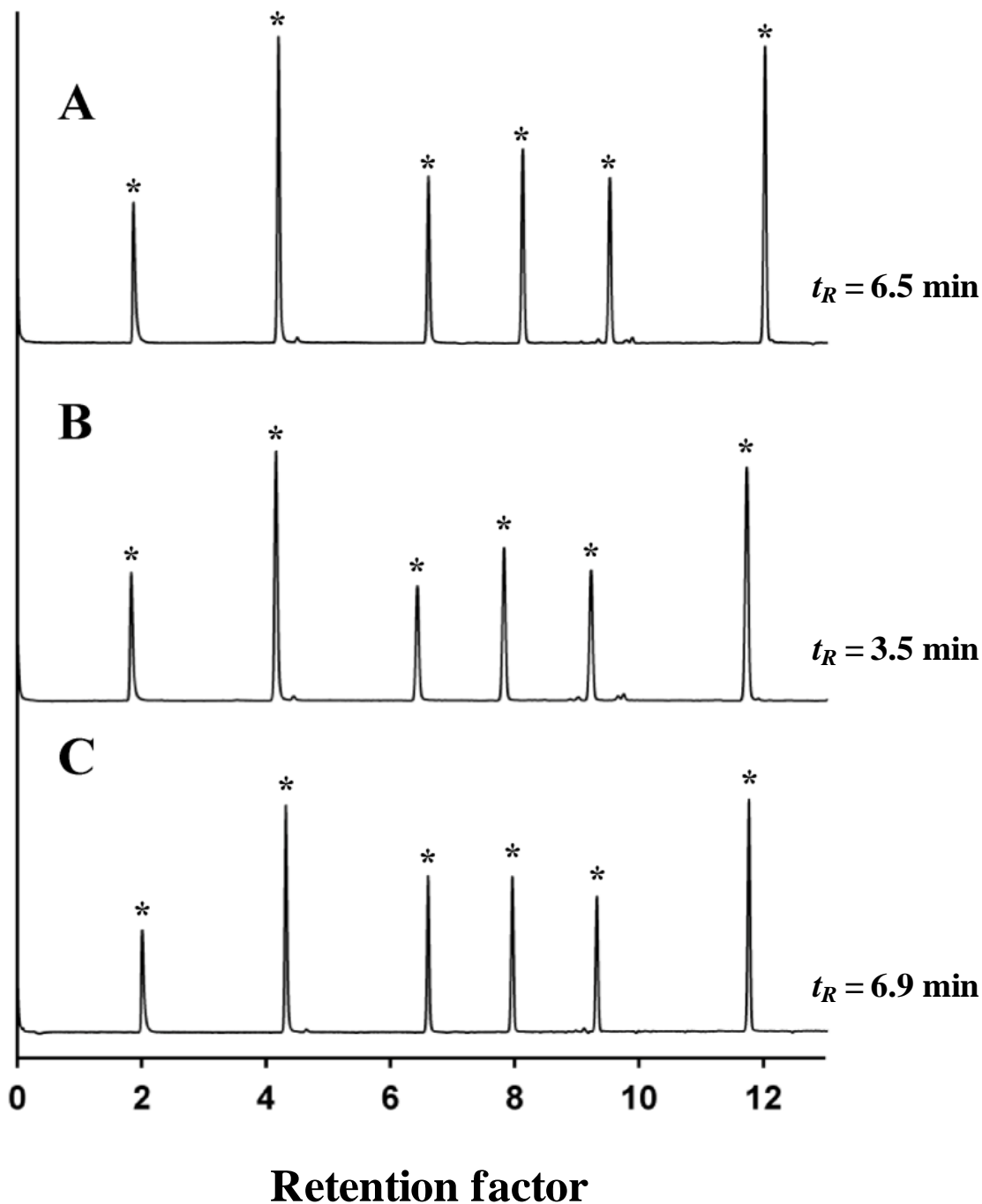


Figure 5.4: Dimensionless chromatograms corresponding to the 3 different cases represented by triangle 1 in Figure 5.3 and illustrated by showing the separation of the simplified 6-compound mixture on (A) a 150 mm column at 600 bar ($n_p = 155$ in 6.5 min), (B) a 150 mm column at 1200 bar ($n_p = 146$ in 3.5 min) and (C) a 200 mm coupled column configuration at 1200 bar ($n_p = 181$ in 6.9 min). All peak capacities were determined based on the peaks denoted with an asterisk (*i.e.* every peak).

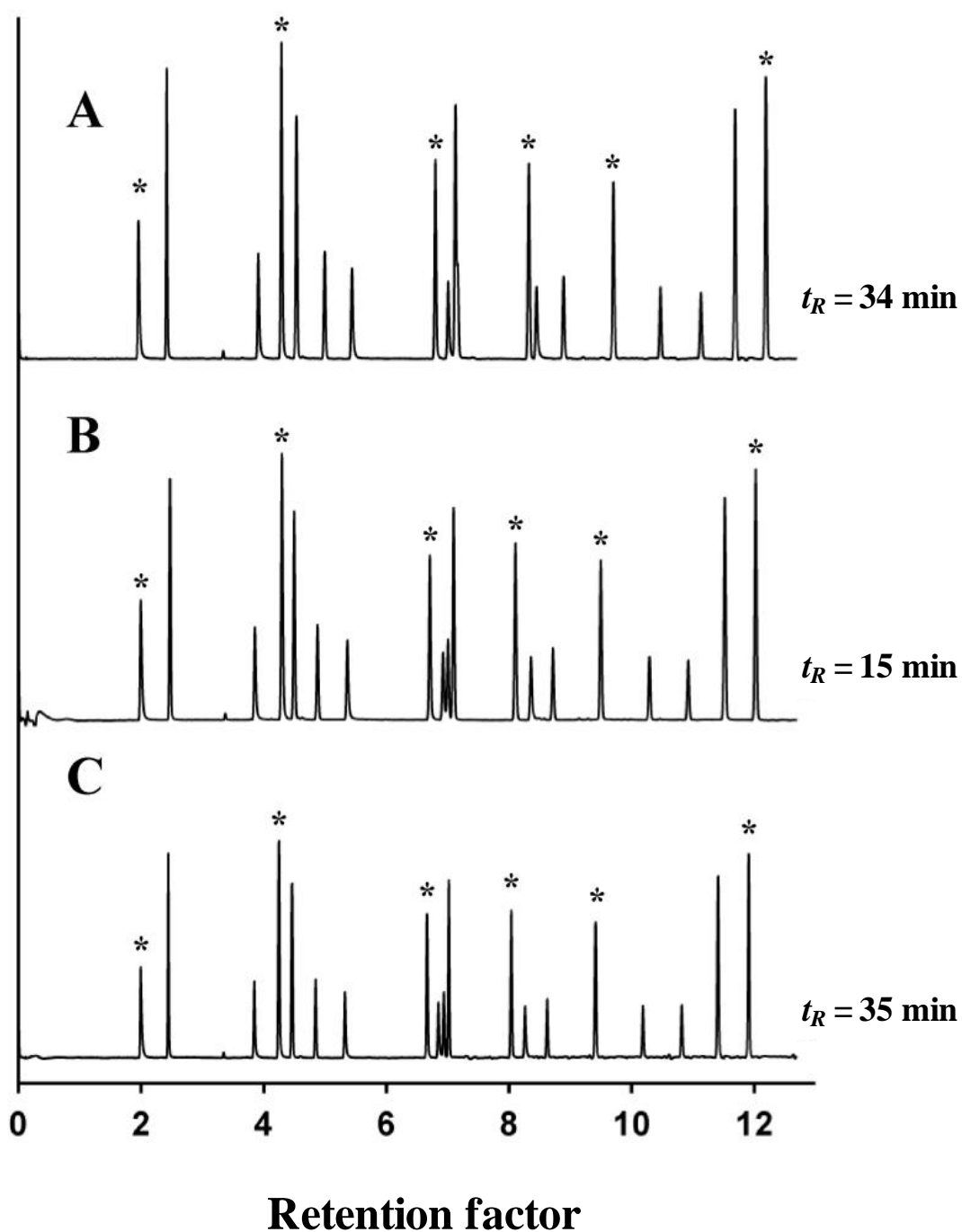


Figure 5.5: Dimensionless chromatograms corresponding to the 3 different cases represented by triangle 2 in Figure 5.3 and illustrated by showing the separation of the complex 19-compound mixture on (A) a 300 mm coupled column configuration at 600 bar ($n_p = 222$ in 34 min), (B) a 300 mm coupled column configuration at 1200 bar ($n_p = 227$ in 15 min) and (C) a 450 mm coupled column configuration at 1200 bar ($n_p = 287$ in 35 min). All peak capacities were determined based on the peaks denoted with an asterisk (*i.e.* 6 compounds from the simplified mixture).

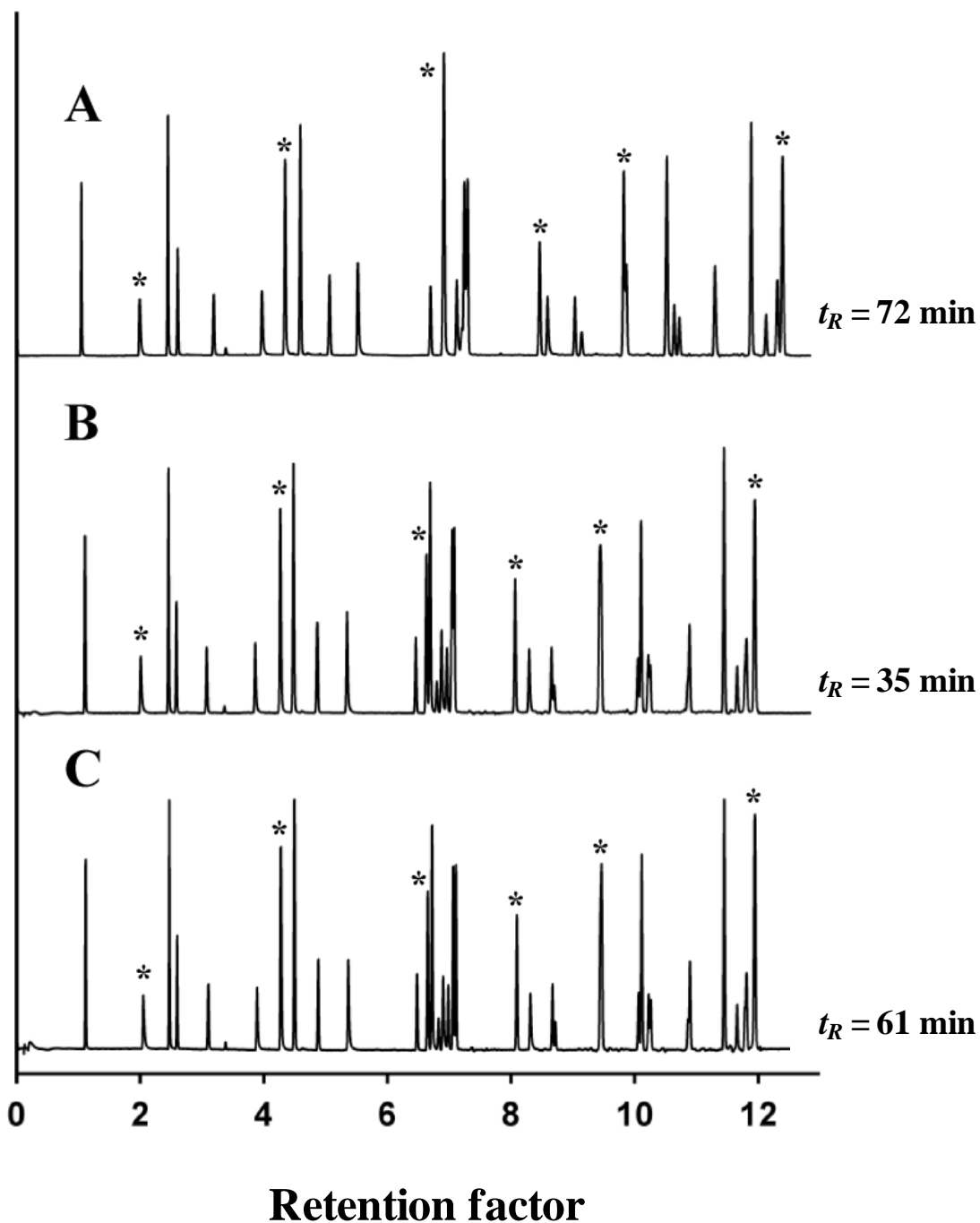


Figure 5.6: Dimensionless chromatograms corresponding to the 3 different cases represented by triangle 3 in Figure 5.3 and illustrated by showing the separation of the more complex 37-compound mixture on (A) a 450 mm coupled column configuration at 600 bar ($n_p = 278$ in 72 min), (B) a 450 mm coupled column configuration at 1200 bar ($n_p = 287$ in 35 min) and (C) a 600 mm coupled column configuration at 1200 bar ($n_p = 325$ in 61 min). All peak capacities were determined based on the peaks denoted with an asterisk (*i.e.* 6 compounds from the simplified mixture).

A separation of intermediate difficulty, using a more complex 19-compound mixture was used to illustrate “triangle 2” of Figure 5.3. The reference separation was in this case performed on a 300 mm coupled column system (2 x 150 mm) operated at 600 bar (Figure 5.5A), generating a peak capacity of 222 in 34 min. Subsequently switching to a 1200 bar operation, keeping the same 300 mm coupled system, allows for a 56% gain in time (15 min) while a similar peak capacity of 227 is achieved (Figure 5.5B). Looking at the performance that can be achieved in the same time-frame as in the reference case shown in Figure 5.5A, Figure 5.5C shows the performance of a 450 mm coupled system (3 x 150 mm) operated at 1200 bar. In this case, a 29 % increase in peak capacity is obtained ($n_p = 287$) in about the same time (35 min) as in the 600 bar reference case.

To illustrate the gain in performance linked to “triangle 3” of Figure 5.3, a highly complex 37-compound mixture was separated on a 450 mm coupled column system (3 x 150 mm) operated at 600 bar (reference case, Figure 5.6A). This case corresponds to a peak capacity of $n_p = 278$ in 72 min. Increasing the operating pressure to 1200 bar while keeping on the same 450 mm coupled column system allows to represent the case wherein the analysis time can be reduced while nearly the same peak capacity is maintained (Fig. 5.6B). This resulted in a 51% reduction of the analysis time (35 min) for a similar peak capacity of 287 (3% n_p -increase). Again, trying to maximize the peak capacity while keeping about the same analysis time as in Figure 5.6A, a 600 mm coupled column system was employed at 1200 bar (Figure 5.6C), yielding a 14% gain in peak capacity ($n_p = 325$) in 61 min (17% decrease in time).

5.2.2 Practical illustration of the advantage of coupled columns at 1200 bar

The chromatogram in Figure 5.7A shows the separation of the complex mixture using a single core-shell column ($L=150$ mm) at its optimum flow rate ($F=0.4$ mL/min). As such, it represents the state-of-the-art peak capacity of the current day practice for the separation of small-molecular-weight compounds, as can be seen in Figure 5.7. Figure 5.7B and Figure 5.7C on the other hand show the peak capacities that can be obtained when operating the particles at their kinetic-performance limit (KPL), respectively using a 300 and 600 mm long column (obtained by respectively coupling two and four 150 mm columns), and corresponding to a 1200 bar separation. The KPL of a given chromatographic support can be defined as the efficiency (N) or peak capacity (n_p) it can generate using a set of columns with widely varying length and each operated at the maximal available or allowable pressure (ΔP_{max}). As shown in [10], the necessary and sufficient condition to operate a column at the KPL simply corresponds to operating it at the maximal available pressure or the maximal pressure one wishes to subject its columns to (note that this not necessarily should be UHPLC pressure).

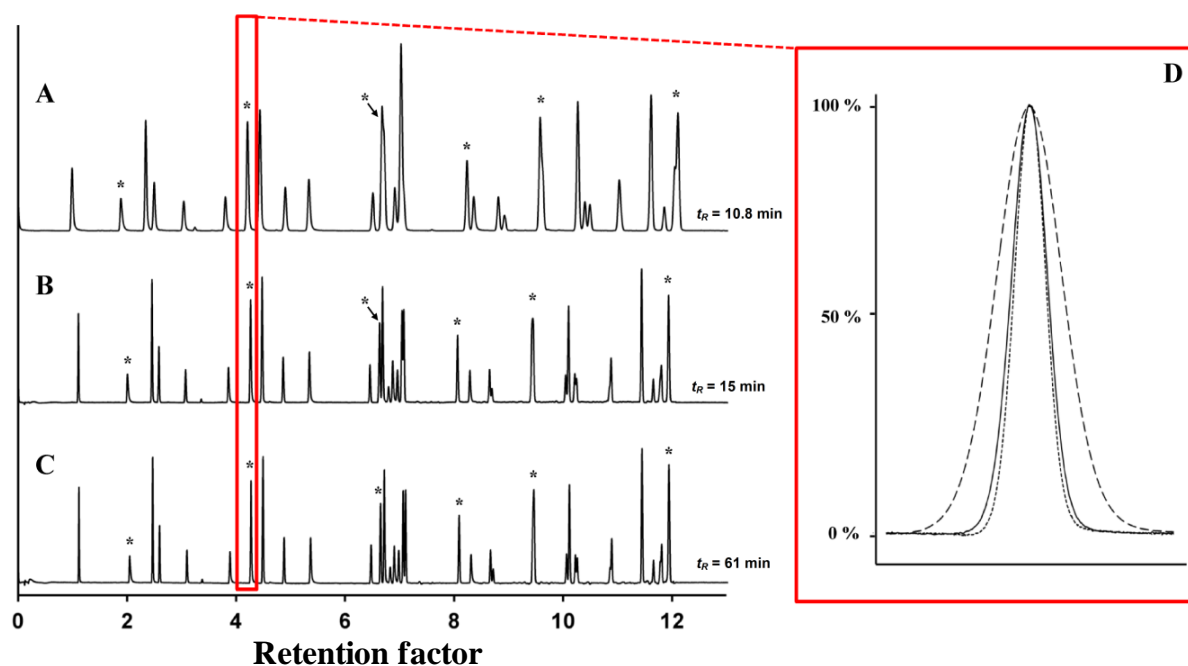


Figure 5.7: Illustration depicting chromatograms of the highly complex mixture on (A) a 150 mm column at F_{opt} operated at 400 bar (dashed line), (B) a 300 mm coupled column system operated at 1200 bar (plain line) and (C) a 600 mm coupled column system also operated at 1200 bar (dotted line). A zoom-in on the quinoline peak eluting at $k=4.2$ obtained by normalizing the peak height is shown in (D). The peaks denoted by asterisks relate to the components of the 6-compound mixture used for peak capacity measurements.

To calculate the peak capacity of the chromatograms in Figure 5.7A-C via Equation (2.37), the peak widths and retention times of the six compounds of the simplified test mixture (denoted by the asterisks) were used. It was found that the single column separation conducted at the optimum flow rate yields a total peak capacity n_p of 162 in 10.8 min (t_R of the last component). The chromatogram in Figure 5.7B on the other hand, produces a peak capacity of 227 in 15 minutes. This corresponds to an increase in peak capacity of 40%, while also the analysis time only increased by 39%. Usually an increase in peak capacity requires a much larger sacrifice in analysis time than the almost linear increase needed here (39% of extra analysis time for a 40% increase in peak capacity). This unusual large gain in peak capacity is due to the fact that the conditions used in Figure 5.7A are, despite their popularity, in fact far away from the KPL, *i.e.*, far away from the kinetic optimum of the particles, so that increasing the column length and pressure not only increases the available number of theoretical plates but also operates the particles closer to their kinetic optimum. The 600 mm long system considered in Figure 5.7C also operates at the KPL of the particles and produces a peak capacity of 325 in 61 min.

Reviewing the literature on the gradient peak capacity performance of fully-porous particles employed under UHPLC conditions, typical peak capacities are of the order of $n_p = 140 - 170$ for a 10 minutes separation, $n_p = 180 - 200$ for a 20 minutes separation and $n_p = 280$ for a 60 minutes separation [36,37]. The much higher peak capacity obtained in the two KPL-cases (Figures 5.7B-C) compared to the “traditional” operating mode represented in Figure 5.7A can also readily be observed from the zoom-in of the peaks shown in Figure 5.7D, showing an overlap of the quinoline peaks (eluting around $k = 4.2$) in the three different cases. In this overlap, the height of the three different peaks was normalized to emphasize the variation in peak width, hence variation in n_p . As the overlap is plotted in relative time coordinates (retention factor coordinates to be more precise), and as the elution window is (nearly) the same in these coordinates (Figure 5.7A-C), the smaller width of the 1200 bar peaks (30 and 600 mm) is a direct measure for the increased peak capacity that can be achieved at this pressure.

The gain in peak capacity can also be clearly noted from the zoom-in on the elution window between $k = 6.2$ and $k = 7.4$ presented in Figure 5.8. It should however be remarked that the improved separation observed in Figure 5.8B and Figure 5.8C is not only due to the increased peak capacity (increasing from 233 to 324 when calculated based on the 6 components denoted by the asterisks in Figure 5.7), but also may be due to temperature and/or pressure-

dependent selectivity effects [30,32] that worked out advantageously in this case. This may explain the observed 1.3% decrease in retention factor when operated at 1200 bar. A similar effect can be noted for the group of peaks eluting just before $k = 12$ (see Figure 5.7), where the second to last peak shifts relatively more to the left than the other peaks when operated at 1200 bar. This indicates that the improved separation observed in Figure 5.7B-C is not only due to an increased N , but also to some synergistic temperature and pressure-dependent selectivity effects. In other areas of the chromatogram, these selectivity effects worked out adversely, as can for example be seen with the doublet eluting around $k = 8.5$.

In general, most compounds appear to be more sensitive to temperature than to pressure, as is reflected by the fact that most compounds display a slight decrease of their retention factor when going from the 400 bar operation in Figure 5.7A to the 1200 bar operation in Figure 5.7B-C (if their pressure-sensitivity would have been dominating, the retention would have increased).

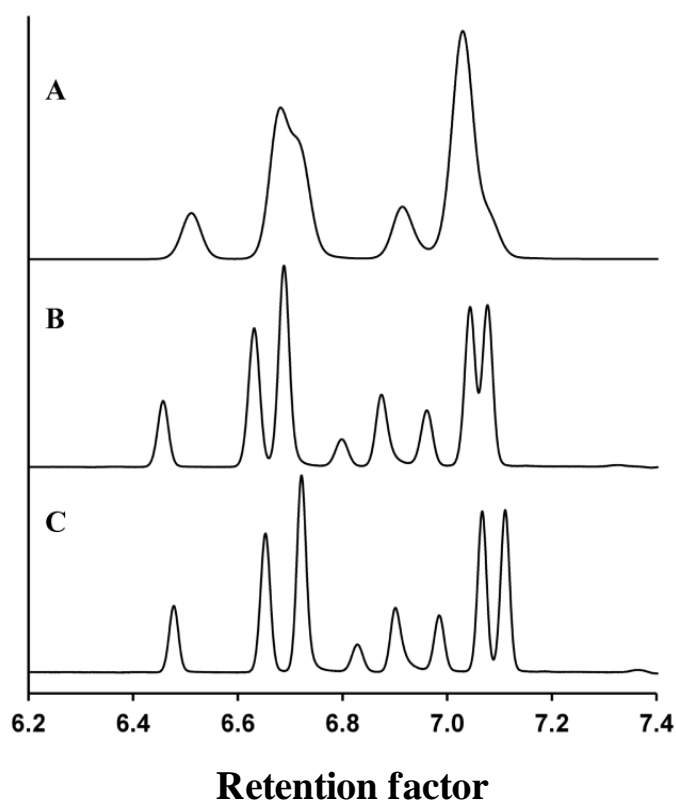


Figure 5.8: Zoom-in on the elution range between $k = 6.2$ and 7.4 of the dimensionless chromatograms shown in Figure 5.7 for (A) a 150 mm column at F_{opt} , (B) a 300 mm coupled columns operated at 1200 bar and (C) a 600 mm coupled column also operated at 1200 bar.

5.3 Kinetic-performance limit for the separation of peptides

The second part of this study comprises of an explorative study to assess the separation performance in gradient mode of peptide separations using long (coupled) columns packed with core-shell particles operated at $\Delta P_{max} = 1200$ bar. In Paragraph 5.1.3 it was demonstrated that the maximum peak capacities were obtained at ΔP_{max} and by using coupled columns. This is now applied to explore the gradient peak capacity limits of core-shell particles for peptide separations. As test samples, a tryptic digest of β -lactoglobulin, a tryptic digest of bovine serum albumin, β -galactosidase, α -lactalbumin, β -lactoglobulin, lysozyme and apotransferrin (6PMD), and a tryptic digest of *E. coli* have been analyzed. As a trade-off between the available efficiency and the analysis time, a 450 mm coupled column system (3 x 150 mm) was selected as the reference system. The performances measured on this system were subsequently compared to the performances obtained on longer column lengths (900 mm).

5.3.1 Peptide separations on a 450 mm core-shell column at 1200 bar

When the column length, particle size, and operating pressure are fixed, the only way to further optimize the separation performance is by increasing the gradient time t_G . This implies that better separations are obtained by varying t_G/t_0 , however at the cost of analysis time.

In Figure 5.9, an increased peak capacity can be observed by increasing t_G/t_0 from 17 to 192. This results in a better separation of peptides and less co-eluting peptide-peaks, which can be visualized by comparing Figure 5.9A with Figure 5.9D. A good argument to validate the decrease in peak overlap is by noticing the lowering of the ‘peak bulge’ with increasing t_G/t_0 . A detailed view from the same relative part of the chromatograms, are displayed in Figure 5.10, where it can be seen that better resolved peaks are obtained when the gradient time is increased. By plotting the true baseline, obtained by subtracting 2 blank signals (given in red on Figure 5.10), together with a part of the 6PMD chromatogram, illustrates the increased performance when using longer gradient times. The valleys between each peak, touch the baseline for $t_G/t_0 = 192$, whereas this is not the case for the shorter gradient times.

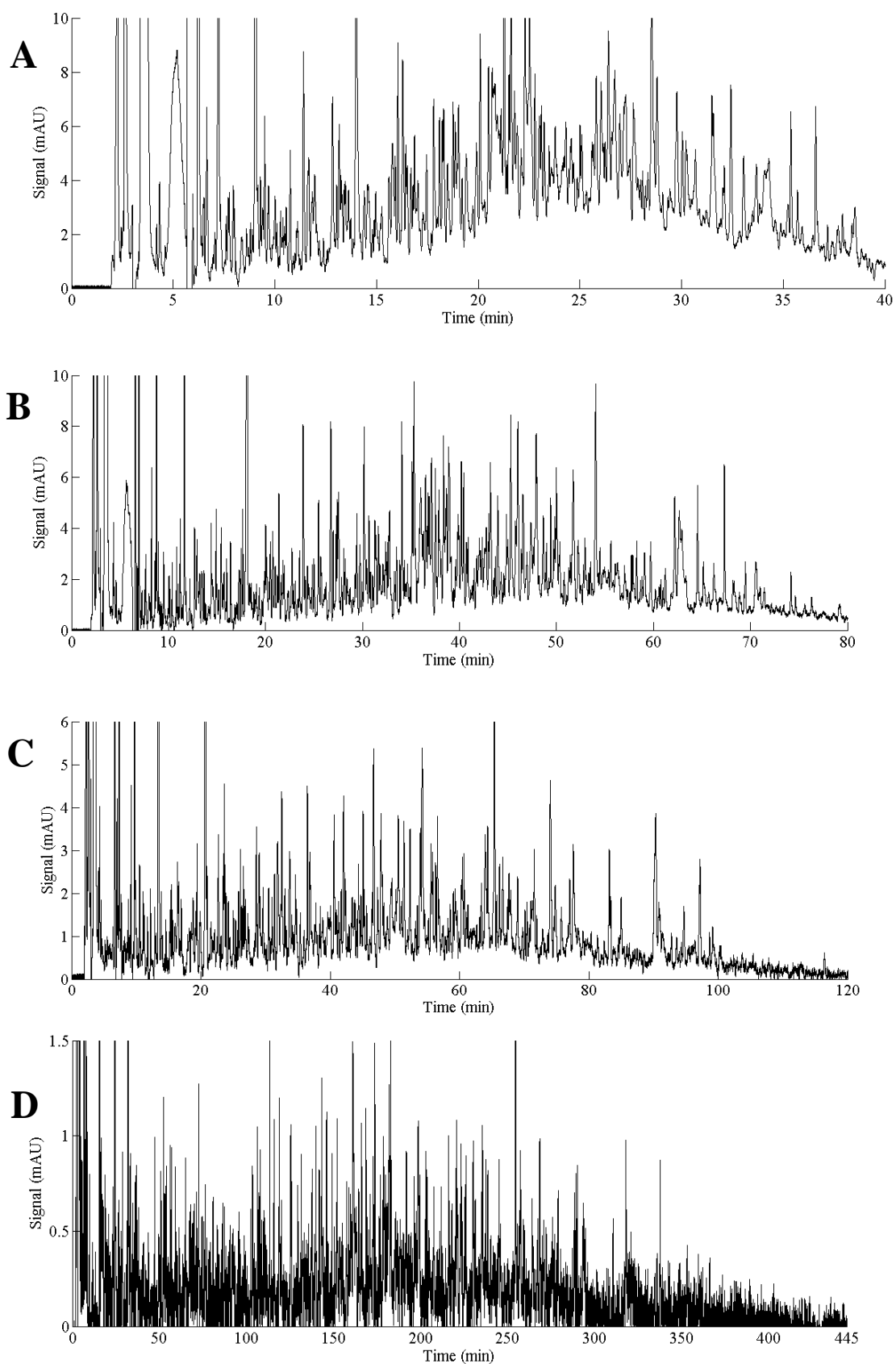


Figure 5.9: Effect of gradient time on the separation performance for the separation of a 6 PMD on a 450 mm Kinetex 2.6 μ m core-shell column (flow rate = 0.35 mL/min) with (A) $t_G/t_0 = 17$, (B) $t_G/t_0 = 35$, (C) $t_G/t_0 = 52$, (D) $t_G/t_0 = 192$. The different gradient times used were respectively 40, 80, 120 and 445 min. With increasing gradient time the peptides are better resolved.

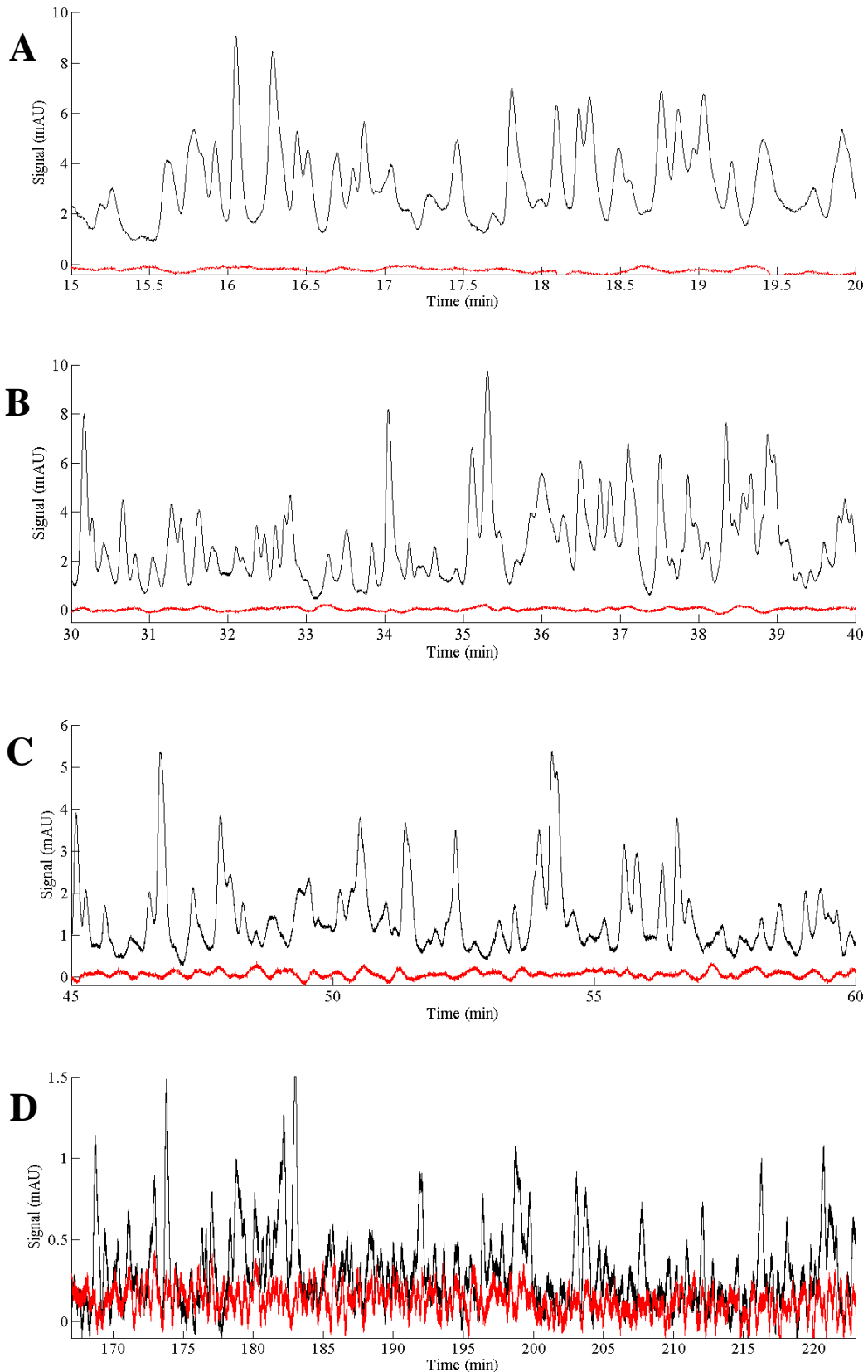


Figure 5.10: A detailed view of the corresponding chromatograms of Figure 5.9, representing the same relative gradient window. The chromatogram for the 6PMD separation was measured at (A) $t_G/t_0 = 17$, (B) $t_G/t_0 = 35$, (C) $t_G/t_0 = 52$, (D) $t_G/t_0 = 192$ or respectively 40, 80, 120 and 445 min gradient time. The true baseline is depicted in red, while the absorbance of the peptides are reported in black. When gradient time is increased, resolution is improved and peaks become better baseline separated.

The need for optimizing gradient time in order to improve separation performance can be illustrated when using a more complex *E. coli* digest sample, see Figure 5.11. According to the UniProt Database the *E. coli* proteome consists of 4595 proteins (www.uniprot.org). Tryptic digestion of this very complex mixture will result in roughly 45.000 peptides. The fact that each peak actually consists of many co-eluting peaks can be better visualized by comparing Figure 5.11A with Figure 5.9C, where the chromatogram of 6PMD for the same gradient time ($t_G = 120$ min) was recorded. Figure 5.11C shows that the peaks are not enough separated from each other to touch the baseline, whereas in the less complex 6PMD chromatogram all peaks are nearly baseline separated over the entire gradient window (Figure 5.10C). When Figure 5.11C is compared with Figure 5.11D, the effect of doubling the gradient time shows that the distance between the observed baseline and the true baseline decreases with a factor of two. This again provides a strong argument for the statement that peak capacity is increased when gradient time increases when column length is fixed and operating pressure is fixed.

5.3.2 Quantitative assessment of peak capacity

Peak capacities were measured for the separation of a tryptic digest of β -lactoglobulin and 6PMD for different gradient times, operated at 1200 bar system pressure. The measured peak capacities n_p , calculated with the 4σ width of a peak $w_{4\sigma}$, are reported as followed [38–40]:

$$n_p = I + \frac{t_G}{\frac{1}{n} \sum_1^n w_{4\sigma}} \quad (5.16)$$

n is the number of peaks selected for the calculation and t_G the gradient run time. The 4σ -width was estimated from the peak width at half height, which was subsequently multiplied by a factor 4/2.35.

Before proceeding to the actual calculation results, it is important to realize that it is difficult to obtain a complete baseline separation of all the components over the entire gradient window when considering complex peptide mixtures. This can be seen from the chromatograms in Figures 5.9-5.11. To report a fair peak capacity, it is important to accurately know the position of the baseline, since an accurate determination of the peak width at half height first requires that the peak height can be determined accurately. In the present study, the exact position of the baseline was determined by subtracting two

subsequent blank runs (red data in Figures 5.10-5.14). The baseline that is obtained in this way agrees well with the position of the signal between the peaks of the β -lactoglobulin digest chromatograms (black data in Figure 5.12), confirming the validity of using this simple digest

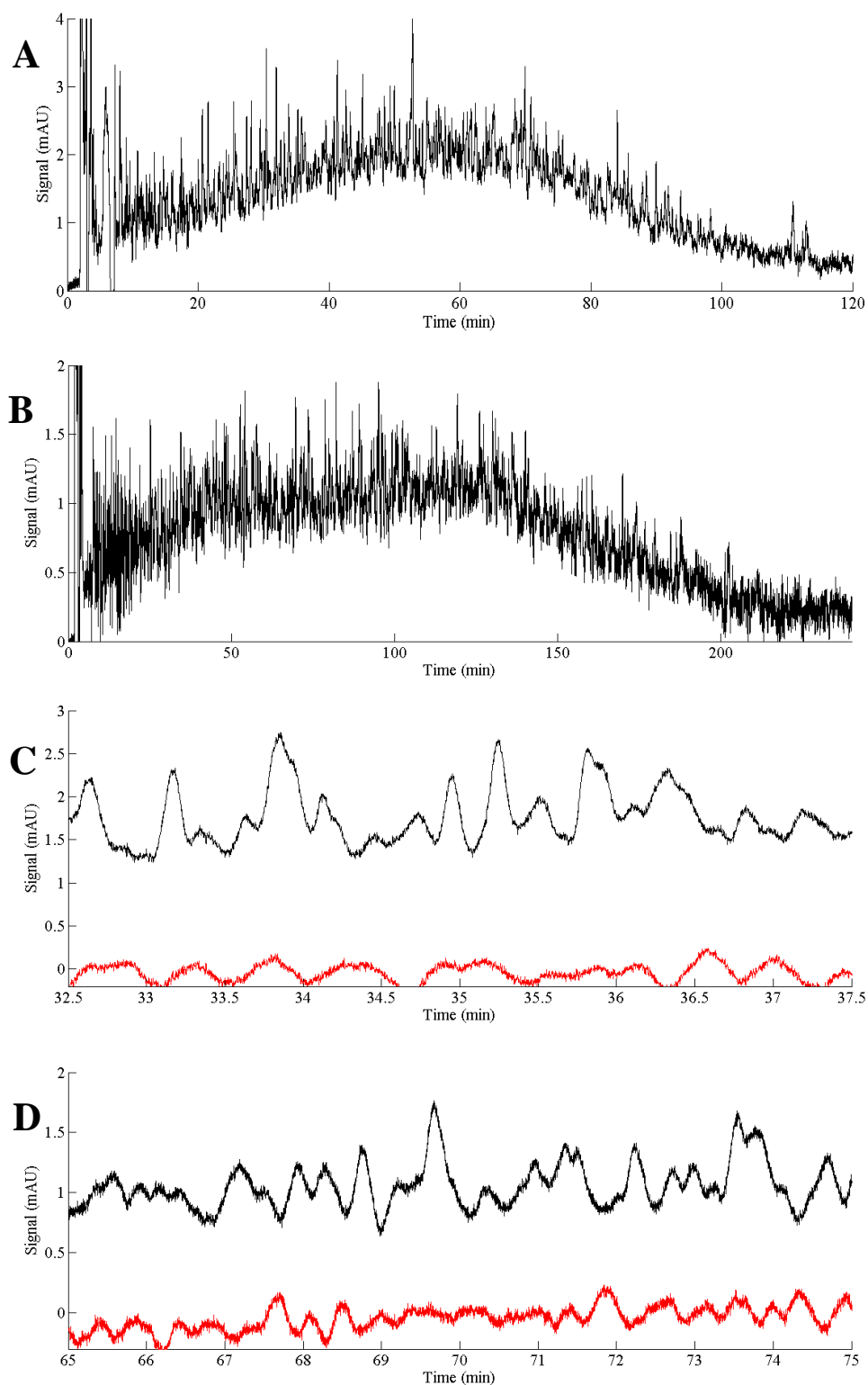


Figure 5.11: Separation of *E. coli* digest (black) on a 450 mm column at 1200 bar with a gradient time of (A) $t_G = 120$ min, (B) $t_G = 240$ min. A detailed view of respectively chromatograms A and B are displayed in (C) and (D) with corresponding t_G/t_0 of 52 and 104. The red line represents the true baseline.

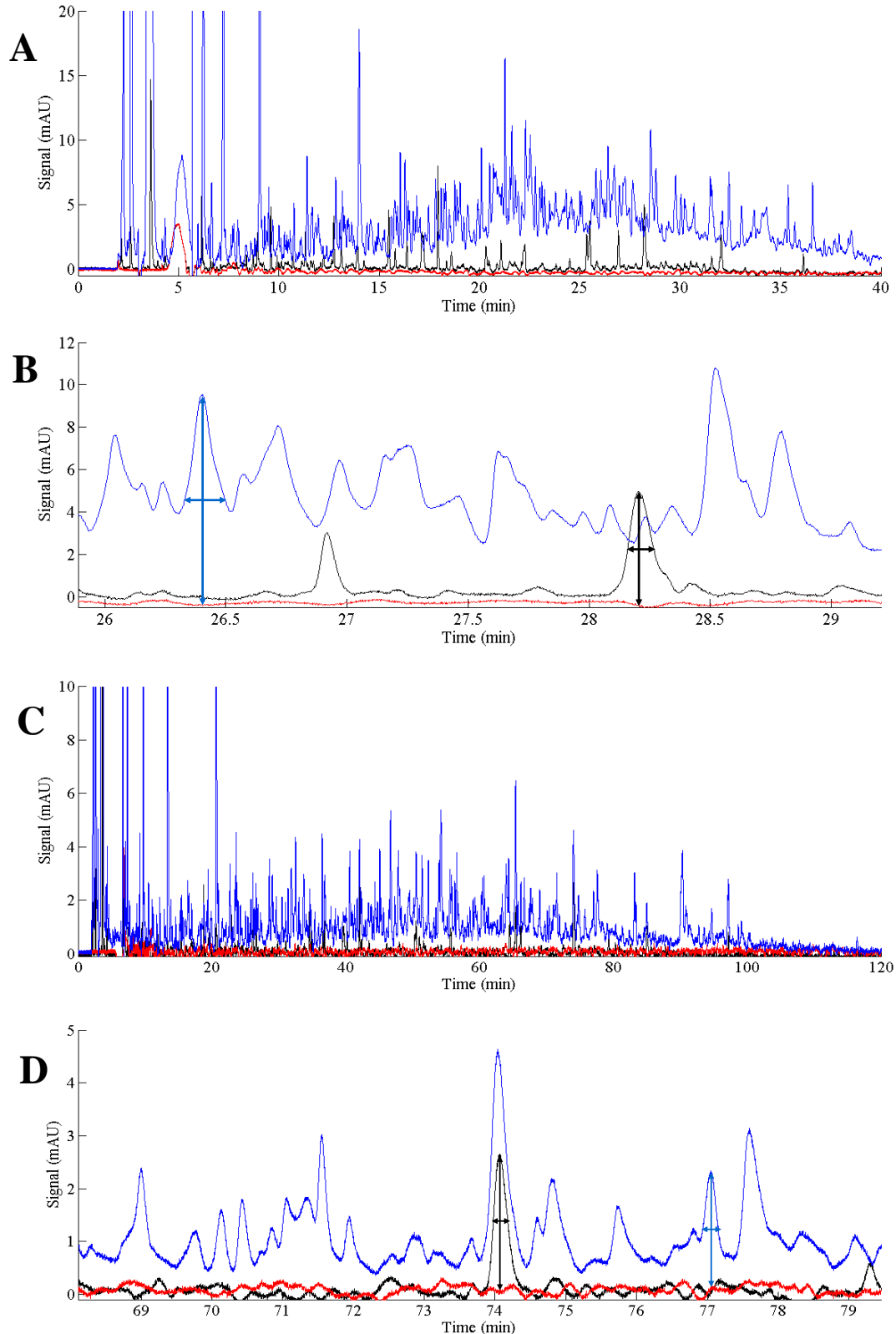


Figure 5.12: (A) Comparison of a complex 6 protein mixture digest (blue), a single protein digest (black) and the true baseline (red) chromatogram on a 450 mm column at 1200 bar using a gradient time of 40 min. During this short gradient run, all peptides of β -lactoglobulin are separated, while the 6PMD mixture remains unresolved. (B) Peak widths at half height (see arrow construction) were calculated based on the true baseline (red). (C) Similar analysis as in A, using a longer gradient time $t_G = 120$ min. (D) Detailed view of the chromatogram given in C, and determination of peak width at half height for assessing peak capacity.

The arrow construction in Figure 5.12 shows how the determination of the peak width at half height has been assessed. It also immediately illustrates that an accurate determination of the peak capacity is only possible for those chromatograms where the peaks return to the baseline instead of co-eluting with others, as is the case for the 6PMD mixture (blue data in Figure 5.12). By performing a theoretic tryptic digest of the proteins of 6PMD using the Peptidemass tool of the ExPASy database (www.expasy.org), it was estimated that the sample contains 500-600 peptides. A rough estimation of the peak capacity obtained for the 6PMD signals can be made by determining the peak width according to the method described above. A peak capacity of 281 was obtained for a 40 min gradient run and 550 for a $t_G = 120$ min. The poor separation performance estimation has everything to do with the fact that it is difficult to select single peaks for assessing the peak capacity. This effect is elaborated in Paragraph 5.1.3. Chromatograms of the separation quality of a more simple peptide mixture, obtained from the tryptic digest of β -lactoglobulin are shown in Figure 5.13. When performing a theoretical tryptic digest, it was found that the digest contains 25 to 43 peptides (with respectively 0 and 1 missed cleavage). This less complex sample was used to accurately determine the peak capacity, because peak overlap is minimized as illustrated in the detailed views of Figure 5.13A and Figure 5.13B. The single peaks that touch the baseline can be used to determine the peak capacity by using Equation (5.16). A peak capacity of 483 was calculated for a gradient time of 40 min, measured on a 450 mm coupled column system. The peak capacity measured on the same system for the same simple peptide mixture increased to 757 by increasing the gradient time to 120 min.

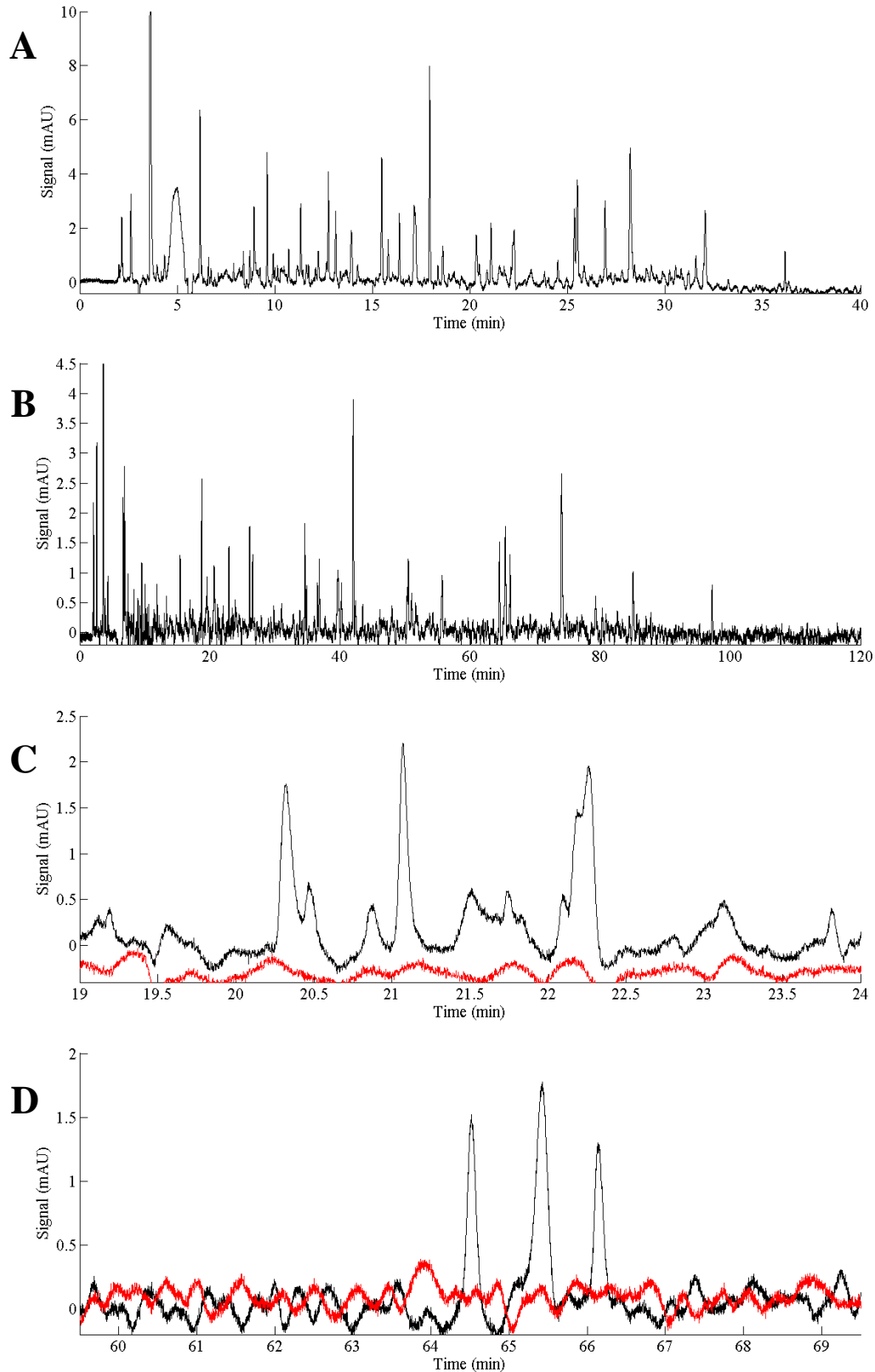


Figure 5.13: Chromatogram of β -lactoglobulin tryptic digest used to accurately assess peak capacity, using a gradient time of (A) $t_G = 40$ min, (B) $t_G = 120$ min on a 450 mm coupled column system operated at 1200 bar. (C) Detailed view of a small part of chromatogram A. (D) Detailed view of a part of chromatogram B, which is scaled relative in timeframe so the same area of the chromatogram as in Figure C is observed. The longer gradient time results in nice baseline resolved peaks, allowing accurate peak capacity determination.

5.3.3 Peptide separations on a 900 mm long column at 1200 bar

The flow rate in the 450 mm column reference case is kept at 0.35 mL/min, which is estimated to be about a factor of two or three larger than the optimal flow rate. By using the Wilke-Chang equation it can be estimated that peptides have a diffusion coefficient that is about two to three times smaller than that of the small-molecular-weight compounds. Since the optimal flow rate is related to the molecular diffusion coefficient and the particle diameter (which is fixed), there was still a progress margin to further increase the peak capacity by decreasing the flow rate with a factor of two or three. This was achieved by coupling three more columns, so that the system consisted of six coupled columns with a total column length $L = 900$ mm. This not only doubles the available stationary phase, but separations are also performed closer to the optimal flow rate.

Before proceeding to these experiments, first the amount of sample volume that could be injected without causing a mass overload was tested. Figure 5.14 shows the effect of injecting a higher amount of a tryptic digest of β -lactoglobulin on the 6 x 150 mm core-shell column system for a gradient time of 480 min. The repeatable overlap of a 5 μ L (red) and 10 μ L (black) injection in Figure 5.14B shows that peak shape remains unaffected (there is no evidence for extra broadening of the peak due to mass overload). Chromatograms obtained for higher injected masses of the sample allow a good read-out of well defined peak widths and related peak capacity.

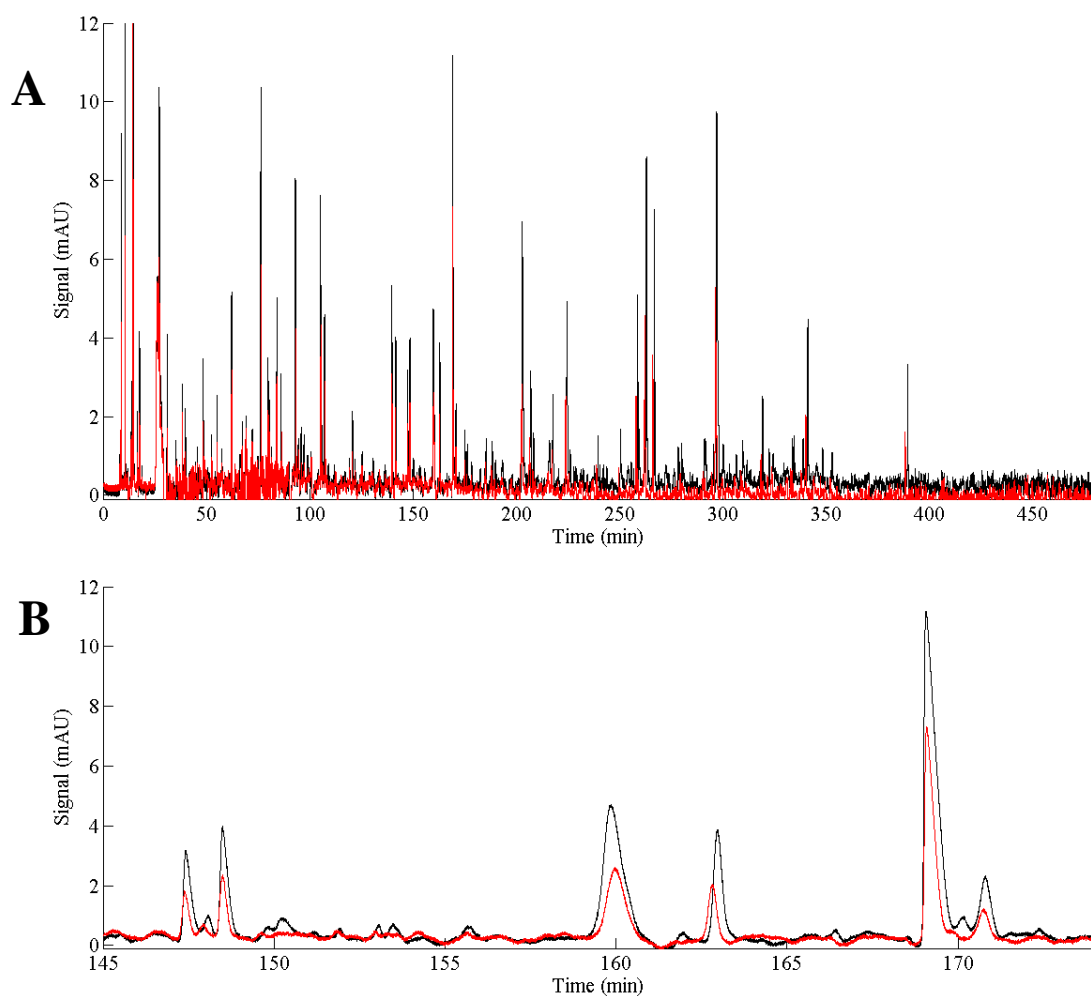


Figure 5.14: Effect of higher injection volume for the separation of β -lactoglobulin: (A) 5 μL injection volume of sample (red) and 10 μL injection volume of sample (black) (B) Detailed view of a part of the chromatogram.

Figure 5.15 shows chromatograms for the separation of respectively a tryptic digest of β -lactoglobulin (Figure 5.15A) and 6PMD (Figure 5.15C) for a 480 min gradient run. The realized peak capacities (respectively $n_p=1363$ and 1360) are in good agreement with each other, most certainly because the 6 PMD-sample is nearly perfectly baseline separated. The realized peak capacity (1360 in 480 minutes) compares very favorably with some of the “record” studies published in the past, see Table 5.1

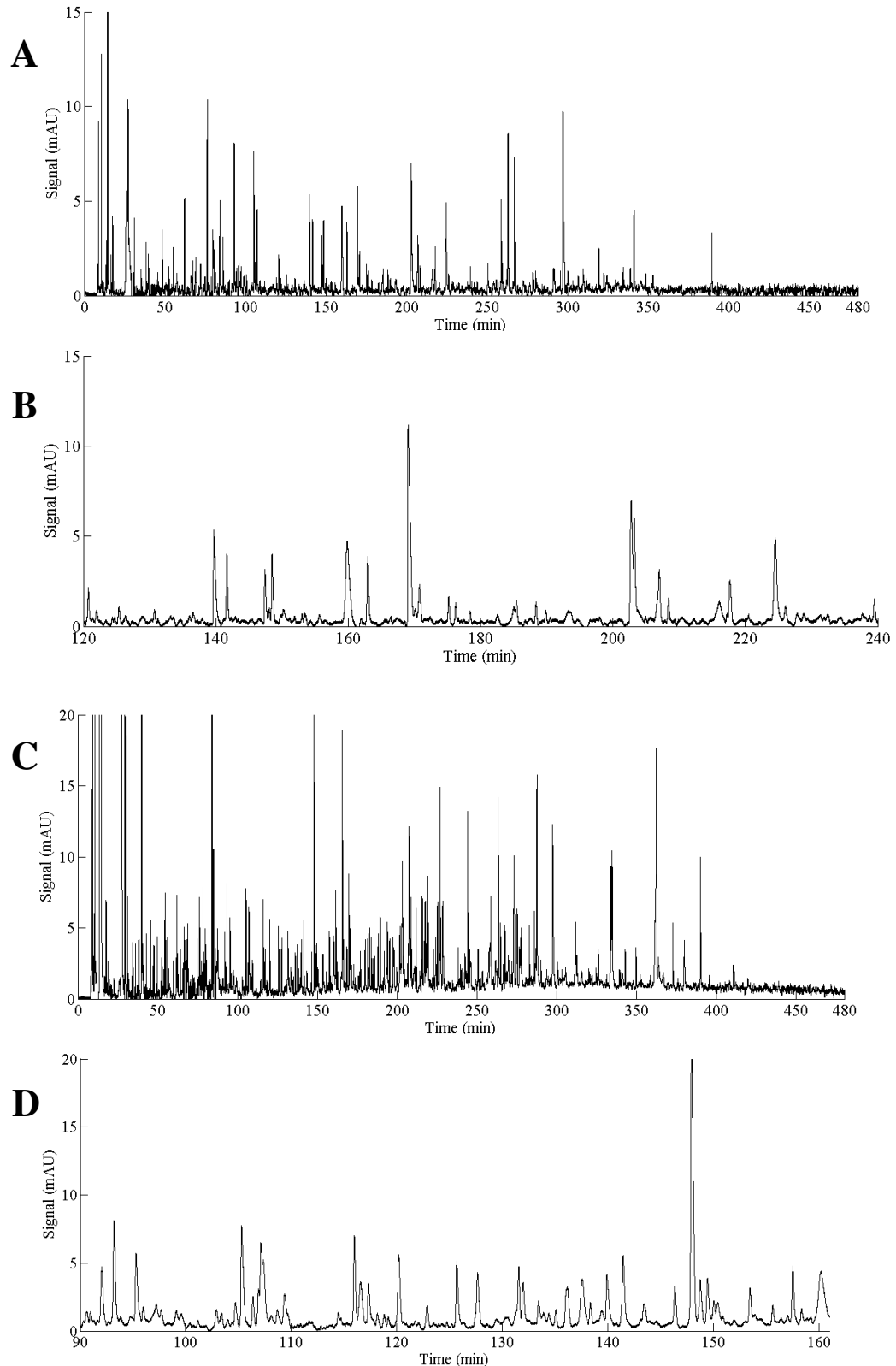


Figure 5.15: Separation on a 900 mm Kinetex 2.6 μm core-shell column (flow rate = 0.175 mL/min) of with 480 min gradient time of (A) a tryptic digest of β -lactoglobulin with $t_G/t_0 = 52$ and (C) a tryptic digest of 6PMD with $t_G/t_0 = 52$. A detailed view of respectively chromatograms A and C are displayed in (B) and (D). Good baseline separation occurs in the chromatogram which allows the selection of single peaks, and this results in a nearly equal peak capacity of 1363 and 1360 for respectively chromatograms A and C.

Table 5.2 reviews the peak capacities realized on the most important column lengths and chromatographic conditions studied. The observed deviation between the peak capacities for the β -lactoglobulin and 6PMD chromatograms illustrates the underestimation of the separation performance, when co-eluting peaks are used to assess peak capacity. In order to achieve an accurate determination of peak capacity, it is necessary to have a good baseline-separated chromatogram (as visualized in Figure 5.15) with an optimized gradient time frame. Therefore, the β -lactoglobulin digest sample is best suited for assessing peak capacity when the performance of different LC setups (with optimized column length to work at the KPL of the chromatographic support and/or optimized gradient time) need to be compared. To conclude, Table 5.2 and evaluation of Figures 5.9, 5.13 and 5.15 also shows the advantages of using coupled columns operated at 1200 combined with optimizing the gradient time according to sample complexity.

TABLE 5.1: Peak capacities reported in literature for one-dimensional LC separations of peptides.

Stationary phase	Column dimensions	Gradient time (min)	Peak capacity	Reference
silica monolith	3 m x 100 μ m	2400 min	1600	[41]
1.4 μ m particles (120Å)	400 mm x 50 μ m	400 min	1000	[42]
3 μ m particles(300Å)	870 mm x 20 μ m	150 min	1088	[43]
3 μ m particles(300Å)	1.5 m x 50 μ m	200 min	1500	[44]

TABLE 5.2: Overview of the peak capacities obtained for a tryptic digest of β -lactoglobulin and 6PMD for the assessed column lengths and separation conditions.

Column length (mm)	Flow rate (mL/min)	Gradient time (min)	Peak capacity (β -lactoglobulin digest)	Peak capacity (6PMD)	Deviation (%)
450	0.35	40	483	281	-42%
450	0.35	120	757	550	-27%
900	0.175	480	1363	1360	0%

6 Conclusion

Despite the fact that the presently considered core-shell particles are relatively large (2.6 μm) and are reputed for their low pressure drop, a significant gain in kinetic performance can be achieved by doubling the applicable instrument pressure from 600 to 1200 bar, provided the total column length is optimized for a given target analysis time or a given target peak capacity. The kinetic-performance limit curve of the chromatographic support, which visualizes this trade-off between speed and efficiency, can be used by chromatographic practitioners to select the best conditions to analyze a sample.

A large gain in both analysis time and peak capacity can be achieved when operating the columns at their kinetic optimum, which has been demonstrated for the separation of small molecules (waste water pollutants, parabenes, alkyl phenones). By comparing systems operated at their respective kinetic-performance limit at 600 and 1200 bar, it can be concluded that doubling the pressure allows to halve the analysis time without any significant sacrifice in peak capacity. This effect is somewhat less (46% time-saving) for separations of mixtures containing only a few components, but is more pronounced (56%) for separations of more complex mixtures, as demonstrated using a sample mixture containing 37 small molecules. Similarly, comparing the kinetic-performance limit operation at both pressures for the case of equal analysis time, the gain in peak capacity that was observed by going from 600 to 1200 bar ranged from 17% to 29% (again ranked from separations of easy mixtures to more elaborate separations). A maximum peak capacity of $n_p = 325$ could be achieved for small molecules in one hour (61 min) of analysis time when a train of 4 columns (4 x 150 mm) was operated at 1200 bar.

When a trade-off has been made between efficiency and the analysis time needed to separate a complex mixture of peptides, the column length and particle size has been optimized in such a way that the system works at the kinetic optimum. To further improve the separation performance the gradient time needs to be increased, which comes with the cost of increased analysis time. For a reference system of 3 coupled columns (3 x 150 mm), the peak capacity increased with 57% from 483 (for a short gradient run of 40 min) to 757 ($t_G = 120\text{min}$) for the separation of a tryptic digest of β -lactoglobulin. A record peak capacity for this study of 1363 has been recorded for the separation of the same tryptic digest in 8 hours when 6 columns packed with core-shell particles was operated at 1200 bar.

This research demonstrates the advantages offered by the combination of UHPLC and coupling of core-shell particle columns, followed by optimization of the separation conditions according to sample complexity.

References

- [1] Martin, A.J.P., Synge, R.L.M., A new form of chromatogram employing two liquid phases. *Biochemical Journal* 1941, 35, 1358-1368.
- [2] van Deemter, J., Zuiderweg, F., Klinkenberg, A., Longitudinal diffusion and resistance to mass transfer as causes of nonideality in chromatography. *Chemical Engineering Science* 1956, 5, 271-289.
- [3] MacNair, J.E., Patel, K.D., Jorgenson, J.W., Ultrahigh-pressure reversed-phase capillary liquid chromatography: isocratic and gradient elution using columns packed with 1.0-micron particles. *Analytical chemistry* 1999, 71, 700-708.
- [4] Giddings, J.C., *Unified Separation Science*, Wiley-Interscience, New York 1991.
- [5] Snyder, L.R. and K., *Introduction to modern liquid chromatography second edition*, n.d.
- [6] Cabooter, D., Fanigliulo, a, Bellazzi, G., Allieri, B., et al., Relationship between the particle size distribution of commercial fully porous and superficially porous high-performance liquid chromatography column packings and their chromatographic performance. *Journal of chromatography. A* 2010, 1217, 7074-81.
- [7] Bristow, P., Standardization of test conditions for high performance liquid chromatography columns. *Chromatographia* 1977, 10, 279-289.
- [8] Desmet, G., Clicq, D., Gzil, P., Geometry-independent plate height representation methods for the direct comparison of the kinetic performance of LC supports with a different size or morphology. *Analytical chemistry* 2005, 77, 4058-70.
- [9] Neue, U.D., Peak capacity in unidimensional chromatography. *Journal of chromatography. A* 2008, 1184, 107-30.
- [10] Broeckhoven, K., Cabooter, D., Lynen, F., Sandra, P., Desmet, G., The kinetic plot method applied to gradient chromatography: theoretical framework and experimental validation. *Journal of chromatography. A* 2010, 1217, 2787-95.
- [11] Novotny, M., in: *Journal of Chromatography Library*, 1984, pp. 194-259.
- [12] Patel, K.D., Jerkovich, A.D., Link, J.C., Jorgenson, J.W., In-depth characterization of slurry packed capillary columns with 1.0-microm nonporous particles using reversed-phase isocratic ultrahigh-pressure liquid chromatography. *Analytical chemistry* 2004, 76, 5777-86.
- [13] MacNair, J.E., Lewis, K.C., Jorgenson, J.W., Ultrahigh-pressure reversed-phase liquid chromatography in packed capillary columns. *Analytical chemistry* 1997, 69, 983-9.
- [14] Jerkovich, A.D., Mellors, J.S., Jorgenson, J.W., Majors, R.E., in *Ultrahigh Pressure. America* 2003, 21.

- [15] Desmet, G., Cabooter, D., Gzil, P., Verelst, H., et al., Future of high pressure liquid chromatography: do we need porosity or do we need pressure? *Journal of chromatography. A* 2006, 1130, 158-66.
- [16] Horvath, C.G., Preiss, B.A., Lipsky, S.R., Fast liquid chromatography. Investigation of operating parameters and the separation of nucleotides on pellicular ion exchangers. *Analytical Chemistry* 1967, 39, 1422-1428.
- [17] Kirkland, J.J., Techniques for High-Performance Liquid-Liquid and Ion Exchange Chromatography with Controlled Surface Porosity Column Packings . *Journal of Chromatographic Science* 1969, 7 , 361-365.
- [18] Fekete, S., Fekete, J., Fast gradient screening of pharmaceuticals with 5 cm long, narrow bore reversed-phase columns packed with sub-3 μm core-shell and sub-2 μm totally porous particles. *Talanta* 2011, 84, 416-423.
- [19] Fanigliulo, A., Cabooter, D., Bellazzi, G., Comparison of performance of high performance liquid chromatography columns packed with superficially and fully porous 2.5 μm particles using kinetic plots. *Journal of* 2010, 33, 3655-3665.
- [20] Cabooter, D., Billen, J., Terryn, H., Lynen, F., et al., Detailed characterisation of the flow resistance of commercial sub-2 micrometer reversed-phase columns. *Journal of chromatography. A* 2008, 1178, 108-17.
- [21] Fekete, S., Oláh, E., Fekete, J., Fast liquid chromatography: The domination of core-shell and very fine particles. *Journal of chromatography. A* 2011.
- [22] Guillarme, D., Grata, E., Glauser, G., Wolfender, J.-L., et al., Some solutions to obtain very efficient separations in isocratic and gradient modes using small particles size and ultra-high pressure. *Journal of chromatography. A* 2009, 1216, 3232-43.
- [23] Guillarme, D., Ruta, J., Rudaz, S., Veuthey, J.-L., New trends in fast and high-resolution liquid chromatography: a critical comparison of existing approaches. *Analytical and bioanalytical chemistry* 2010, 397, 1069-82.
- [24] Fekete, S., Ganzler, K., Fekete, J., Efficiency of the new sub-2 μm core-shell (KinetexTM) column in practice, applied for small and large molecule separation. *Journal of pharmaceutical and biomedical analysis* 2011, 54, 482-90.
- [25] Cabooter, D., Billen, J., Terryn, H., Lynen, F., et al., Kinetic plot and particle size distribution analysis to discuss the performance limits of sub-2 microm and supra-2 microm particle columns. *Journal of chromatography. A* 2008, 1204, 1-10.
- [26] Guiochon, G., Gritti, F., Shell particles, trials, tribulations and triumphs. *Journal of chromatography. A* 2011, 1218, 1915-38.
- [27] Liekens, A., Denayer, J., Experimental investigation of the difference in B-term dominated band broadening between fully porous and porous-shell particles for liquid chromatography using the. *Journal of Chromatography A* 2011, 1218, 4406-4416.

- [28] Dolan, J.W., Snyder, L.R., Maintaining fixed band spacing when changing column dimensions in gradient elution. *Journal of chromatography. A* 1998, 799, 21-34.
- [29] Vaast, A., Broeckhoven, K., Dolman, S., Comparison of the gradient kinetic performance of silica monolithic capillary columns with columns packed with 3 μm porous and 2.7 μm fused-core silica particles. *Journal of Chromatography A* 2012, 1228, 270-5.
- [30] Neue, U.D., Kele, M., Performance of idealized column structures under high pressure. *Journal of chromatography. A* 2007, 1149, 236-44.
- [31] Fallas, M.M., Neue, U.D., Hadley, M.R., McCalley, D.V., Investigation of the effect of pressure on retention of small molecules using reversed-phase ultra-high-pressure liquid chromatography. *Journal of chromatography. A* 2008, 1209, 195-205.
- [32] Verstraeten, M., Broeckhoven, K., Lynen, F., Choikhet, K., et al., Comparison of the quantitative performance of constant pressure versus constant flow rate gradient elution separations using concentration-sensitive detectors. *Journal of chromatography. A* 2011, 1232, 65-76.
- [33] Neue, U.D., Marchand, D.H., Snyder, L.R., Peak compression in reversed-phase gradient elution. *Journal of chromatography. A* 2006, 1111, 32-9.
- [34] Carr, P.W., Stoll, D.R., Wang, X., Perspectives on Recent Advances in the Speed of High-Performance Liquid Chromatography. *Analytical Chemistry* 2011, 83, 1890-1900.
- [35] Eeltink, S., Decrop, W.M.C., Steiner, F., Ursem, M., et al., Use of kinetic plots for the optimization of the separation time in ultra-high-pressure LC. *Journal of separation science* 2010, 33, 2629-35.
- [36] Broeckhoven, K., Cabooter, D., Desmet, G., Maximizing Throughput with Optimized Column Lengths and Particle Diameters. *LC-GC Europe* 2011, 396.
- [37] Zhang, Y., Wang, X., Mukherjee, P., Petersson, P., Critical comparison of performances of superficially porous particles and sub-2 microm particles under optimized ultra-high pressure conditions. *Journal of chromatography. A* 2009, 1216, 4597-605.
- [38] Neue, U., Theory of peak capacity in gradient elution. *Journal of Chromatography A* 2005, 1079, 153-161.
- [39] Wang, X., Stoll, D.R., Schellinger, A.P., Carr, P.W., Peak capacity optimization of peptide separations in reversed-phase gradient elution chromatography: fixed column format. *Analytical chemistry* 2006, 78, 3406-16.
- [40] Petersson, P., Frank, A., Heaton, J., Euerby, M.R., Maximizing peak capacity and separation speed in liquid chromatography. *Journal of separation science* 2008, 31, 2346-57.

- [41] Horie, K., Sato, Y., Kimura, T., Nakamura, T., et al., Estimation and optimization of the peak capacity of one-dimensional gradient high performance liquid chromatography using a long monolithic silica capillary column. *Journal of chromatography. A* 2012, 1228, 283-91.
- [42] Shen, Y., Zhang, R., Moore, R.J., Kim, J., et al., Automated 20 kpsi RPLC-MS and MS/MS with chromatographic peak capacities of 1000-1500 and capabilities in proteomics and metabolomics. *Analytical chemistry* 2005, 77, 3090-100.
- [43] Shen, Y., Zhao, R., Berger, S.J., Anderson, G. a, et al., High-efficiency nanoscale liquid chromatography coupled on-line with mass spectrometry using nanoelectrospray ionization for proteomics. *Analytical chemistry* 2002, 74, 4235-49.
- [44] Kim, M.-sik, Choie, W.-suk, Shin, Y.S., Yu, M.-hee, Lee, S.-won, Development of Ultra-High Pressure Capillary Reverse-Phase Liquid Chromatography / Tandem Mass Spectrometry for High-Sensitive and High-Throughput Proteomics 2004, 25, 1833-1839.

Appendix I: Nederlandstalige samenvatting

Optimalisatie Van Piekcapaciteit Door Gebruik Van Gekoppelde Core-Shell Kolommen Bij 1200 Bar

J. De Vos^a, A. Vaast^b, K. Broeckhoven^b, G. Desmet^b and S. Eeltink^{*b}

^a Faculteit Wetenschappen, Universiteit Gent, Krijgslaan 281, 9000 Gent, België

^b Departement Chemische Ingenieurswetenschappen, Vrije Universiteit Brussel, Pleinlaan 2, 1050 Brussel, België

(*)Corresponderende auteur
E-mail : jedvos.devos@ugent.be

In dit onderzoek wordt piekcapaciteit gerapporteerd voor scheidingen op kolommen, gevuld met state-of-the-art core-shell deeltjes ($d_p = 2,6 \mu\text{m}$), rond hun kinetisch optimum bij een ultra-hoge druk van 600 en 1200 bar. Het koppelen van kolommen was nodig om het kinetisch optimum te realiseren. Terwijl met behulp van één enkele 150 mm kolom (werkend bij de optimale stroomsnelheid van 0,4 mL/min) een piekcapaciteit van 162 in 10,8 minuten werd bekomen voor kleine moleculen, bood het koppelen van vier kolommen van 150 mm tot een totale geoptimaliseerde kolom van 600 mm een piekcapaciteit van 325 in 61 min bij 1200 bar voor deze type testmengsels. Voor het scheiden van peptiden op een geoptimaliseerde 900 mm-kolom werd een maximale piekcapaciteit van 1363 in een 480 minuten gradiënt meting opgemeten. De toename in performantie, die kan worden gegenereerd bij het overschakelen van een volledig geoptimaliseerde werkingsmodus van 600 bar tot een volledig geoptimaliseerde 1200 bar modus is aanzienlijk. De analysetijd voor kleine moleculen kon gehalveerd worden met behoud van piekcapaciteit. Wanneer de analysetijd constant werd gehouden, leed dit tot een toename van 20% in piekcapaciteit. Dit biedt voordelen voor industriële toepassingen waar in korte tijd veel testmengsels moeten worden geanalyseerd.

Trefwoorden: Core-shell deeltjes; Ultra-hoge-druk; Kinetische performantie; Gradiënt piekcapaciteit; Kinetische plot; Gekoppelde kolommen

1 Inleiding

De nieuwe generatie van de core-shell deeltjes biedt een grote sprong voorwaarts in chromatografische performantie in vergelijking met hun volledig-poreuze tegenhangers (1-5). Hoewel sommige redenen voor deze verbetering nog niet volledig begrepen zijn, bieden core-shell-deeltjes ontegensprekelijk een verminderde stromingsweerstand (ϕ_0) en een verhoogde efficiëntie (2). De stromingsweerstand van een kolom gevuld met volledig poreuze deeltjes ligt gewoonlijk in het bereik van $\phi_0 = 700-800$, terwijl stromingsweerstand van $\phi_0 = 500$ gemeten zijn voor kolommen gevuld met core-shell-deeltjes (6,7). De best mogelijke kolommen gevuld met core-shell-deeltjes zijn de tegenwoordig de meest performante

kolommen, omdat ze een minimale gereduceerde plaathoogte-waarde kunnen opleveren van $h_{min} = 1.5$ tot 1.8, terwijl het nog steeds zeer moeilijk is kolommen gevuld met volledig-poreuze-deeltjes te vinden die h_{min} van ongeveer 2 produceren. Door het combineren van deze waarden uit de literatuur kan de berekening van de minimale scheidings-impedantie E_{min} gedefinieerd door Golay en Knox worden berekend (8):

$$E_{min} = h_{min}^2 \Phi_0 \quad [1]$$

volgt dat de overschakeling van volledig-poreuze naar core-shell-deeltjes leidt tot een afname van de scheidings-impedantie van $E_{min} = 2800$ en hoger tot $E_{min} = 1600$ en minder. De E_{min} -waarde bepaalt direct de maximale snelheid waarmee een bepaald type deeltje een gegeven scheidingsefficiëntie N of piekcapaciteit n_p kan behalen. De core-shell-deeltjes verwezenlijken dus bijna een verdubbeling van de scheidingssnelheid ten opzichte van de volledig-poreuze deeltjes, als beide typen deeltjes worden vergeleken bij dezelfde druk en op basis van hun kinetische-performantie limiet (KPL). De KPL van een bepaalde deeltjessoort verbindt de maximale piekcapaciteit waarden die met dat deeltjestype kan worden bereikt als functie van de toegestane analysetijd (9,10).

Een andere belangrijke technologische vooruitgang in het afgelopen decennium op het gebied van LC was de introductie van ultra-hoge-druk instrumenten, vaak aangeduid als UHPLC (11,12). Een toename in scheidingssnelheid met factor 2 tot 2,5 kan verkregen worden bij het overschakelen van 400 naar 1000 bar (aanzienlijk minder als slechts een kleine efficiëntie in de grootte-orde van 10.000 nodig is en aanzienlijk meer als een zeer grote efficiëntie vereist is) (13).

In deze studie zijn de gradiënt piekcapaciteit limieten en scheidingssnelheden onderzocht die kunnen worden bereikt door de combinatie van beide technologische vooruitgangen. Hiervoor werden performanties in gradiënt-elutie modus gerapporteerd van scheidingen op prototype Kinetex kolommen gevuld met 2,6 μm core-shell-deeltjes. Deze kunnen tot 1200 bar druk weerstaan. Door het koppelen van kolommen kan de totale kolomlengte aangepast worden om het systeem te laten werken bij de KPL van het beschouwde partikeltype en de grootte (2,6 μm). Om het potentiële voordeel van verhoogde drukken te kwantificeren, wordt de kinetische-performantie vergeleken bij twee verschillende systeemdrukken (resp. 600 en 1200 bar) voor scheidingen van moleculen met een klein moleculair gewicht. De voordelen van werken met gekoppelde kolommen bij hoge drukken werd verder geïllustreerd voor het scheiden van trypsine digesten van proteïnen.

2 Experimenteel

2.1 Chemicaliën en materialen

Acetonitrile (ACN, HPLC supra-gradiënt kwaliteit) werd gekocht van Biosolve B.V. (Valkenswaard, Nederland). Gedeïoniseerd HPLC-grade water ($\leq 0,055 \mu\text{S}$) werd terplaatse geproduceerd met behulp van een Milli-Q waterzuiveringssysteem (Millipore, Molsheim, Frankrijk). Voor de scheiding van peptiden werd mierenzuur (FA, $\geq 99\%$), gekocht bij Biosolve B.V. (Valkenswaard, Nederland), toegevoegd aan de mobiele-fase. Een testmengsel (piekcapaciteit metingen) bestaande uit 6 afvalwater verontreinigende stoffen is samengesteld uit 2-naphtalenecarboxyl zuur, quinoline, 2-naphtalenol, benzofuran, indeen en fluoreen. Om de performantie van testmengsels met een grotere complexiteit te illustreren werd een

mengsel bestaande uit 19 componenten gebruikt die dezelfde componenten omvat als het vereenvoudigde testmengsel hierboven, waaraan 9-hydroxyfluoreen, 2-hydroxychinoline, methyl 4-hydroxybenzoaat, ethyl-4-hydroxybenzoaat, propyl-4-hydroxybenzoaat, butyl-4-hydroxybenzoaat, dibenzofuran, indaan, 1-indanon, acetofenon, propiofenon, butyrofenon en valerofenon werd toegevoegd. Bovendien werd een complex mengsel van 37 componenten bereid, vertrekkende van het 19 componenten mengsel met toevoeging van cafeïne, acetanilide, fenol, trans-4-fenyl-3-buteen-2-on, 3-methylacetofenon, benzeen, dibenzothiofeen sulfon, toluen, benzothiofeen, benzofenon, xyleen, naftaleen, ethylbenzeen, acenaftyleen, 1,3,5-tri-isopropylbenzeen, hexanofenon, mesityleen en propylbenzeen. De testmengsels van alle voorgaande componenten werden bereid door 100 ppm van elk van de componenten in 50/50 (V%) ACN/H₂O op te lossen, waaraan uracil (99%, HPCE) werd toegevoegd als t₀-marker. Alle componenten hierboven werden gekocht bij Sigma-Aldrich (Steinheim, Duitsland). Voor mengsels van peptiden werd een trypsine digest uitgevoerd op β-lactoglobuline en een mengsel van 6 proteïnen (6PMD): bovine serum albumin, β-galactosidase, α-lactalbumin, β-lactoglobuline, lysozyme en apotransferrin. De concentraties bedroegen respectievelijk 0.26 μg/μL en 1.4 μg/μL. Scheidingen werden uitgevoerd op een aantal prototype Kinetex 2,1 x 150 mm en 2,1 x 100 mm C₁₈ kolommen (2,6 μm deeltjesgrootte, 100 Å), ontworpen om een hogere systeemdruk (1200 bar) te kunnen weerstaan.

2.2 Instrumentatie en LC condities

De metingen werden uitgevoerd op een Agilent 1290 Infinity systeem bestaande uit een binaire pomp, een autosampler, een gethermostatiseerd kolom compartiment en een variabele-golflengte detector. Het toestel werd bediend met de Agilent ChemStation software. De absorptie-waarden zijn gemeten bij 210 nm met een frequentie van 40 Hz en piekbreedtes werden bepaald met de breedte op halve hoogte. Het volume geïnjecteerde staal bedroeg 0,5 μL voor kleine moleculen en 10 μL voor de mengsels van peptiden.

Metingen van piekcapaciteit gerapporteerd voor het testmengsel van kleine moleculen werd uitgevoerd op één kolom apart en op de opstelling met gekoppelde kolommen. Alle scheidingen van kleine moleculen werden uitgevoerd in gradiënt mode, met een lineaire mobiele-fase helling van 15% (ϕ_0) tot 72% (ϕ_e) waterige ACN met $t_G/t_0 = 15$ (constante verhouding voor de verschillende debieten). Dit resulteert in een elutievenster met een retentiefactor k variërend tussen 1,8 en 12,2. Voor de scheiding van mengsels van peptiden was de mobiele-fase A 0.05% FA in water, mobiele-fase B was 0.04% FA in 80:20% (v/v) ACN:H₂O en een lineaire gradiënt van 0 tot 50% B werd gebruikt.

2.3 Gradiënt kinetische plot methode

Er bestaan verschillende definities voor het bepalen van de experimentele piekcapaciteit (14). Alle waarden van piekcapaciteit in deze studie werden bepaald op basis van de 6 componenten in het vereenvoudigde testmengsel van kleine moleculen beschreven in Paragraaf 2.1, en zijn berekend volgens de volgende vergelijking:

$$n_{p,exp} = I + \sum_{i=1}^n \frac{t_{R,i+1} - t_{R,i}}{4 \cdot \sigma_{t,i+1}} \quad [2]$$

In deze uitdrukking staat $\sigma_{t,i}$ voor de standaarddeviatie van de piek van de i -de component. Met behulp van de kinetische-plot methode, kan de KPL van een bepaald type

deeltje direct worden berekend met behulp van de experimenteel bepaalde piekcapaciteit ($n_{p,exp}$), de analysetijd van de laatste component ($t_{R,exp}$) en de drukval (ΔP_{exp}) over een bepaalde kolomlengte (9). Zoals beschreven in de literatuur, kan dit gebeuren door extrapolatie van de bovengenoemde experimenteel bepaalde parameters naar hun corresponderende waarde op de KPL door gebruik te maken van (10):

$$n_{p,KPL} = I + (n_{p,exp} - I) \cdot \sqrt{\lambda} \quad [3]$$

$$t_{R,KPL} = \lambda \cdot t_{R,exp} \quad [4]$$

met de lengte-elongatie factor λ gedefinieerd als:

$$\lambda = \frac{P_{max}}{P_{exp}} \quad [5]$$

3 Resultaten

3.1 Dimensieloze chromatogrammen

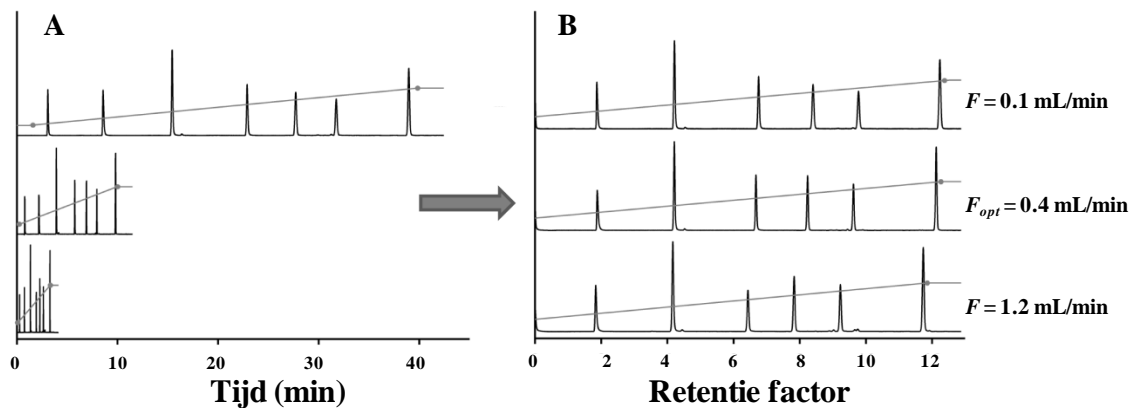
Alle experimenten werden uitgevoerd bij (i) dezelfde oorspronkelijke samenstelling van de mobiele-fase ϕ_0 , (ii) dezelfde gradiënt helling ($\beta \cdot t_0$) waarin β gegeven wordt door:

$$\beta = \frac{\phi_e - \phi_0}{t_G} \quad [6]$$

en (iii) dezelfde verhouding t_{dwell}/t_0 , om ervoor te zorgen dat een identieke piek selectiviteit en relatief elutievenster wordt verkregen, onafhankelijk van de kolomlengte of toegepast debiet. De dwell-tijd t_{dwell} wordt hier gedefinieerd als de tijd tussen het moment van de injectie en het tijdstip waarop de helling van de gradiënt het begin van de kolom bereikt. Aangezien het systeem-dwell volume (112 μL) onvermijdelijk zorgt voor een t_{dwell} voor één enkele kolom, werd de constante t_{dwell}/t_0 -conditie verzekerd bij langere kolomlengtes door het toevoegen van een isocratische hold voor de start van het gradiënt programma. Deze regel is nodig wanneer metingen op verschillende kolomlengtes met elkaar vergeleken moeten worden, en is bijgevolg belangrijk voor het bepalen van kinetische-performantie limieten.

Ter illustratie van het constante elutiepatroon dat verkregen kan worden bij verschillende debieten (F) op één kolom van 150 mm, wordt verwezen naar Figuur 1. De chromatogrammen aan de linkerkant worden uitgezet als functie van de tijd, terwijl de chromatogrammen aan de rechterkant uitgezet worden als functie van de retentiefactor k en nog steeds dezelfde informatie tonen (15). De retentiefactor stelt een aangepaste dimensieloze tijd voor, gedefinieerd door $k = \frac{t_R - t_0}{t_0}$. De laatste benadering toont dat de selectiviteit en het elutievenster inderdaad (bijna geheel) onaangetaast is bij verschillende stormingssnelheden als dezelfde ϕ_0 en $\beta \cdot t_0$ -waarden worden gebruikt. Dezelfde conclusies gelden ook voor veranderingen in lengte. De onafhankelijkheid van de elutiepatroon bij andere debieten, rekening houdend met vooropgestelde regels, is echter niet volledig perfect. De twee laatste componenten elueren algemeen iets eerder wanneer het debiet toeneemt. Deze afwijkingen kunnen worden toegeschreven aan een meer uitgesproken werking van viskeuze opwarming bij hogere stromingssnelheden (16,17). Dergelijke effecten zijn typisch voor scheidingen

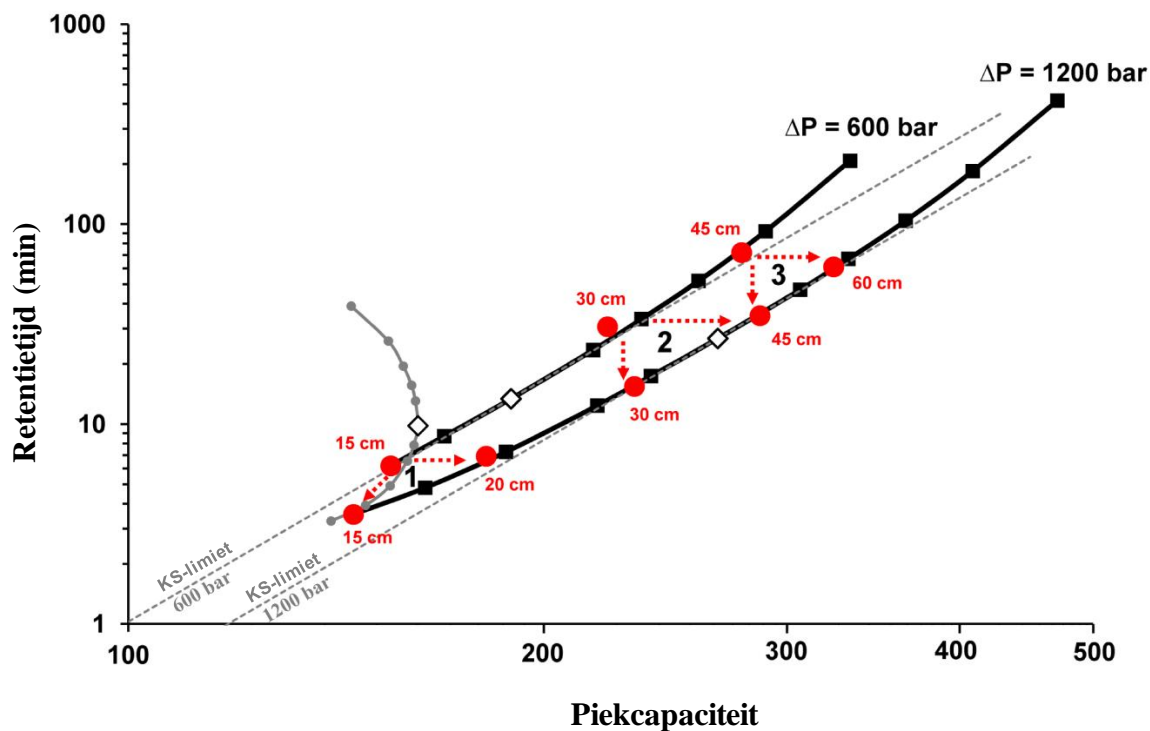
uitgevoerd bij hogere druk en kunnen niet worden vastgelegd in een eenvoudige regel, zoals de constante ϕ_0 - en $\beta \cdot t_0$ -regel.



Figuur 1: Chromatogrammen voor de scheiding van 6 afvalwater vervuilende stoffen opgenomen bij drie verschillende debieten en uitgezet als een functie van (A) de absolute tijd en (B) de retentie k (dimensieloze tijd $k = (t-t_0)/t_0$). De volgorde van de eluerende pieken komt overeen met 2-naphtalenecarboxyl zuur, quinoline, 2-naphtalenol, benzofuran, indeen en fluoreen.

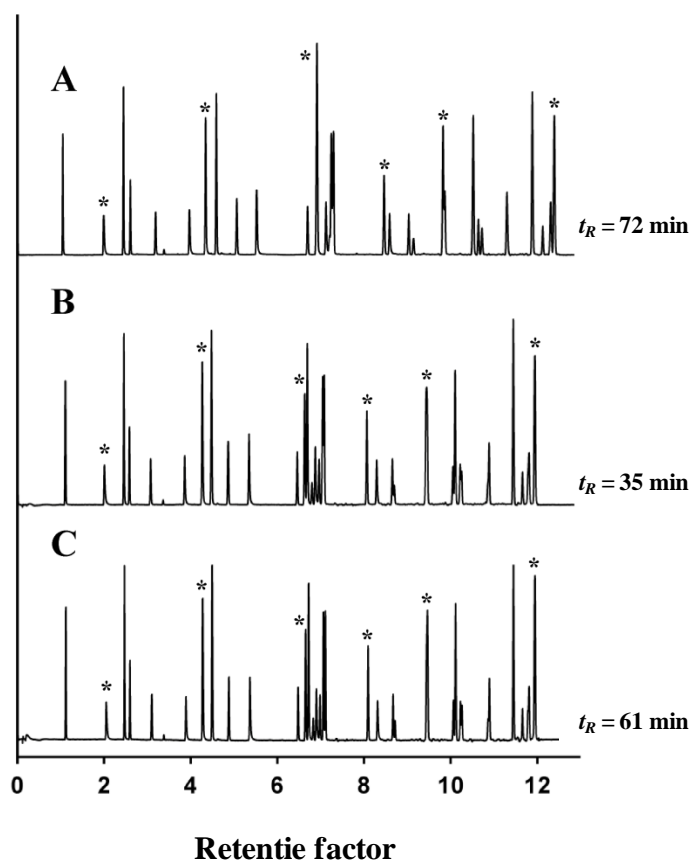
3.2 Kinetische plot analyse: effect van druk op de scheidingsperformantie

Een kinetische plot van experimentele datapunten (die overeenkomt met een grafiek van de KPL van een bepaald type deeltje) kan geïnterpreteerd worden op twee manieren: het meten van de performantie op één kolom en met de kinetische-plot methode de overeenkomstige KPL berekenen (zie Paragraaf 2.3), of het meten van de werkelijke performanties op verschillende kolomlengtes. In deze studie, zijn beide benaderingen toegepast zoals afgebeeld in Figuur 2. De volle grijze curve geeft de piekcapaciteit gemeten op één kolom voor verschillende debieten weer. De zwarte lijnen zijn berekend door toepassen van vergelijkingen (2-5) op de datapunten gemeten op één kolom waarbij een maximale systeemdruk van 600 en, respectievelijk 1200 bar werd verondersteld. De zwarte lijnen drukken dus de KPL van de onderzochte core-shell deeltjes. De grijze curve in stippellijnen is de Knox en Saleem limiet curve, die de KPL curve slechts in één enkel punt snijdt. Dit is het punt waar de chromatografische kolom gebruikt wordt bij zijn kinetisch meest voordelige punt. Met andere woorden daar waar de kolom exact lang genoeg is om de optimale snelheid van de mobiele-fase te bereiken bij de maximale opgelegde druk. Er kan een duidelijke verbetering in performantie opgemerkt worden tussen de 600 en 1200 bar KPL curven, die aantonen dat het voordelig is om deeltjes te gaan gebruiken die 1200 bar in plaats van slechts 600 bar kunnen weerstaan.



Figuur 2: Extrapolatie van de gemeten n_p versus t_R data opgemeten op één enkele 150 mm-kolom (grijze curve, ●) tot de KPL curve die overeenkomt met respectievelijk een 600 en een 1200 bar scheiding (zwarte curve). De tijd die hier staat afgebeeld is de retentietijd van de laatst eluerende component. De geconstrueerde Knox en Saleem limiet lijnen raken de KPL-curves op het punt overeenkomen met het optimale debiet (witte diamanten ◇). De experimentele data gemeten op verschillende gekoppelde kolomlengtes bij 600 en 1200 bar worden weergegeven door de rode stippen (●). Er worden drie verschillende driehoeken van datapunten onderscheiden, die gelabeld zijn van 1-3.

In Figuur 3 worden de voordelen weergegeven van het uitvoeren van scheidingen bij hogere drukken. Deze chromatogrammen geven de scheiding weer van een complex mengsel dat 37 kleine molecules bevat. De scheiding gebeurde op een 450 mm systeem met gekoppelde kolommen (3x 150 mm) met een systeemdruk van 600 bar (Figuur 3A). Bij deze scheiding hoort een piekcapaciteit van 278 in 72 min. Als de druk opgedreven wordt naar 1200 bar, zonder de kolomlengte te wijzigen waardoor de piekcapaciteit nagenoeg ongewijzigd blijft (3% toename in n_p), kan de winst in scheidingssnelheid (51% afname in analysetijd) worden uitgedrukt. Anderzijds kan ook naar het geval gekeken worden waarbij de piekcapaciteit gemaximaliseerd wordt terwijl de analysetijd in dezelfde grootteorde blijft (zie Figuur 3C; opgemeten in 61 min). Door het koppelen van vier kolommen tot een totale kolomlengte van 600 mm en daarbij een systeemdruk van 1200 bar te gebruiken, werd de maximale piekcapaciteit $n_p = 325$ opgemeten (14% winst t.o.v. het chromatogram in Figuur 3A) voor deze studie.



Figuur 3: Dimensieloze chromatogrammen die overeenkomen met driehoek 3 in Figuur 2. Ze illustreren scheidingen van een 37 componenten mengsel op een (A) 450 mm kolomconfiguratie bij 600 bar ($n_p = 278$ in 72 min), (B) 450 mm gekoppelde kolommen bij 1200 bar ($n_p = 287$ in 35 min) en (C) een 600 mm kolomconfiguratie bij 1200 bar ($n_p = 325$ in 61 min). Alle piekcapaciteiten werden bepaald op basis van de pieken aangeduid met een sterretje (dwz. 6 verbindingen uit het vereenvoudigde mengsel).

3.3 Toepassing van werken bij de kinetische-performantie limiet: scheidingen van peptiden

Als de kolomlengte en deeltjesgrootte vastligt, dan is de enige parameter die nog kan geoptimaliseerd worden de gradiënttijd t_G . Deze gradiënttijd wordt gekozen afhankelijk van de complexiteit van het testmengsel. Als een extreem complex mengsel bestaande uit een trypsine digest van β -lactoglobuline of van 6 proteïnen geanalyseerd wordt, dan is ook de kolomlengte een belangrijke factor. Om te bepalen welke opstelling en condities goed gescheiden pieken oplevert voor het laatste staal (afgekort als 6PMD) werden piekcapaciteiten berekend voor het eenvoudige β -lactoglobuline digest staal en 6PMD bij verschillende kolomlengtes en gradiënttijden met:

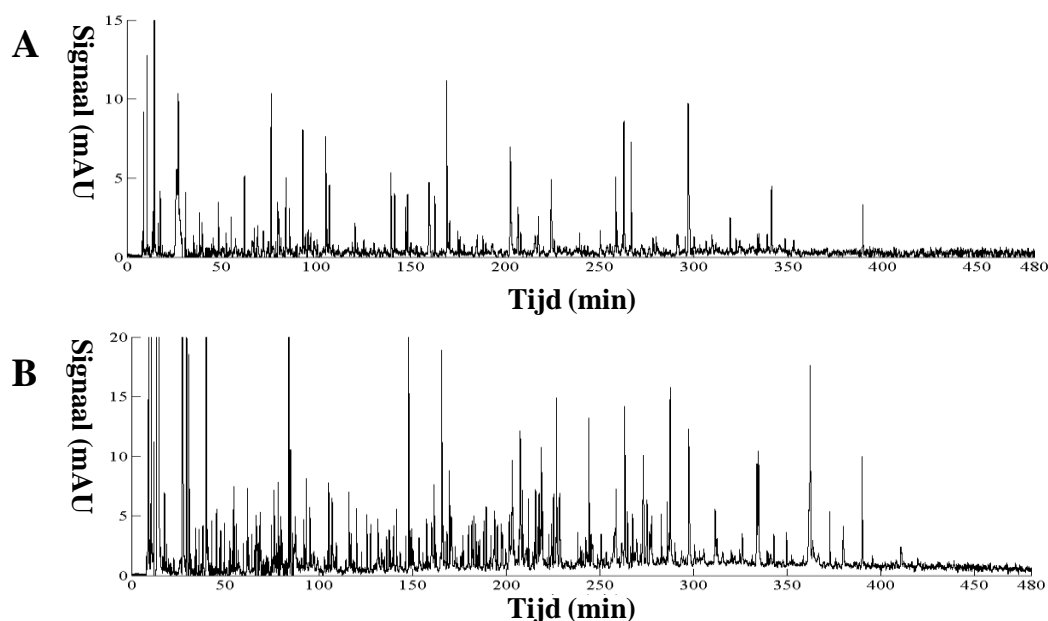
$$n_p = 1 + \frac{t_G}{\frac{1}{n} \sum_1^n w_{4\sigma}} \quad [7]$$

waarbij n het aantal geselecteerde pieken is voor de berekening. De 4σ -breedte werd geschat uit de piekbreedte op halve hoogte; die vervolgens vermenigvuldigd werd met een factor $4/2.35$. De resultaten werden samengevat in Tabel 1. Hierbij valt op dat de piekcapaciteit van

6PMD onderschat wordt bij korte gradiënttijden en korte kolomconfiguraties. Als men de hoeveelheid stationaire fase gaat verdubbelen door gebruik te maken van zes gekoppelde kolommen (900 mm) benadert de piekcapaciteit van 6PMD die van het simpele β -lactoglobuline digest staal. Dit komt enerzijds door de lange gradiënttijd en grotere beschikbare stationaire fase, maar anderzijds ook door het feit dat metingen op een 900 mm bij 1200 bar een debiet zullen bereiken dat dicht in de buurt van de optimale stromingssnelheid ligt. Uit de chromatogrammen in Figuur 4 kan worden afgeleid dat er goede gescheiden pieken optreden in het chromatogram van 6PMD en de β -lactoglobuline digest, wat ervoor zorgt dat er zeker enkelvoudige pieken worden geselecteerd voor het berekenen van de piekcapaciteit. Bij kortere kolomlengtes en kortere gradiënttijden konden geen enkelvoudige pieken geselecteerd worden voor deze berekening, waardoor piekcapaciteit onderschat werd.

TABEL 1: Overzicht van de piekcapaciteiten verkregen voor een trypsine digest van β -lactoglobuline en 6PMD voor de gebruikte kolomlengtes en scheidingscondities.

Kolomlengte (mm)	Debiet (mL/min)	Gradiënttijd (min)	Piekcapaciteit (β -lactoglobuline digest)	Piekcapaciteit (6PMD)	Afwijking (%)
450	0.35	40	483	281	-42%
450	0.35	120	757	550	-27%
900	0.175	480	1363	1360	0%



Figuur 4: Scheiding op een 900 mm Kinetex kolom (debiet = 0,175 ml / min) met een 480 min gradiënttijd van een (A) trypsine digest van β -lactoglobuline en (B) een trypsine digest van 6PMD.

4 Conclusie

Een aanzienlijke winst in kinetische performantie kan bereikt worden door het verdubbelen van de systeemdruk van 600 naar 1200 bar, mits de totale kolomlengte wordt geoptimaliseerd voor een opgelegde analysetijd of een vooraf bepaalde hoeveelheid piekcapaciteit. De curve van de kinetische-performantie limiet van het chromatografisch medium visualiseert de wisselwerking tussen snelheid en efficiëntie. Door vergelijken van systemen die gebruikt worden bij hun kinetische-performantie limiet bij 600 en 1200 bar, kan worden geconcludeerd dat een verdubbeling in druk de analysetijd kan halveren, zonder noemenswaardig in te boeten in piekcapaciteit voor de scheiding van kleine moleculen. De winst in piekcapaciteit, bij ongeveer dezelfde analysetijd, die waargenomen werd door van 600 naar 1200 bar over te schakelen, bedroeg minimaal 17% en maximaal 29%. Een maximale piekcapaciteit $n_p = 325$ kan bereikt worden voor scheidingen van kleine moleculen in een uur voor vier gekoppelde kolommen (4 x 150 mm) bij 1200 bar. Om verdere verbetering van de performantie van de scheiding te verwezenlijken (bv. voor het scheiden van complexe mengsels van peptiden in biomarker studies) kan de gradiënttijd worden verhoogd om de performantie te verbeteren, maar dit gaat dan weer ten koste van een toegenomen analysetijd. Voor een referentiesysteem van 3 gekoppelde kolommen (3 x 150 mm), steeg de piekcapaciteit met 57% van 483 ($t_G = 40$ min) tot 757 ($t_G = 120$ min) voor scheidingen van een simpele digest. Een record piekcapaciteit in deze studie van 1363 werd bereikt door het scheiden van hetzelfde tryptische digest mengsel op 6 kolommen gevuld met core-shell deeltjes in 8 uur, bij een systeemdruk van 1200 bar. Dit onderzoek geeft de voordelen weer van de combinatie van UHPLC en koppeling van kolommen gevuld met core-shell-deeltjes, gevolgd door optimalisatie van de scheidingscondities naargelang de complexiteit van het testmengsel.

5 Samenvatting

De nieuwe generatie van core-shell deeltjes leidt tot een kwantsprong in de chromatografische performanties in vergelijking met hun volledig poreuze tegenhangers. Een andere belangrijke technologische verbetering, ontstaan in de afgelopen jaren was de introductie van ultra-hoge-druk instrumenten, vaak aangeduid als UHPLC. In de huidige studie worden de grenzen van de gradiënt piekcapaciteit en de verbeteringen in analysetijden (50% reductie in analysetijd) onderzocht, die bereikt kunnen worden door beide ontwikkelingen te combineren. Meer specifiek werd de gradiënt performantie bepaald van de prototype Kinetex kolommen (ontworpen om een druk te weerstaan tot 1200 bar) gevuld met 2,6 micrometer core-shell deeltjes. De gradiënt-performantie limieten worden gevisualiseerd met behulp van kinetische plots van de analysetijd *versus* de piekcapaciteit voor scheidingen van kleine moleculen. De winst in performantie (20%) wordt verder aangetoond en gevalideerd met scheidingen van complexe mengsels met componenten met een laag moleculair gewicht. Om te werken bij de kinetische-performantie limiet werd de kolomlengte geoptimaliseerd (kolom koppeling). Bovendien werd de verbeterde piekcapaciteit voor gekoppelde kolommen bij 1200 bar geïllustreerd voor scheidingen van mengsels van peptiden. Dit resulteerde in piekcapaciteit 1363 voor een meting in gradiëntmodus van 480 minuten voor de scheiding van β -lactoglobuline op een 900 mm-kolom bij 1200 bar.

6 Erkenning

De auteurs willen Dr. Tivadar Farkas en Dr. Jason Anspach van Phenomenex (Torrance, CA, VS) bedanken voor de donatie van de prototype Kinetex kolommen. Prof. Dr. Bart Devreese wordt ook bedankt voor het doneren van de mengsels van proteïnen.

7 Referenties

1. P.W. Carr, D.R. Stoll, X. Wang, *Anal. Chem.*, **83**, 1890 (2011).
2. G. Guiochon and F. Gritti, *J. Chromatogr. A*, **1218**, 1915 (2011).
3. S. Fekete, K. Ganzler, J. Fekete, *J. Pharm. Biomed. Anal.*, **54**, 482 (2011).
4. D. Guillarme, E. Grata, G. Glauser, J.-L. Wolfender, J.-L. Veuthey, S. Rudaz, *J. Chromatogr. A*, **1216**, 3232 (2009).
5. D. Guillarme, J. Ruta, S. Rudaz, J.-L. Veuthey, *Anal. Bioanal. Chem.*, **397**, 1069 (2010).
6. D. Cabooter, J. Billen, H. Terry, F. Lynen, P. Sandra, G. Desmet, *J. Chromatogr. A*, **1178**, 108 (2008).
7. A. Fanigliulo, D. Cabooter, G. Bellazzi, D. Tramarin, B. Allieri, A. Rottigni, G. Desmet, *J. Sep. Sci.*, **33**, 3655 (2010).
8. P.A. Bristow, J.H. Knox, *Chromatographia*, **10**, 279 (1977).
9. G. Desmet, D. Clicq, P. Gzil, *Anal. Chem.*, **77**, 4058 (2005).
10. K. Broeckhoven, D. Cabooter, F. Lynen, P. Sandra, G. Desmet, *J. Chromatogr. A*, **1217**, 2787 (2010).
11. K.D. Patel, A.D. Jerkovich, J.C. Link, J.W. Jorgenson, *Anal. Chem.* **76**, 5777 (2004).
12. MacNair, J.E., Lewis, K.C., Jorgenson, J.W., *Analytical chemistry*, **69**, 983 (1997).
13. G. Desmet, D. Cabooter, P. Gzil, H. Verelst, D. Mangelings, Y. Vander Heyden, D. Clicq, *J. Chromatogr. A* **1130**, 158 (2006).
14. U.D. Neue, *J. Chromatogr. A*, **1184**, 107 (2008).
15. A. Vaast, K. Broeckhoven, S. Dolman, G. Desmet, S. Eeltink, *J. Chromatogr. A*, **1228**, 270 (2012).
16. M.M. Fallas, U.D. Neue, M.R. Hadley, D.V. McCalley, *J. Chromatogr. A* **1209**, 195 (2008).
17. M. Verstraeten, K. Broeckhoven, F. Lynen, K. Choikhet, M. Dittmann, K. Witt, P. Sandra, G. Desmet, *J. Chromatogr. A*, **1232**, 65 (2012).

Appendix II: Linear solvent strength model

AII.1 Gradient retention factor

The change in mobile phase composition with time during a gradient run is called the gradient shape. Linear gradients are used for most gradient separations. These can be described by the initial and final mobile phase compositions (defined as the volume fractions φ_0 and φ_f) and the gradient time t_G . The change in solvent composition during the gradient is called the gradient range $\Delta\varphi$:

$$\Delta\varphi = \varphi_f - \varphi_0 \quad (\text{AII.1.1})$$

The mobile phase composition at position x and time t during the gradient is then given by:

$$\varphi = \varphi_0 \text{ when } 0 < t < \frac{x}{u} \quad (\text{AII.1.2})$$

$$\varphi = \varphi_0 + \frac{\Delta\varphi}{t_G} \left(t - \frac{x}{u} \right) \quad (\text{AII.1.3})$$

where x/u or t_m is the time needed to reach position x when moving in the mobile phase. Since a molecule is either in the mobile phase or in the stationary phase the residence time t can be written as:

$$t = t_m + t_s \quad (\text{AII.1.4})$$

Now Equation (AII.1.3) can be written as:

$$\varphi = \varphi_0 + \frac{\Delta\varphi}{t_G} (t_s) \quad (\text{AII.1.5})$$

Isocratic retention can be written as a function of φ :

$$\ln k = \ln k_w - S \varphi \quad (\text{AII.1.6})$$

where k_w is the extrapolated value of k in pure water ($k_w = k(\varphi=0)$) and S is the solvent strength parameter which is constant for a given solute and organic solvent. Equations (AII.1.5) and (AII.1.6) can be combined into the following relationship [1]:

$$\ln k = \ln k_0 - b \frac{t_s}{t_0} \quad (\text{AII.1.7})$$

where k_0 is the retention at the beginning of the gradient and b is the gradient steepness:

$$\ln k_0 = \ln k_w - S \varphi_0 \quad (\text{AII.1.8})$$

$$b = S \frac{\Delta\varphi}{t_G} t_0 \quad (\text{AII.1.9})$$

Note that in other literature the gradient steepness is defined as:

$$\beta = \Delta\varphi \frac{t_0}{t_G} \quad (\text{AII.1.10})$$

The expression for the retention time t_R can be found starting from the definition of the local retention factor k (see Equation (AII.1.11)) by separation of the variables:

$$k = \frac{dt_s}{dt_m} \quad (\text{AII.1.11})$$

Because the total residence time t_R equals $t_{m,R} + t_{s,R}$ the boundaries of the integration are the following:

$$0 < t_s < t_{s,R} = t_R - t_0$$

$$0 < t_m < t_{m,R} = t_0$$

which leads to:

$$\int_0^{t_0} dt_m = \int_0^{t_R - t_0} \frac{dt_s}{k} \quad (\text{AII.1.12})$$

Insertion of Equation (AII.1.7) into Equation (AII.1.12) gives the expression for the gradient retention factor $k_{\text{effective}}$, which is equal to the instantaneous value of k when the band has migrated halfway through the column [1]:

$$\frac{1}{b} \ln(b \cdot k_0 + 1) = \frac{t_R - t_0}{t_0} = k_{\text{effective}} \quad (\text{AII.1.13})$$

Equation (AII.1.12) can be rewritten to find the expression for the retention time t_R :

$$t_R = \frac{t_0}{b} \ln(b \cdot k_0 + 1) + t_0 \quad (\text{AII.1.14})$$

When the parameters S and k_w in the expressions for k_0 and b (Equation (AII.1.8) and Equation (AII.1.9)) are known, t_R can be calculated for other gradient times and gradient conditions using Equation (AII.1.14).

AII.2 Retention factor at the end of the column

The retention factor of a compound at the end of the column $k_{elution}$ can be found by inserting the left hand side of Equation (AII.1.13) into Equation (AII.1.7) where $t_s = t_R - t_0$. The column dead time t_0 is subtracted because it takes t_0 time for the beginning of the gradient to reach the end of the column. Therefore the gradient is only felt by the compound during a time $t_R - t_0$. The expression is as follows [2]:

$$k_{elution} = \frac{k_0}{b \cdot k_0 + 1} \quad (\text{AII.1.15})$$

Note that when b approaches zero, the separation becomes isocratic, that is, the retention at the beginning of the column (k_0) and at the end (k_e) are equal.

AII.3 Extending the generality of the retention factor calculations

Equation (AII.1.13) for the retention factor $k_{effective}$ only holds when the peak elutes during the gradient. Due to the intrinsic dwell time t_0 or an imposed isocratic hold (the dwell time t_D between the solvent mixer and the head of the column), the gradient will only reach the column after a time $t_0 + t_D$. This means that t_R must be between $t_0 + t_D$ and $t_0 + t_D + t_G$ (with t_G the gradient time). Peaks eluting before $t_0 + t_D$ and after $t_0 + t_D + t_G$ are not well described by Equation (AII.1.13) and the respective chromatograms can thus not be taken into account. Therefore, the expression for $k_{effective}$ was adjusted for these peaks by adding an isocratic hold at the start and the end of the gradient. Now, peaks can elute before (region 1 in Figure AII.1), during (region 2 in Figure AII.1) and after (region 3 in Figure AII.1) the gradient, each region having a different expression for $k_{effective}$ (see Equations (AII.1.16)-(AII.1.19))

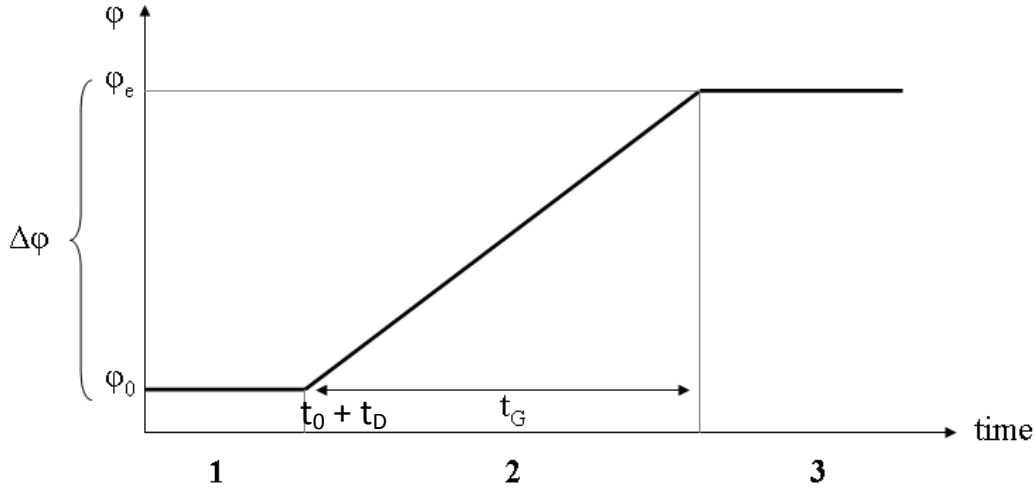


Figure AII.1: A linear gradient profile with three regions where a peak can elute: 1) during the isocratic part before the gradient reaches the column head 2) during the linear gradient 3) during the isocratic part after the gradient.

Region 1: $t_0 < t_R < t_0 + t_D$

$$k_{effective} = k_0 \quad (\text{AII.1.16})$$

Region 2: $t_0 + t_D < t_R < t_0 + t_D + t_G$

$$k_{effective} = \frac{t_D}{t_0} + \frac{1}{b} \ln \left(\left(t_0 - \frac{t_D}{k_0} \right) \frac{b}{t_0} k_0 + 1 \right) \quad (\text{AII.1.17})$$

Region 3: $t_R > t_0 + t_D + t_G$

$$k_{effective} = k_e - \frac{k_e t_D}{k_0 t_0} + \frac{t_D + t_G}{t_0} + \frac{k_e}{k_0 b} \left(1 - \exp \left(b \frac{t_G}{t_0} \right) \right) \quad (\text{AII.1.18})$$

$$\text{where } k_e = k_w \cdot \exp(-S \varphi_e)$$

AII.4 Determination of retention properties of components using LSS-theory

The k_w - and S -values of the compounds can be determined by fitting Equation (AII.1.13) (combined with Equation (AII.1.8)) for two or more gradient runs (different t_G , all other settings kept constant). The fitting is carried out in Matlab using the routine *lsqcurvefit*. This

routine solves nonlinear data-fitting problems in the least-squares sense. The routine basically guesses values for k_w and S , and fits those values in such a way that the related fitted gradient retention factor k_{fitted} approximates the measured gradient retention factor $k_{measured}$. That is, given the input data φ_0 and $\Delta\varphi/t_G$ and the observed output data $k_{measured}$, the k_w - and S -values are found for which the sum of least squares (see (AII.1.19)) is minimal:

$$\min \sum_{i=1}^n (k_{fit,i} - k_{measured,i})^2 \quad (\text{AII.1.19})$$

where n is the number of components that is measured in the gradient elution experiment.

References

- [1] Snyder, L.R., Dolan, J.W., *High-Performance Gradient Elution The Practical Application of the Linear-Solvent-Strength Model*, John Wiley & Sons, 2007.
- [2] Neue, U., Theory of peak capacity in gradient elution. *Journal of Chromatography A* 2005, 1079, 153-161.

Appendix III: Signal enhancement by trapping

AIII.1 Introduction

Impurity profiling of pharmaceutical samples is an important application in pharmaceutical industry. The EU consistently published threshold values for impurities in pharmaceutical substances, see Table AIII.1. Detection of low-abundant peptides in proteomic samples is also of key importance in biomarker discovery.

Table AIII.1: Threshold values for impurities in pharmaceutical substances; EU guidelines. ¹The amount of drug substance administered per day, ²Higher reporting thresholds should be scientifically justified, ³Lower thresholds can be appropriate if the impurity is unusually toxic.

Maximum daily dose ¹	Reporting threshold ^{2,3}	Identification threshold ³	Qualification threshold ³
≤ 2 g/day	0.05 %	0.10% or 1.0 mg/day intake (whichever is lower)	0.15% or 1.0 mg/day intake (whichever is lower)
> 2 g/day	0.03 %	0.05 %	0.05 %

To tackle the problem of enhancing the detector signal of low-abundant peaks in the chromatogram, a column packed with a stationary phase with increased retention characteristics for the sample compared to the analytical column can be used. Remobilization of the analytes can be done by using a low-thermal mass heating system or by using a strong solvent. The first approach practically requires a low thermal mass heating sleeve around the trapping segment, which is capable of temporarily delivering 100-200°C to lower the retention factor of the trapped components. The second approach requires a switching valve between the analytical column and the trapping segment, and is further investigated.

AIII.2 Experimental set-up and aim

An Agilent 1100 series binary pump was used to pump a water-acetonitrile gradient (from 20% to 90% ACN) through an analytical column (COL 1, see Figure AIII.1). To test retention behavior on the set-up, isocratic elution mode (30% ACN) was used. An Agilent 1290 auto-injector and thermostated column compartment were used. Two switching valves made it

possible to send fractions of COL 1 to one of the two trapping segments (Trap 1 or Trap 2) or a capillary (Cap 1). An Agilent 1290 series binary pump delivered the solvent to flush the trap or capillary. A variable wavelength detector with a low dispersion cell (80 Hz sample rate, 245 nm) was used for the experiments. As can be noted in Figure AIII.1, the switching valves allow to select Cap 1 (when the user wants to bypass a main peak in the sample that elutes from the analytical column), send a fraction from Col 1 to Trap 1 while Trap 2 is flushed to the detector or send a fraction from Col 1 to Trap 2 while Trap 1 is flushed to the detector.

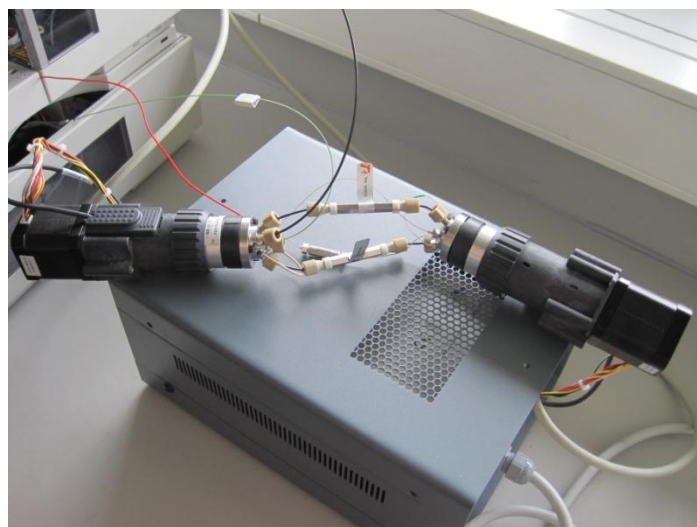
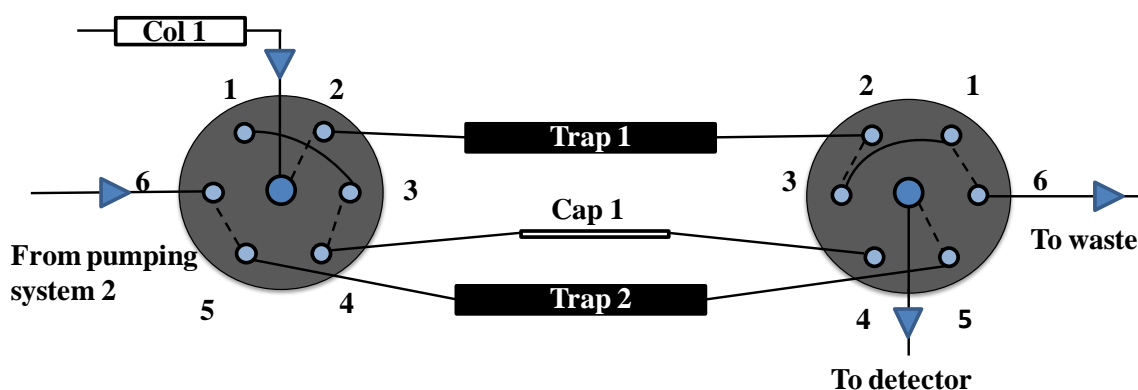


Figure AIII.1: In the upper part a schematic of a trapping interface can be found consisting of 2 switching valves, 2 trap columns (Trap 1 and Trap 2) and a capillary (Cap1). Fractions from Col 1 are feeded to Trap 1, while Trap 2 is flushed to the detector. The lower part shows the actual set-up.

A test sample of 10 phenones (acetanilide, acetophenone, 3-methylacetophenone, propiophenone, butyrophenone, benzophenone, valerophenone, hexanophenone, heptanophenone and octanophenone) with uracil added as a t_0 -marker was used. The concentration of all components was 100 ppm. See Figure AIII.2.

An Acclaim C18 (300 μm ID x 150mm), Acclaim C8 (1 mm ID x 150mm) and an Acclaim C8 (300 μm ID x 150mm) column were tested as analytical Col 1. All these columns were packed with 5 μm particles which had 120 \AA pore size. The trap column consisted of a Hypercarb 1 mm ID x 15 mm segment.

In this study, the influence of changing column stationary phase and column dimensions on the test sample above were investigated. The trapping set-up was tested for one selected component in the test mixture.

AIII.3 Results and discussion

AIII.3.1 Retention characteristics of the analytical column and the trapping segment

Preliminary studies of the retention behavior of the phenones mixture on the different analytical columns and the Hypercarb trap column was first investigated. The separation at typical gradient conditions ($\phi_0=20\%$, $\phi_0 = 90\%$ and $t_G = 20$ min) is depicted in Figure AIII.2. An example of plots depicting retention factor *versus* fraction ACN on an Acclaim C8 (1 mm ID x 150mm) analytical column is given in Figure AIII.3A. The test mixture was analyzed in isocratic mode (30, 50, 70 and 90% ACN in water), in this way the retention behavior of the components could be evaluated. On the analytical column, the components show normal retention behavior (more hydrophobic components retain longer) and no deviations from LSS-theory (see Appendix II) are observed.

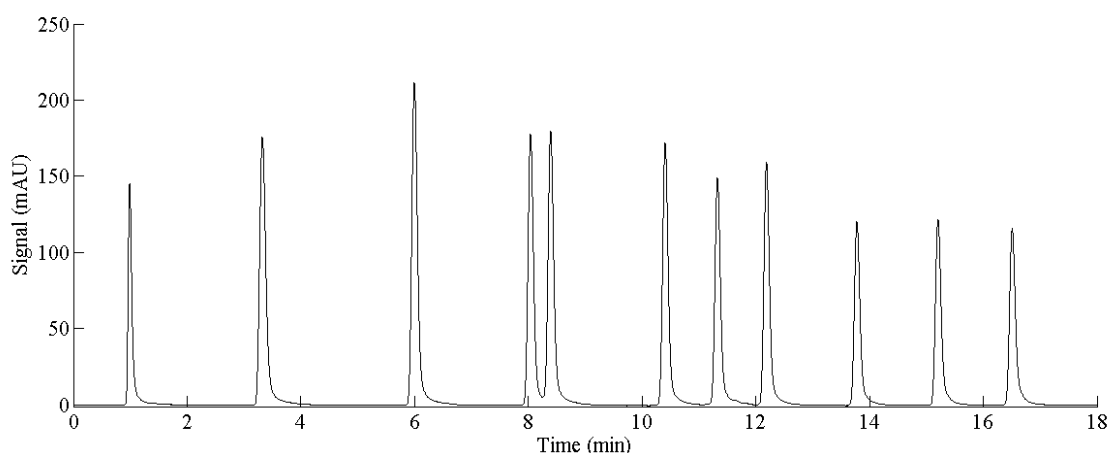


Figure AIII.2: Separation of the test mixture (uracil and 10 phenones) in gradient elution mode ($\phi_0=20\%$, $\phi_0 = 90\%$ and $t_G = 20$ min).

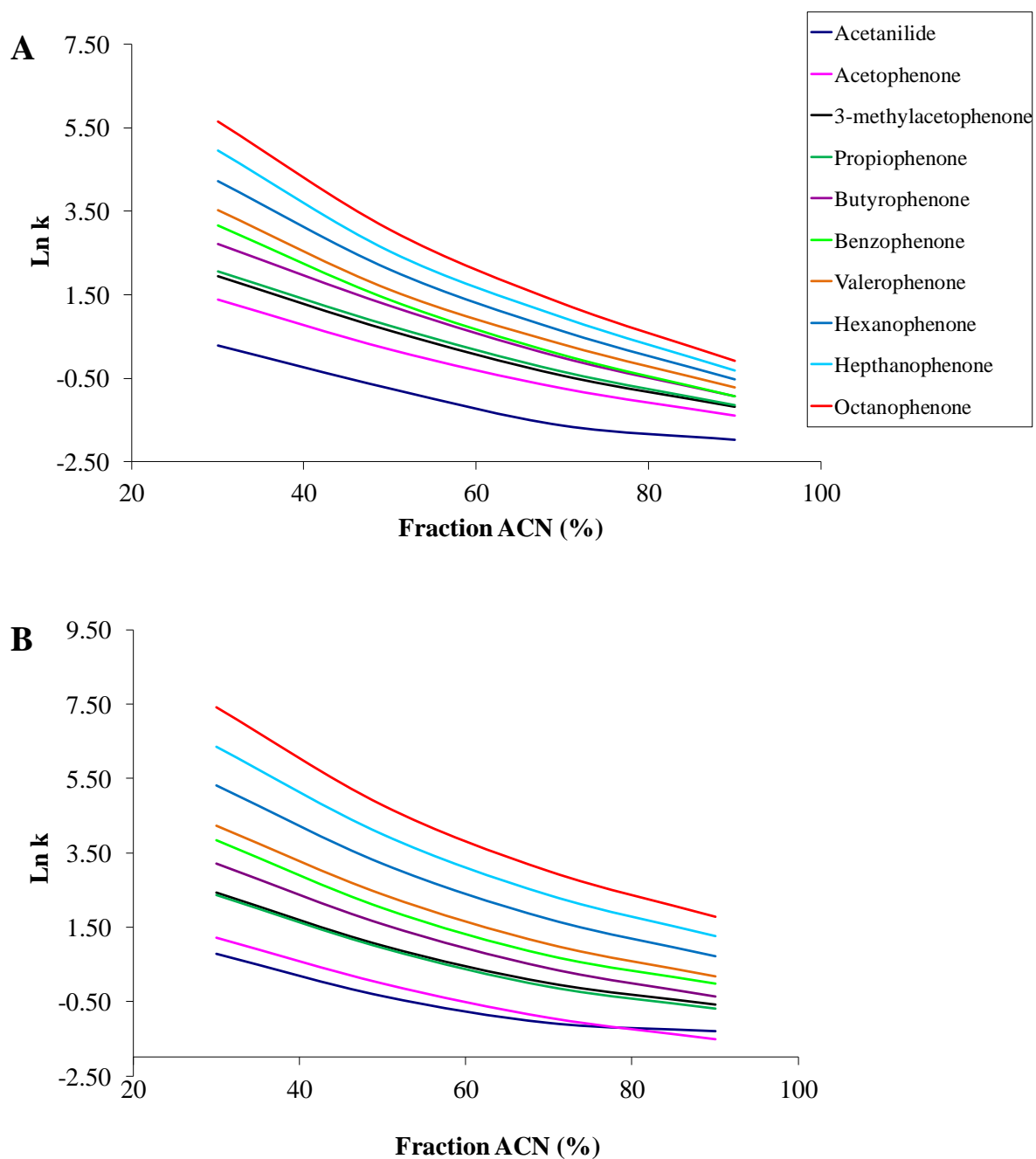


Figure AIII.3: Retention characteristics of the test mixture measured on (A) an Acclaim C8 (1 mm ID x 150 mm) and (B) a Hypercarb 1 mm ID x 15 mm segment.

Figure III.3B illustrates the retention behavior of the test components on the Hypercarb column. An anomalous retention behavior for acetanilide can be observed when high fractions of acetonitrile are used. It is possible that measurement errors were made when detecting the acetanilide-peak (which elutes after 3 s, which is 0.5 s slower than the t_0 -peak for a flow rate of 2.2 mL/min and 90% ACN). The figure also illustrates the peculiar retention behavior of the components on the Hypercarb stationary phase (porous graphitic carbon). Note that the retention of 3-methylacetophenone and propiophenone on this material is different compared to the tested analytical columns. When LSS-theory is applied, k_w and S values for the different

components can be calculated. These can be used to calculate a theoretical plate number in isocratic mode and the related peak widths. With this information, a selected conditions can be evaluated and the effect of different parameters (flow rate, temperature,...) can be theoretically evaluated. Peak enhancement factors can be theoretically evaluated.

AIII.3.2 Preconcentration experiment

The set-up was further tested with valerophenone. An isocratic elution experiment (30% ACN) on an Acclaim C8 column (300 μm ID) learned that the component eluted at 14 min. The trapping column collects the fractions of valerophenone until the entire tail of the peak is eluted from the analytical column. A reproducible trapped peak can be observed in Figure AIII.4 (red chromatogram). However, significant difference in area was observed. Optimization of the set-up and operation conditions will be subject for a PhD study.

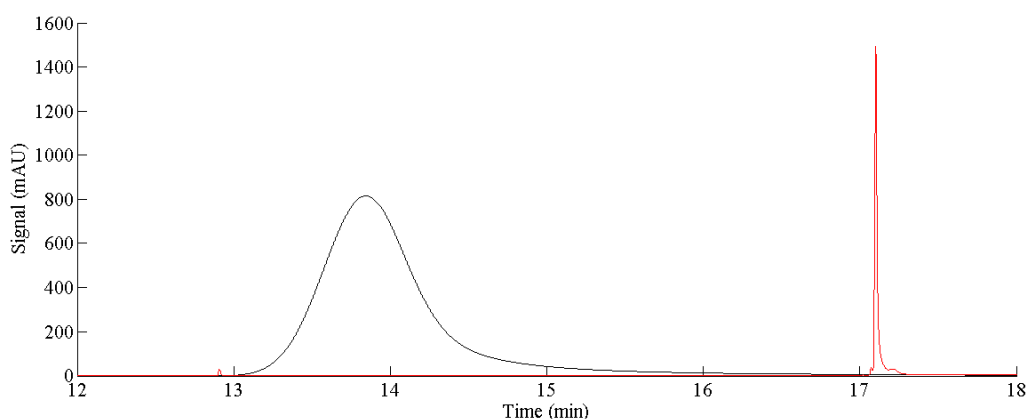


Figure AIII.4: Overlay of chromatograms of valerophenone eluted (0.5 mL/min, 100% ACN) from a trapping column (red) and eluted (0.032 mL/min, 30% ACN in water) from an Acclaim C8 column (black). The effect of trapping on peak width is visualized.